Spring 2020

# Exploring wellbore and reservoir temperature profiles in fluid circulation and production operations

Ahmed Qasim Al Saedi



Department: Geosciences and Geological and Petroleum Engineering

# EXPLORING WELLBORE AND RESERVOIR TEMPERATURE PROFILES IN FLUID CIRCULATION AND PRODUCTION OPERATIONS

by

AHMED QASIM ATIYAH AL SAEDI

A DISSERTATION

Presented to the Faculty of the Graduate School of the

MISSOURI UNIVERSITY OF SCIENCE AND TECHNOLOGY

In Partial Fulfillment of the Requirements for the Degree

DOCTOR OF PHILOSOPHY

in

PETROLEUM ENGINEERING

2020

Approved by:

Ralph Flori, Advisor
Shari Dunn-Norman
Mingzhen Wei
David Rogers
Kelly Homan

## PUBLICATION DISSERTATION OPTION

This dissertation has been prepared in the form of four articles, formatted in style used by the Missouri University of Science and Technology:

Paper I: Pages 11-47 “New analytical solutions of wellbore fluid temperature profiles during drilling, circulating, and cementing operations.” This manuscript have been published in *Journal of Petroleum Science and Engineering*.

Paper II: Pages 48-86 “Influence of Frictional or Rotational Kinetic Energy on Wellbore Fluid-Temperature Profiles During Drilling Operations.” This manuscript have been published in *SPE Drilling & Completion Journal*.

Paper III: Pages 87-129 “Exploring alteration of near-wellbore geothermal gradient during fluid circulation and production.” This manuscript have been published in *Journal of Petroleum Science and Engineering*.

Paper IV: Pages 130-163 “Estimating the initial-formation temperature and flowing-temperature gradient with transient-temperature analysis: Applications in gas reservoirs. “ This manuscript have been published in *Journal of Natural Gas Science and Engineering*.

# ABSTRACT

The wellbore heat flow occurs during different well operations resulting from any temperature differences between the wellbore fluid and the adjacent formation. Understanding the direction and mechanism of heat flow whether it is conduction or convection help to represent this heat exchange mathematically. However, the only available factor used to understand the heat flow behavior is the measured wellbore temperature which can be obtained from the direct measurement while drilling or circulation operations, well logging, well test, or from the production operations. Also, the initial geothermal formation temperature resulting from the geothermal gradient will help to understand the undistributed formation temperature and the heat flow behavior.

In general, there are two type of models; the first type depends on the conservation of heat energy theory for both steady and unsteady satiations. And the second model type depend on the analogy between the pressure and temperature diffusivity equations.

In this study, and in addition to the old boundary conditions that used to solve the heat energy system we introduce two new boundary condition that can expanse the insight of the predictive temperature and then the heat flow rate. Another model was present to investigate a new factor that can be effect the wellbore temperature resulting from the Kinetic rotational energy of the drillstring in drilling operations. The thermal radius and the heat transfer behavior was also investigated for drilling, circulation, and production operations. Finally, a full derivation of the line-source solution of the temperature diffusivity equation, which provide a required recipe to studying the falloff and build-up temperature record of transient temperature test.

# ACKNOWLEDGMENTS

First, thanks to Allah (God) for giving me the many blessings, opportunity, and strength to complete this long research journey. Second, I would like to express my sincere gratitude to my PhD advisors, Dr. Ralph Flori and Mr. Shah Kabir, for their invaluable support throughout my research. They have always been excellent mentors, contributors, supporters, and friends during the whole study.

I would also like to thank my committee members, Dr. Shari Dunn-Norman , Dr. Mingzhen Wei, Dr. David Rogers, and Dr. Kelly Homan for their valuable advice and recommendations. I am very grateful to the Higher Committee for Education Development (HCED) in Iraq for granting me a PhD scholarship and financial support.

A special thanks to my family, especially, my parents, for their love, support, encouragement, and prayers throughout my study.

Ultimately, I would like to thank my lovely wife and my kids for their love and great patience throughout my study. Without their steadfast support and kind encouragement, this study would have never been completed.

# TABLE OF CONTENTS

Page

# LIST OF ILLUSTRATIONS

PAPER I Page



PAPER II

PAPER IV

# LIST OF TABLES

# 1. INTRODUCTION

Historically, the formulation of the wellbore temperature profiles during drilling, circulating, and cementing operations relied upon the boundary condition or BC at the bottomhole location, wherein the tubular and annular temperatures become equal. The first part of this study presents two other formulations to explore alternative to bottomhole BC's that may potentially occur in wellbores. Application of the energy balance in the wellbore for both forward and reverse circulations underpins all three formulations. The wellbore temperature profiles generated by implementing the energy balance in the system depends on the type of the boundary condition used. Initially, we generated various temperature profiles using these models. In general, we observed that the maximum temperature occurs at the end of the tubular or some distance away from the bottom. For open and cased-hole sections, the difference in heat-transfer coefficients triggers different magnitudes of heat transfer and affects the corresponding temperature profiles.

We compared the performance of our models with those presented in the literature. Thereafter, we sought to validate the models with diverse set of field data. Given the ability of all three models to handle changes in the geothermal gradient due to the characteristics of the sediments, salt domes, and gas hydrates, we explored their performance in situations where there is significant heat transfer. The holistic approach pursued here provided the necessary insights into various temperature profiles in a given situation.

However, temperature-profile distributions in a wellbore during drilling operations might take different forms when applying the energy balance in the overall system. For steady-state conditions, wherein the wellbore is considered as a closed system, adding any source of

additional energy to this system can influence the predicted temperature profiles. This study presents a new analytical model to investigate the influence of rotational energy arising from the drillstring on the wellbore-temperature behavior.

A significant part of drilling operation is the rotation of the drillstring. Depending on the drilling rig, various equipment provides this kind of energy, such as the rotary table or top drive. In addition, downhole motors or turbines can add additional rotation to the drill bit. This type of energy source may be construed as a supplemental heat source that can be added to the formulations of drillpipe-and annular-temperature profiles. Overall, this part presents two models involving frictional and rotational energy. These models yield the same solution if we do not include the energy source, and they can apply equally well for any energy balance system. The proposed mathematical models provide new insights into different energy terms that can be included to compute the temperature profiles in the drillpipe and annulus.

The constant undisturbed formation temperature profile controlling heat transfer into the wellbore appears counterintuitive in light of transient cooling of the formation that occurs upon fluid circulation in drilling and also heating during fluid production. The third part presents a mathematical model that shows that the heat transfer occurs from the wellbore/formation interface, not from some distance away from the wellbore wherein the initial formation temperature profile remains undisturbed. This new model allows investigation of heat transfer behavior from the formation into the wellbore during drilling or fluid circulation, and from the wellbore into the reservoir in the production mode.

Application of the line-source solution for the temperature diffusivity equation for a steady-state system provides the necessary ingredients for computing the temperature behaviors at different times and radii. This line-source solution can be used throughout the

wellbore to determine the undisturbed formation temperature, which may be used to obtain the geothermal gradient dependent on the radius and fluid circulation time. Therefore, the initial geothermal gradient works as a time-dependent variable, and the resultant second-order polynomial relationships can describe the undisturbed formation temperature. This study provides the required tools to assess the wellbore heat-transfer behavior and their effect on the wellbore temperature profiles. Also, the new mathematical model illuminates the impact of heat transfer by comparing its performance with the original formulations. Besides, this paper presents a complete derivation of the line-source solution of the temperature diffusivity equation to justify the proposed approach.

The formation temperature constitutes one of the essential factors that affect the wellbore fluid temperature behavior in production mode. The amount and direction of the radial heat transfer between the surrounding formation and the wellbore depend on the temperature differential and thermal properties of the media. Traditional studies probing geothermal gradients depended principally on extrapolating the transient bottomhole temperature to infinite shut-in time for obtaining the undisturbed formation temperature. After that, a straight line from the surface to the bottomhole condition constituted the geothermal gradient. Of course, the implicit assumption in this approach is that a linear geothermal gradient exists in light of unavailability of depth-wise temperature measurements.

The last part presents a new transient-temperature analysis approach to determine the undisturbed formation temperature. Specifically, we show the application of the line-source solution that has roots in the temperature-diffusivity equation. Secondly, using the distributed temperature measurements associated with transient-pressure testing, we proved that the bottomhole or static temperature is time-dependent, leading to alteration of the geothermal

gradient in a well's proximity. Finally, the lowering of the temperature-derivative plateau with increasing depth during well shut-in periods indicated an increase in thermal conductivity, resulting in a nonlinear geothermal gradient.

# 2. LITERATURE REVIEW

Although commercial drilling in the US started in the 1920's, the fluid circulation models appeared a few decades later. We note that the earlier analytical models of Edwardson et al. (1962) and Tragesser et al. (1967), although useful to gain a physical understanding of the transient flow problem, are impractical in a field situation because they require a detailed knowledge of the drilling history.

Raymond (1969) presented the first numerical model for computing circulating-fluid temperatures during unsteady and pseudosteady-state conditions to handle multiple casing strings. This approach requires a finite difference solution of the governing equations dealing with the unsteady-state, heat-transfer problem. Subsequently, improvements to this model were presented by Keller et al. (1973), Wooley (1980), and Beirute (1991), among others.

Subsequently, analytical solutions became feasible for less complicated systems, such as that for a single casing string. For example, Holmes and Swift (1970) presented a solution for the steady-state heat transfer in a drillpipe and annulus surrounded by the formation. In contrast, Kabir et al. (1996) and Hasan et al. (1996) obtained solutions for forward and reverse-circulation cases for the variable mud-tank temperature of the circulating fluid. They validated their fluid-temperature model with field data from Holmes and Swift (1970) and Davies et al. (1994).

In the modern era, deeper drilling depths in deviated wellbores and demanding environments, such as that in a deepwater setting present considerable operational challenges. Given the influence of fluid temperature on the fluid properties and the consequent drilling operation itself, one cannot overemphasize the importance of estimating the fluid temperature

profiles in both conduits. To that end, Kumar and Samuel (2013) expanded the scope of the previous models by including well deviation and heat generated by wellbore friction. Others studied the drilling fluid temperature profile during the gas-hydrate drilling process, such as the mathematical model presented by Gao et al. (2017), and the numerical model given by Li et al. (2017). We point out that all the previous studies solved the flow problem of interest using the boundary condition or BC of first kind or the Dirichlet condition.

In drilling operations, the frictional forces originate from pressure losses or the contact area between the drilling tool and the drilled formation. Furthermore, the torque and drag forces result from rotating the drill string, such as those presented by Samuel (2007), Aadnoy and Djurhuus (2008), Aadnoy et al. (2010), and Mirhaj et al. (2016), among others. These factors may influence the drilling fluid temperature profiles by incorporating the necessary heat energy system model as presented by Kumar et al. (2012a, 2012b) for drilling operations, and for casing while drilling operations by including the plastering effect as in Kumar and Samuel (2012).

Historically, many studies provided the necessary mathematical tools to describe the temperature distribution inside the wellbore. Earlier studies presented the basic analytical models and provided the physical understanding of the steady-state and transient flow problems as those given by Edwardson et al. (1962) and Tragesser et al. (1967). Raymond (1969) provided the first numerical model for computing circulating-fluid temperatures during unsteady and pseudosteady-state conditions to handle multiple casing strings.

Furthermore, improvements to this model have been made by Keller et al. (1973) by adding new forms of energy as a result of frictional pressure losses throughout the drillpipe and annulus to the heat energy system with the limitations of the provided data. This model

was further investigated by Marshall and Bentsen (1982) by using a full set of data. Subsequently, analytical solutions became feasible for less complicated systems, such as that for a single casing string. For example, Holmes and Swift (1970) presented a solution for the steady-state heat transfer in a drillpipe and annulus surrounded by the formation. In contrast, Kabir et al. (1996) and Hasan et al. (1996) obtained solutions for forward and reverse-circulation cases, for a variable mud-tank temperature of the circulating fluid. More recently, Kumar and Samuel (2013) expanded the scope of the previous models by including well deviation and heat generated by wellbore friction. They validated their fluid-temperature model with field data involving deviated and horizontal wellbores.

Conservation of energy for both conductive and convective heat transfer underpins all studies while assessing the wellbore temperature profiles. When a temperature difference exists, conductive heat transfer occurs between the adjacent formation with the cooler wellbore, and between the outer and inner diameter of different tools inside the wellbore. In this context, the convective heat transfer occurs in the drilling or circulating fluid itself. In a drilling operation, the adjacent formation temperature remains higher than the wellbore fluid temperature, given the formation's geothermal gradient; therefore, the direction of heat flow will be from the reservoir toward the wellbore. This heat flow direction reverses itself during a well's production mode. Two types of studies have emerged based on the direction of heat flow. In the first group the direction of heat flow occurs from the wellbore to the formation, such as those presented by Holmes and Swift (1970), Keller et al. (1973), Marshall and Bentsen (1982), Arnold (1990), Sagar et al. (1991), Kumar and Samuel (2013), Guo et al. (2016), and Gao et al. (2017), among others. The second group considered the heat flow direction from the initial formation temperature into the wellbore, such as those offered by

Raymond (1969), Hasan and Kabir (1994), Hasan et al. (1996), and Kabir et al. (1996). The difference between these two approaches is the amount of heat transfer that occurs after obtaining the wellbore temperature profile. For example, Holmes and Swift (1970) presented a solution for the steady-state heat transfer in a drillpipe and annulus surrounded by the formation. In contrast, Kabir et al. (1996) and Hasan et al. (1996) obtained solutions for forward and reverse-circulation cases for the variable mud-tank temperature of the circulating fluid.

Many studies also attempted to determine the formation temperature based on well logging measurements, such as those of Schoeppel and Gilarranz (1966), Prensky (1992), and Forrest and Scott (2007), among others. In contrast, others attempted to use the extrapolation of the bottomhole transient temperature for the static-formation temperature, as presented in Dowdle and Cobb (1975), Kritikos and Kutasov (1988). Moreover, Kutasov and Eppelbaum (2005) provided a mathematical model to determine the formation temperature from the bottom-hole logs by the generalized Horner method.

More recently, Kutasov and Eppelbaum (2018) presented a new approach to estimating the undisturbed formation temperature from shut-in temperature openhole logs for deep wells. They modified the Horner plot by adopting a new circulation and shut-in time concept to find the undisturbed formation temperature. Regardless of the methodology, once the formation temperature obtained, the geothermal gradient can be established.

For conservation of energy in any system, the formation temperature estimation largely depends on the type of boundary condition used in the solution of that system. We implemented two boundary conditions, the Dirichlet condition as the traditional one and the Robin condition as presented recently by Al Saedi et al. (2018), leading to different

geothermal gradients. The intrinsic idea was to cover a wide range of possible temperature profiles that may emerge due to operational considerations.

The similarity between the pressure diffusivity equation presented by van Everdingen and Hurst (1949) and the temperature diffusivity equation given by Carslaw and Jaeger (1959) allowed many authors to adopt the same solution methods for the pressure diffusivity equation for its temperature counterpart. The temperature diffusivity equation allows to describe the heat transfer and to find the undisturbed radial formation temperature distribution. In general, the undisturbed formation temperature for the wellbore can be characterized by a linear relationship including the geothermal gradient which required a knowledge of the bottomhole and surface temperatures.

Many studies presented the line-source solution for pressure diffusivity equation, such as those given by Mathews et al. (1967) and Dake (1978). Horner (1951) presented an analytical study to find the initial reservoir pressure involving flow and shut-in periods. The study was based on the line-source solution of the pressure diffusivity equation. His solution approach known as the Horner method has served the industry well as documented in many textbooks, such as that in Lee et al. (2003). A comparison between the temperature and pressure buildup study was presented by Dowdle and Cobb (1975); however, no mathematical details appeared. The authors suggested the buildup temperature equation based on the similarities with the pressure buildup equation obtained by Horner (1951). Nonetheless, Dowdle and Cobb (1975) showed that Horner-type analysis could be used to find the static formation temperature under the assumption of short fluid circulation times. However, this method was more investigated to estimate the initial formation temperature as presented by Roux et al. (1980), Hasan and Kabir (1994a), among others. Furthermore, the flowing fluid

temperature of two-phase flow for a complex well demands the application of an energy balance including pressure gradient was presented by Hasan et al. (2009), which expand the window of fluid temperature calculation by depth steps covering the possible variety of the heat loss and geothermal gradient throughout the well path.

Earlier, Kutasov and Eppelbaum (2005) provided a mathematical model to determine the formation temperature from bottomhole logs by generalized Horner method. More recently, Kutasov and Eppelbaum (2018) presented a new approach to estimate the undisturbed formation temperature from shut-in temperature data gathered in openhole systems. They modified the Horner method by adopting a new circulation and shut-in time concept to find the undisturbed formation temperature. Studying flowing fluid temperature behavior by using the distributed temperature measurements in gas wells inspired us to investigate different aspects of temperature behavior to elicit more information beyond those reported recently by Hashmi et al. (2015).

# PAPER

## I. NEW ANALYTICAL SOLUTIONS OF WELLBORE FLUID TEMPERATURE PROFILES DURING DRILLING, CIRCULATING, AND CEMENTING OPERATIONS

A.Q. Al Saedi, R. E. Flori, and C. S. Kabir

Missouri University of Science and Technology,

(Published in Journal of Petroleum Science and Engineering 170 (2018) 206-217)

## ABSTRACT

Historically, the formulation of the wellbore temperature profiles during drilling, circulating, and cementing operations relied upon the boundary condition or BC at the bottomhole location, wherein the tubular and annular temperatures become equal. This study presents two other formulations to explore alternative to bottomhole BC's that may potentially occur in wellbores. Application of the energy balance in the wellbore for both forward and reverse circulations underpins all three formulations.

The wellbore temperature profiles generated by implementing the energy balance in the system depends on the type of the boundary condition used. Initially, we generated various temperature profiles using these models. In general, we observed that the maximum temperature occurs at the end of the tubular or some distance away from the bottom. For open and cased-hole sections, the difference in heat-transfer coefficients triggers different magnitudes of heat transfer and affects the corresponding temperature profiles.

We compared the performance of our models with those presented in the literature. Thereafter, we sought to validate the models with diverse set of field data. Given the ability of all three models to handle changes in the geothermal gradient due to the characteristics of the sediments, salt domes, and gas hydrates, we explored their performance in situations where there is significant heat transfer. The holistic approach pursued here provided the necessary insights into various temperature profiles in a given situation.

## 1. INTRODUCTION

Although commercial drilling in the US started in the 1920's, the fluid circulation models appeared a few decades later. We note that the earlier analytical models of Edwardson et al. (1962) and Tragesser et al. (1967), although useful to gain a physical understanding of the transient flow problem, are impractical in a field situation because they require a detailed knowledge of the drilling history.

Raymond (1969) presented the first numerical model for computing circulating-fluid temperatures during unsteady and pseudosteady-state conditions to handle multiple casing strings. This approach requires a finite difference solution of the governing equations dealing with the unsteady-state, heat-transfer problem. Subsequently, improvements to this model were presented by Keller et al. (1973), Wooley (1980), and Beirute (1991), among others.

Subsequently, analytical solutions became feasible for less complicated systems, such as that for a single casing string. For example, Holmes and Swift (1970) presented a solution for the steady-state heat transfer in a drillpipe and annulus surrounded by the formation. In contrast, Kabir et al. (1996) and Hasan et al. (1996) obtained solutions for forward and reverse-circulation

cases for the variable mud-tank temperature of the circulating fluid. They validated their fluid-temperature model with field data from Holmes and Swift (1970) and Davies et al. (1994).

In the modern era, deeper drilling depths in deviated wellbores and demanding environments, such as that in a deepwater setting present considerable operational challenges. Given the influence of fluid temperature on the fluid properties and the consequent drilling operation itself, one cannot overemphasize the importance of estimating the fluid temperature profiles in both conduits. To that end, Kumar and Samuel (2013) expanded the scope of the previous models by including well deviation and heat generated by wellbore friction. Others studied the drilling fluid temperature profile during the gas-hydrate drilling process, such as the mathematical model presented by Gao et al. (2017), and the numerical model given by Li et al. (2017). We point out that all the previous studies solved the flow problem of interest using the boundary condition or BC of first kind or the Dirichlet condition.

The purpose of this study is to offer new analytical fluid-temperature models with different boundary conditions at the well bottom via the formulation of a second-order differential equation that explores more realistic downhole conditions. The absence of published field thermal data provided the impetus to develop this approach. In our modeling, the change in casing diameter can also be handled.

## 2.MODEL DEVELOPMENT

The conservation of energy balance in a vertical wellbore leads to a second-order differential equation due to changes in depth and time, which has been regarded as a boundary value problem by Powers (2010). The general solution of a boundary-value problem contains

two unknown constants, which can be found by applying the boundary conditions. There are three types of these boundary conditions known as the condition of the first kind or Dirichlet condition, the condition of the second kind or the Neumann condition, and the third kind or Robin condition. For simplicity, we term these models in a sequence of BC's as Model-1, Model-2, and Model-3. All literature on this subject used the boundary condition of the first kind or Model-1.

For clarity, these three boundary conditions appear in Fig. 1 for the flow problem at hand. In Model-1, we assume at $Z = 0$, $T_t = T_{ti}$, and at $Z = L$, $T_t = T_a$. These conditions appear quite reasonable when we attain a stable fluid circulation rate, as Fig. 1a shows. In Model-2, we assume unchanged annular temperature at the well bottom: $dT_a/dz|_{z=L} = 0$.

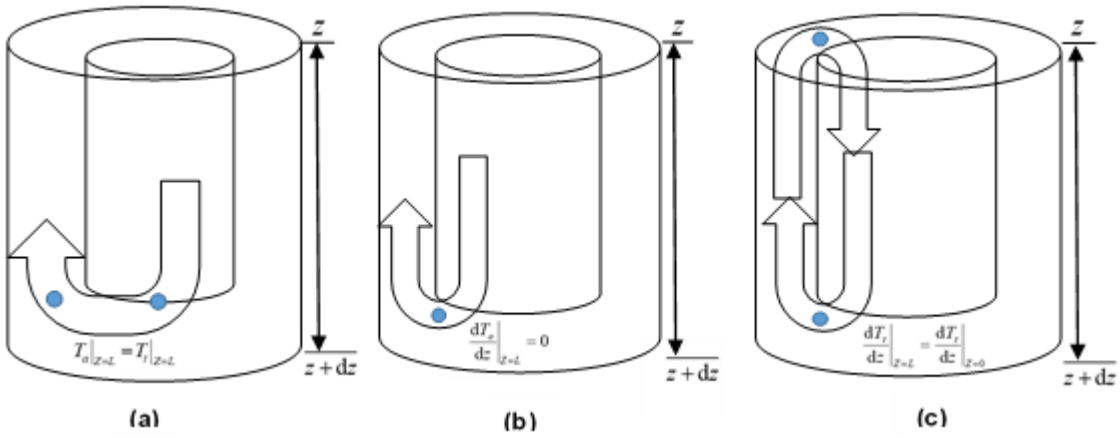


Figure 1. Depiction of three boundary conditions: (a) Model-1, (b) Model-2, and (c) Model-3.

Physically, when the drilling or circulating fluid leaves the tubing or drill-pipe and enters into the annular space no change in temperature should occur, as Fig. 1b depicts.

Therefore, this flow condition justifies the notion that the annular fluid temperature at well bottom remains stable. In Model-3, we presuppose that during the steady-state fluid

circulation, these conditions prevail for both at the wellhead and well bottom; that is, $dT_t/dz|_{z=0} = dT_t/dz|_{z=L} = 0$. Figure 1c portrays the physical representation of this boundary condition.

Two studies from the literature aided verification of the models presented here. They include the steady-state heat-transfer model of Holmes and Swift (1970), and both steady-state heat-transfer model for conduits and the transient conduction of thermal energy within the formation, as given in Kabir et al. (1996).

## 2.1. FORWARD CIRCULATION MODEL

Kabir et al. (1996) presented an analytical model for estimating the fluid temperature in the drillpipe and annulus as a function of well depth and circulating time for both flowing fluids in forward and reverse circulation as Figure 2 shows. This model is based on energy balance between the formation and annulus, and the annulus to the drillpipe. Computations of the temperature profile presuppose steady-state heat flow in the wellbore, and transient heat conduction in the formation. The maximum temperature occurs in the annulus at a depth above the bottomhole location.

As shown in Appendix A, we modified the boundary conditions of the Kabir et al. (1996) model to obtain two new solutions for the tubing or drill-pipe temperature as given by the following expression:

$$T_t = \gamma e^{\xi_1 Z} + \delta e^{\xi_2 Z} + g_G Z - B g_G + T_{es} \tag{1}$$

and for the annular temperature can be written as

$$T_a = (1+\xi_1 B)\gamma e^{\xi_1 Z} + (1+\xi_2 B)\delta e^{\xi_2 Z} + g_G Z + T_{es} \tag{2}$$

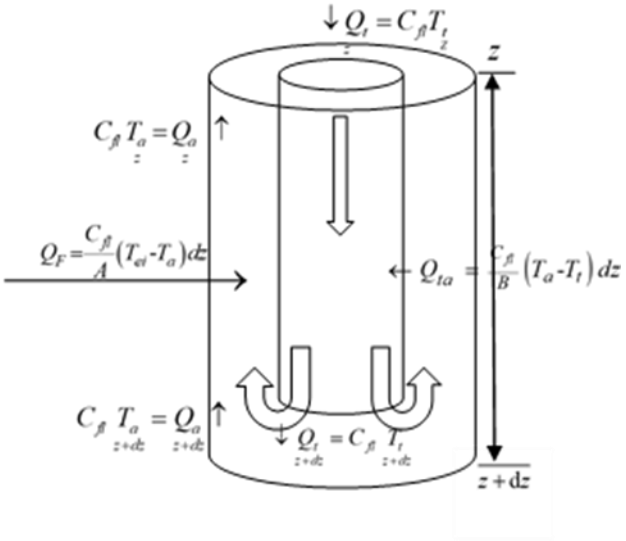


Figure 2. Differential element of heat balance in forward circulation.

where $T_t$ represents the tubing temperature, $T_a$ the annular temperature, the geothermal gradient expressed by $g_G$ in ˚F/ft, and $Z$ refers to vertical depth. The constants, $\xi_1$ and $\xi_2$ depend on thermal properties, while $\gamma$ and $\delta$ depend on the boundary conditions. By adopting the inlet drill-pipe temperature as a solution reference, using the Dirichlet condition, the constants $\gamma$ and $\delta$ for Model-1 can be written as

$$\gamma = \frac{\left[\left(T_{ti} + Bg_G - T_{es}\right)\xi_2 e^{\xi_2 L} + g_G\right]}{\left[\xi_2 e^{\xi_2 L} - \xi_1 e^{\xi_1 L}\right]} \tag{3}$$

$$\delta = T_{ti} + Bg_G - T_{es} - \gamma \tag{4}$$

or

$$\delta = \frac{\left[\left(T_{ti} + Bg_G - T_{es}\right)\xi_1 e^{\xi_1 L} + g_G\right]}{\left[\xi_1 e^{\xi_1 L} - \xi_2 e^{\xi_2 L}\right]} \tag{5}$$

Application of the Neumann condition for Model-2 results in the following constants:

$$\delta = T_{ti} + Bg_G - T_{es} - \gamma \tag{6}$$

$$\gamma = \frac{\left[\left(T_{ti} + Bg_G - T_{es}\right)\xi_2\left(1+\xi_2 B\right)e^{\xi_2 L} + g_G\right]}{\left[\xi_2 e^{\xi_2 L}\left(1+\xi_2 B\right) - \xi_1 e^{\xi_1 L}\left(1+\xi_1 B\right)\right]} \tag{7}$$

Similary, application of the Robin condition for Model-3 provides the following constants:

$$\delta = T_{ti} + Bg_G - T_{es} - \gamma \tag{8}$$

$$\gamma = \frac{\left[\left(T_{ti} + Bg_G - T_{es}\right)\left(\xi_2 e^{\xi_2 L} - \xi_2\right)\right]}{\left[\xi_1 - \xi_1 e^{\xi_1 L} - \xi_2 + \xi_2 e^{\xi_2 L}\right]} \tag{9}$$

## 2.2. REVERSE CIRCULATION MODEL

The application of energy balance, in this case, has the similar form of the forward circulation case with different thermal and boundary constants. With details appearing in Appendix B, the final solution of the drill-pipe temperature can be written as

$$T_t = \alpha e^{\lambda_1 Z} + \beta e^{\lambda_2 Z} + g_G Z + T_{es} + Bg_G \tag{10}$$

and for the annular temperature is given by

$$T_a = \left(1-\lambda_1 B\right)\alpha e^{\lambda_1 Z} + \left(1-\lambda_2 B\right)\beta e^{\lambda_2 Z} + g_G Z + T_{es} \tag{11}$$

Following the solution principles used for forward circulation, and by using the annular temperature as a solution reference, the final mathematical form for the integration constants for the Model-1 boundary conditions are given as

$$\beta = \frac{T_{as} - T_{es} - \left(1-\lambda_1 B\right)\alpha}{\left(1-\lambda_2 B\right)} \tag{12}$$

$$\alpha = \frac{\left[\left(T_{as} - T_{es}\right)\lambda_2 e^{\lambda_2 L} + \left(1-\lambda_2 B\right)g_G\right]}{\left[\left(1-\lambda_1 B\right)\lambda_2 e^{\lambda_2 L} - \left(1-\lambda_2 B\right)\lambda_1 e^{\lambda_1 L}\right]} \tag{13}$$

Similarly, the constants for the application of the Model-2 boundary conditions result in the following constants:

$$\beta = \frac{T_{as} - T_{es} - (1 - \lambda_1 B)\alpha}{(1 - \lambda_2 B)} \tag{14}$$

$$\alpha = \frac{\left[ (T_{as} - T_{es})\lambda_2 e^{\lambda_2 L} + g_G \right]}{\left[ (1 - \lambda_1 B)(\lambda_2 e^{\lambda_2 L} - \lambda_1 e^{\lambda_1 L}) \right]} \tag{15}$$

For Model-3 boundary conditions, we obtained the following expressions:

$$\beta = \frac{T_{as} - T_{es} - (1 - \lambda_1 B)\alpha}{(1 - \lambda_2 B)} \tag{16}$$

$$\alpha = \frac{\left[ (T_{as} - T_{es})(\lambda_2 - \lambda_2 e^{\lambda_2 L}) \right]}{(1 - \lambda_1 B)(\lambda_1 e^{\lambda_1 L} - \lambda_1 + \lambda_2 - \lambda_2 e^{\lambda_2 L})} \tag{17}$$

## 2.3. CALCULATION OF THE OVERALL-HEAT-TRANSFER COEFFICIENT

Holmes and Swift (1970) assumed a constant value for the overall-heat-transfer coefficient across the wellbore face U, and across the drill-pipe hp. Moreover, they showed the impact of changing the overall heat-transfer coefficient across the drill-pipe and annular temperature. By applying a simple mathematical expression to calculate hp as in Ramey (1962), Edwardson et al. (1962), Willhite (1967), and Hasan and Kabir (1994), we can represent the overall-heat-transfer coefficient across the drill-pipe hp or across the casing Ut as follows:

$$U_t \text{ or } h_p = \left[ \frac{r_a}{r_{pi} h_f} + \frac{r_a \ln(r_{po}/r_{pi})}{k_{dp}} + \frac{1}{h_f} \right]^{-1} \tag{18}$$

where $r_a$ is the average of the wellbore diameter and outer diameter of the drill-pipe is in ft. The thermal conductivity of the drill-pipe is given by $k_{dp}$ in Btu/ft-hr-˚F and $h_f$ refers to convective heat-transfer coefficient of the circulating fluid in Btu/ft$^2$-hr-˚F.

Kabir et al. (1996) presented an analytical model for estimating the fluid temperature in the drillpipe and annulus as a function of well depth and circulating time for both flowing fluids in forward and reverse circulation as Figure 2 shows. This model is based on energy balance between the formation and annulus, and the annulus to the drillpipe. Computations of the temperature profile presuppose steady-state heat flow in the wellbore, and transient heat conduction in the formation. The maximum temperature occurs in the annulus at a depth above the bottomhole location.

## 3.VERIFICATION OF MODELS

To verify our models, we adopted the data set used by Holmes and Swift (1970) as shown in Table 1. Applications of both the Holmes and Swift (1970) model and Kabir et al. (1996) model (designated as Model-1) form the foundation for verification of the possible applications of the new models presented in this study; that is, Model-2 and Model-3. Figure 3 compares the Model-1 temperature profiles of the conduit and the annular temperature for Kabir et al. (1996) with that of the Holmes and Swift (1970) study. The difference in temperature profiles due to incorporating the transient conduction of thermal energy within the formation represented by 44 hr to calculate the $T_D$.

The application of Model-2 and Model-3 will result in different temperature profiles due to changes in the BC's. The annular temperature is higher due to the heat gain from the formation than the drill-pipe temperature profile for the forward circulation, while the opposite is true for the reverse circulation case.

Table 1. Well and mud dataset from HOLMES and SWIFT (1970).

| | |
|---|---|
| Well depth, ft. | 15,000 |
| Drill stem OD, in. | 6 5/8 |
| Drill bit size, in. | 8 3/8 |
| Circulation rate, bbl/hr. | 300 |
| Inlet mud temperature, °F. | 75 |
| Mud viscosity, $lb_m$/(ft-hr). | 110 |
| Mud thermal conductivity, Btu/(ft-°F-hour). | 1 |
| Mud specific heat, Btu/($lb_m$-°F). | 0.4 |
| Mud density, $lb_m$/gal. | 10 |
| Formation thermal conductivity, Btu/(ft-°F-hr) | 1.3 |
| Formation specific heat, Btu/($lb_m$-°F). | 0.2 |
| Formation density, $lb_m$/ $ft^3$. | 165 |
| Surface earth temperature, °F. | 59.5 |
| Geothermal gradient, °F/ft. | 0.0127 |

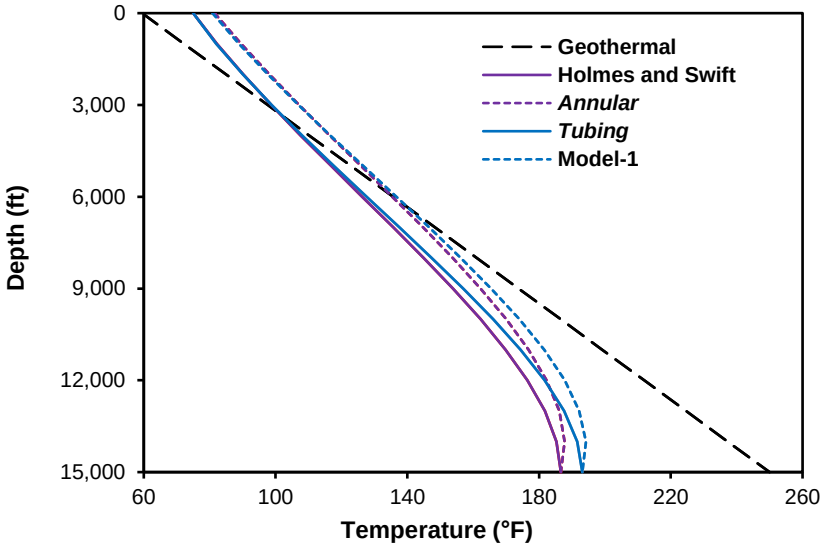


Figure 3. Model-1 performance compared with the Holmes and Swift model.

Figure 4 compares the results of all three models for the forward and reverse-circulation cases. Figures 3 and 4 suggest that the behavior of the temperature profiles change for Model-2 and -3.

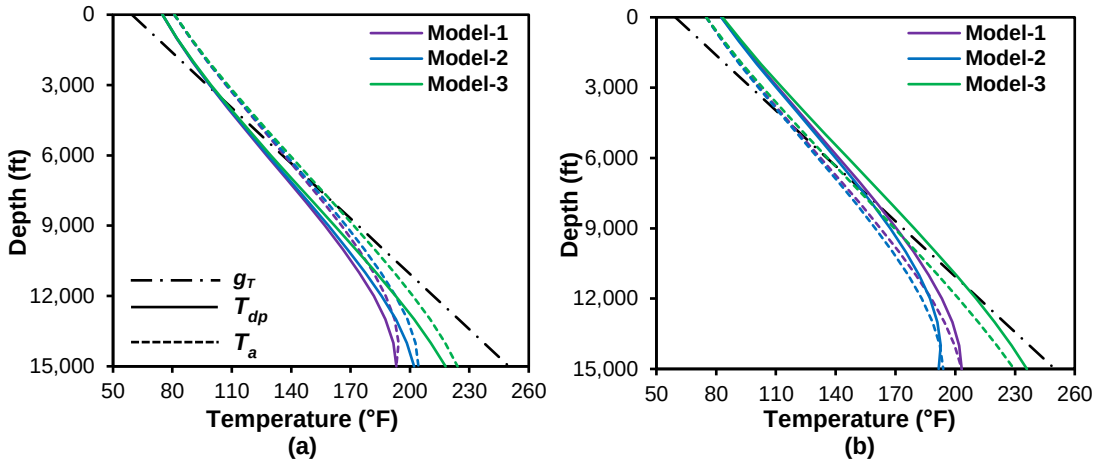


Figure 4. Result of all models: forward circulation (a), reverse circulation (b).

For forward circulation, Holmes and Swift (1970) observed that the maximum mud temperature occurs in the annulus at a depth above the bottom, as well as by Tragesser et al. (1967) and others. In contrast, the maximum annular temperature occurred at the well bottom in Model-2 and Model-3. The difference in drill-pipe temperature is about (9.54 ˚F) and (11.71 ˚F) in the annulus between Model-2 and Model-1. Furthermore, Model-3 and Model-1 suggest 30.13 ˚F and 37.01 ˚F for both the drill-pipe and annulus, respectively. All three models behave in the same way from the surface down to 3,000 ft, and then the signature starts to change all the way to the total depth.

## 4.MODEL VALIDATION WITH FIELD DATA

This section explores three cases wherein field data are available, although the heat-transfer parameters may be incomplete. These cases include that during the drilling operation, in post-cement job operation, and in a gas hydrate formation.

### 4.1. CASE-1

In deep wells, most of the temperature measurement occurs before or after the cementing operation. The differences in wellbore radius for each drilled segment or casing size may influence the temperature measurements or its distribution in the wellbore. Furthermore, the amount of overall heat-transfer coefficient from the adjacent formation to the annulus and then goes inside the drill-pipe change from one section to another as the circulating mud passes through each section. Davies et al. (1994) reported two downhole temperature measurement cases for offshore wells.

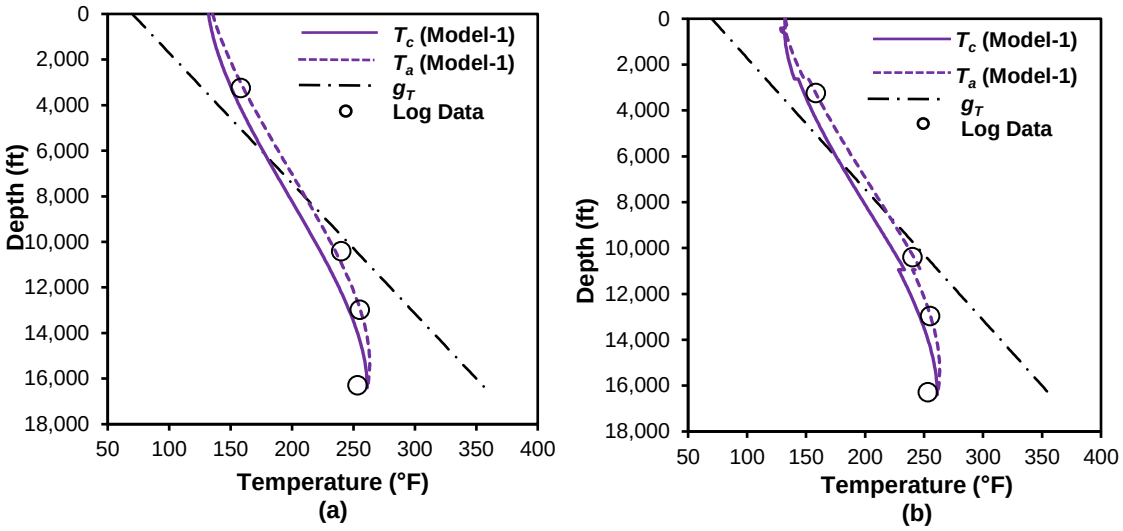


Figure 5. Model-1 reproduces temperature profile of Davies at al. (a), shows influence of wellbore radius on temperature (b).

Figure 5a represents their Case-2 data for the post-cement job situation and reasonable agreement with Model-1. Figure 5b shows the same information but with the influence of the well radius in two sections. The distribution of temperature profile for either the drill-pipe or the casing may change significantly depending on calculations of the overall heat-transfer coefficient across the tubulars.

According to Eq. 18, the temperature profiles may increase or decrease depending on the fluid's overall heat-transfer coefficient $h_f$ and other thermal parameters. The calculation of the overall-heat-transfer coefficient from the formation to annulus change for each section depending on the number of casing installed, previously placed cement, and the convective heat-transfer coefficient of the circulating fluid.

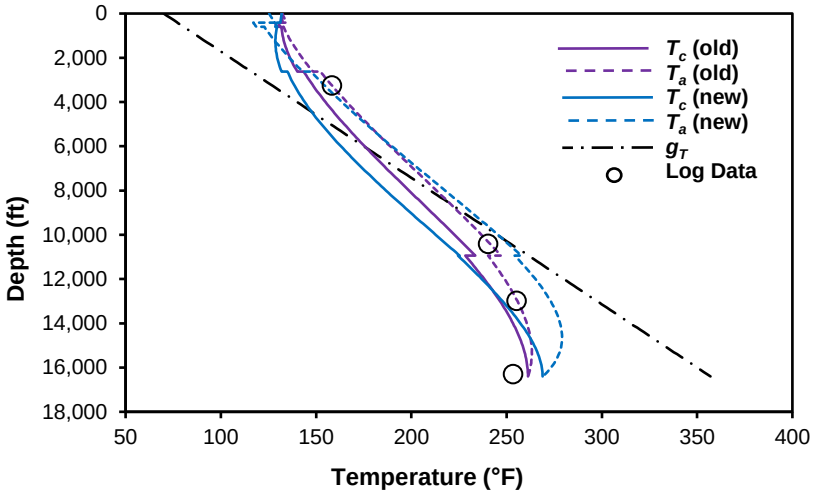


Figure 6. Performance of Model-1, before and after calculating $U_a$, and $U_t$.

Note that the overall-heat-transfer coefficient from the annulus to the drill-pipe depends only on the tubular metal and $h_f$. At the well bottom, an increase of 7 °F in temperature profiles may be obtained if we assume the convective heat-transfer coefficient of the circulating fluid $h_f$ to be 20 Btu/(ft$^2$-hr-$^o$F) to calculate the overall-heat-transfer coefficient across the annulus and the casing for Model-1, as shown in Figure 6. Therefore, an accurate measurement of thermal properties of the tool and fluid ensure confidence in solutions. Also, when we assume an overall-heat-transfer coefficient across the wellbore face and across the drill-pipe to be equal, the behavior of the annular and drill-pipe temperature will change.

### 4.2. CASE-2

Holmes and Swift (1970) calculated the bottomhole temperature for various drilling segments by incorporating his model with the line-source solution after the cessation of mud circulation for the change in bit size occurred during the drilling operation. They showed good agreement between their method and the log measurements. But, the calculation procedure needs inclusion of other parameters, such as the thermal properties of the casing and cement. Figure 7 shows that Model-3 reproduces the field measurements rather well. Note that at the well bottom, the derivative of tubular temperature with respect to depth equals the derivative of the annular temperature with respect to depth; that is, $dT_{dp}/dz = dT_a/dz$, when $Z=L$, as shown in Figure 7.

### 4.3. CASE-3

Guo et al. (2016) presented an analytical model to calculate the temperature inside drill-pipe and the annulus by incorporating the effect of gas-hydrate cuttings entrained in the annulus and the Joule-Thompson (J-T) cooling effect. The J-T effect was used as the second boundary condition to find a solution for the mathematical model, and it was represented as the difference between the annulus and the drill-pipe temperature, which was assumed to be zero. Consequently, the Guo et al. model reverts back to Model-1. This model was applied on well NGHP-01-17A, which was one of the wells in the Andaman Islands. Figure 8a presents the result of Guo et al. (2016). Drilling data for this well indicate two zones of gas hydrate at intervals of 1,794 to 1,870 ft and 1,922 to 1,975 ft below the seafloor. The geothermal temperature of the hydrate-bearing layer is about 51 °F. Moreover, from the data used in this

model, the physical and thermal properties of gas hydrate differ from the drilling mud and formation.

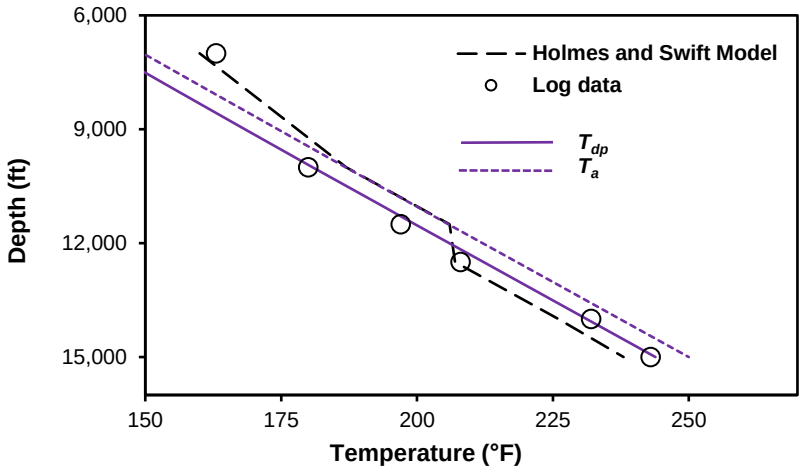


Figure 7. Both Model-3 and the Holmes and Swift model show agreement with field data.

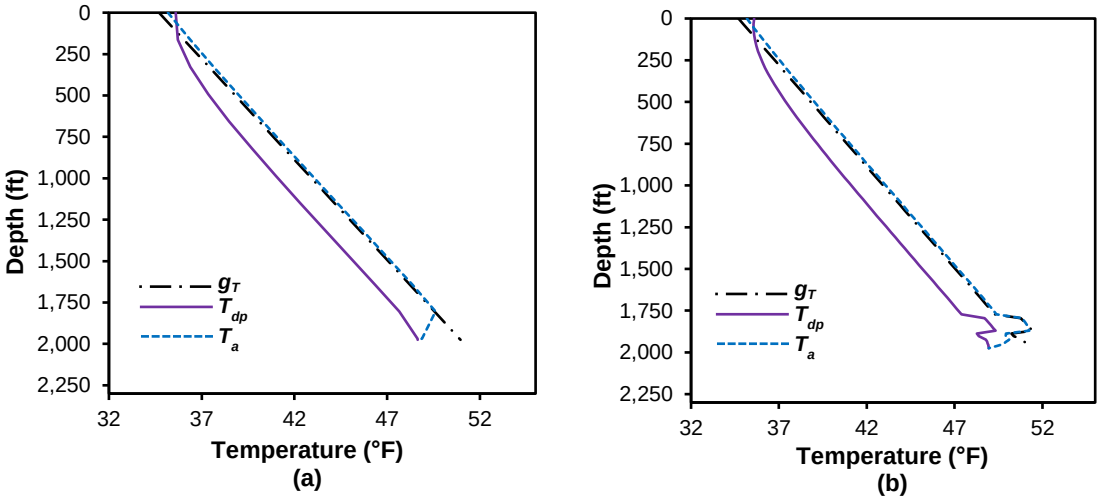


Figure 8. Performance of Guo at el. (2016) approach (a), Model-1 including gas hydrate intervals (b).

Moreover, as figure. 8b shows, we estimated the average mean of the geothermal gradient for each interval: gT1= 0.00896 °F/ft for the first and gT2 = 0.00841 °F/ft for the second

interval. While both figures in figure. 7 reflect the temperature profiles generated by Model-1, the temperature will increase when either Model-2 or Model-3 is enacted. To incorporate the gas hydrate properties for the two indicated zones, we needed to estimate the geothermal gradient caused by the gas hydrate zone.

## 5. APPLICATION OF MODELS

This section explores applications of the proposed models in diverse settings, from uncertain geothermal gradient setting to salt domes to change in the geothermal gradient due to encountering a change in formation's geologic age. The underlying thought is to keep an open mind about the absolute validity of a given model in possible diverse situations.

### 5.1. UNCERTAINTY IN GEOTHERMAL GRADIENT & HEAT-TRANSFER PARAMETERS

We tried to apply the sensitivity analysis by changing the absolute value of a geothermal gradient. Let us illustrate this point with all three models for the Case-2 data of Davies et al. (1994) discussed earlier. We assumed the geothermal gradient to be 0.0175 °F/ft with ± 0.25% uncertainty. As Figure 9a shows, merely increasing the geothermal gradient by 0.25%, Model-2 responds more favorably than Model-1, unlike that shown earlier in Figure 5. By calculating the overall heat-transfer coefficient from formation to annulus and then from the annulus to the tubular for each drilled section, the temperature profile will change, as Figure 10 shows.

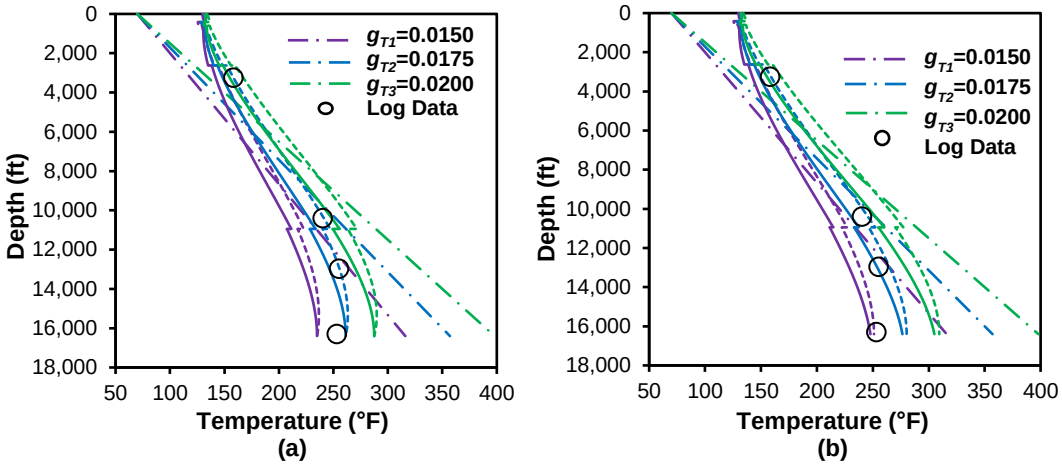


Figure 9. Uncertainty in geothermal gradient, Model-1 (a), Model-2 (b).

Calculating the overall-heat-transfer coefficient has a significant effect on the drill-pipe or casing and the annular temperature profile. In case we have constant values of $U_a$, and $U_t$, the tubular and annular temperature will have the same trend, while it increases for the annular temperature but decreases in the drill-pipe or casing temperature in case of calculating $U_a$ and $U_t$ for each well section. However, increasing or decreasing the geothermal gradient by (0.25%) will cover all possible range of temperature measurement.

## 5.2. PRESENCE OF GAS-HYDRATE INTERVAL

For the Case-2 data set of Davies et al. (1994), let us assume a gas hydrate interval of 6,000 to 6,500 ft, with a density of 56.18 $lb_m/ft^3$, the thermal conductivity of 0.347 Btu/ft-hr-˚F, and heat capacity of 0.5015 $Btu/lb_m$-˚F. These parameters are taken from those suggested by Gao et al. (2017). Usually, the gas hydrate zone temperature is higher than the normal formation; therefore, the new geothermal gradient should exist for this interval. Figure 11 presents the results of three models.

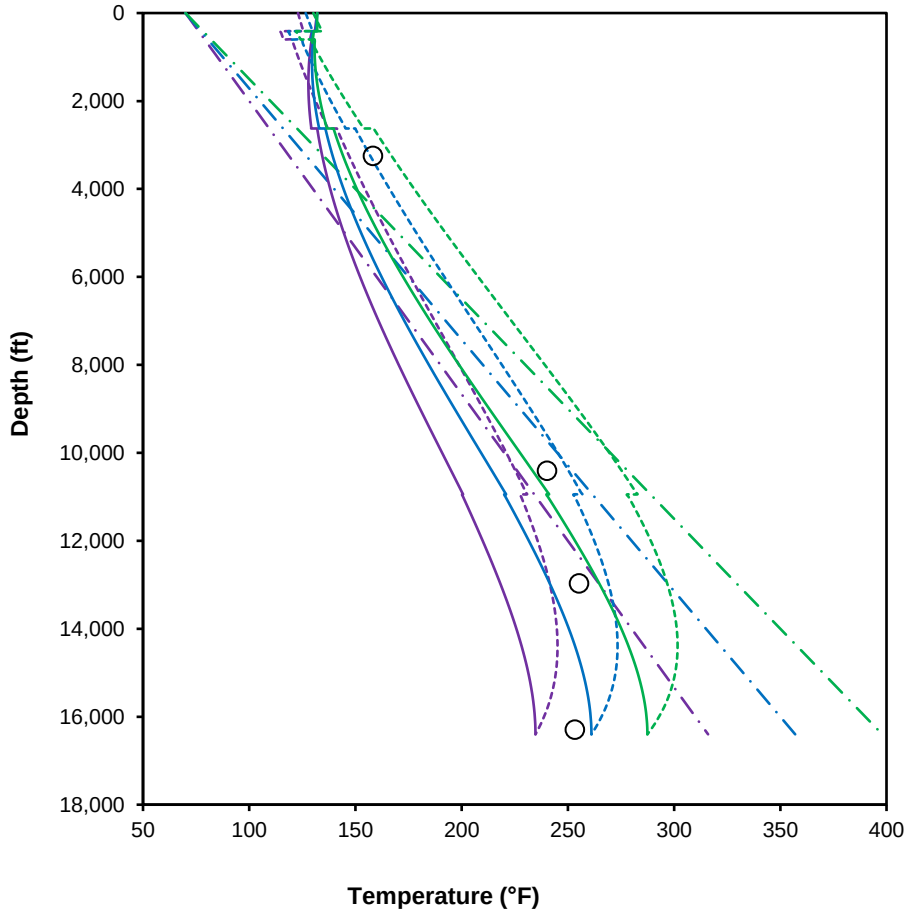


Figure 10. Uncertainty in geothermal gradient for Model-1, calculating of $U_a$, *Ut* case.

## 5.3. PRESENCE OF A SALT-DOME INTERVAL

We assumed a salt dome interval from 12,500 to 13,500 ft. Salt has a thermal conductivity two to three times greater than that of typical sedimentary rocks (Yu at el. 1992). The properties of the salt dome involve density of 129.6 $lb_m/ft^3$, a thermal conductivity of 3.758 Btu/ft-hr-˚F, and heat capacity of 0.2078 $Btu/lb_m$-˚F, and formation temperature of 300 ˚F. The salt dome geothermal gradient was calculated as 0.01604 ˚F/ft. Based on these input parameters, Figure 12 shows the results all three models.

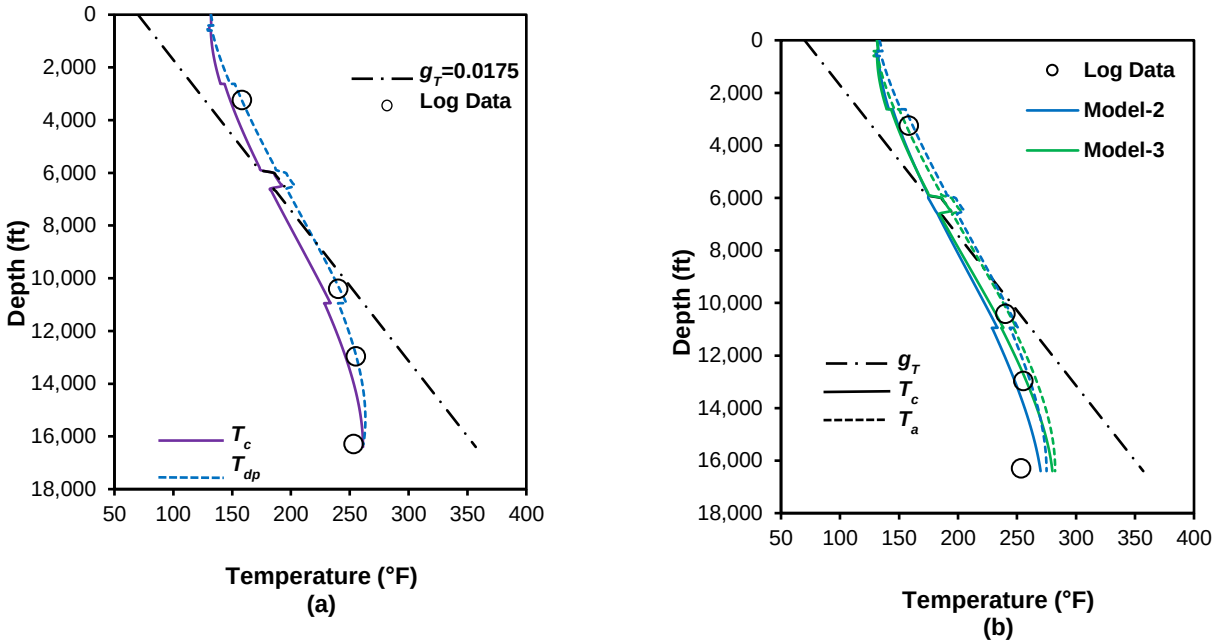


Figure 11. Gas hydrate case, Model-1 (a), Model-2 and Model-3 (b).

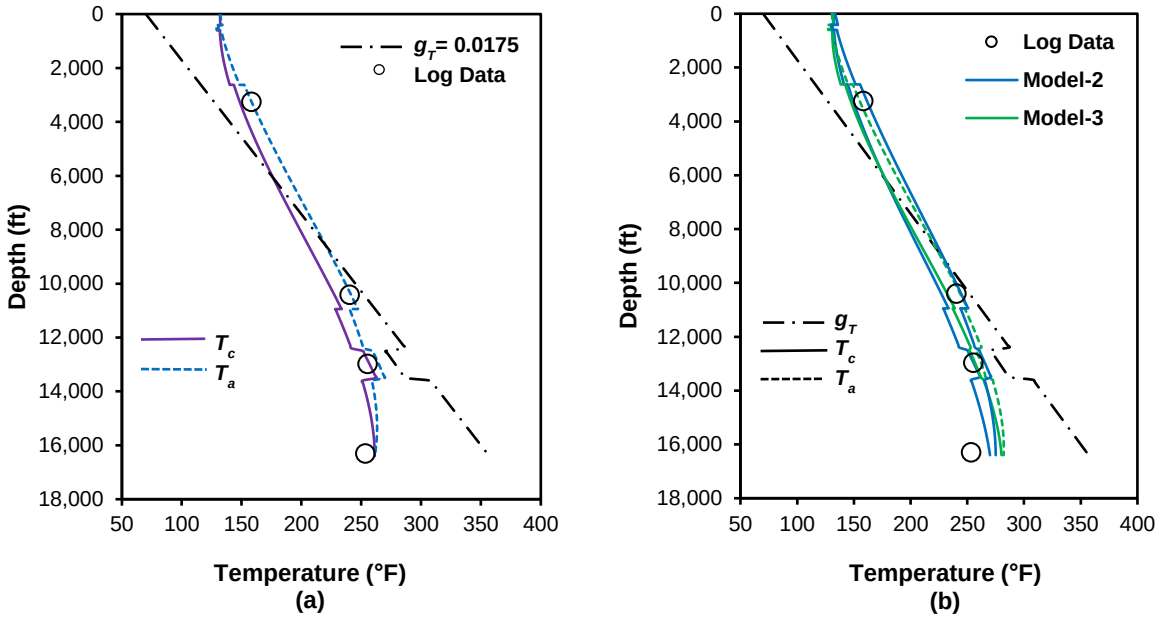


Figure 12. Salt-dome case, Model-1 (a), Model-2 and Model-3 (b).

## 5.4. CHANGE IN GEOTHERMAL GRADIENT

The geothermal gradient ($g_T$) can change due to the change in stratigraphic boundary containing different sediments, as shown recently for a deepwater well by Kabir et al. (2014), wherein that bed boundary involves the Jurassic/Triassic interface. Here, we enacted that change at the interval of 10,945 to 16,400 ft. Increasing or decreasing the $g_T$ will affect both drill-pipe and annular temperature profiles. The main $g_T$ for all models equal to 0.0175 °F/ft. Figure 13 represents the results of decreasing the $g_T$ by 0.001 °F/ft for Model-1. Increase in temperature profiles occurs when Model-2 and Model-3 are enacted.

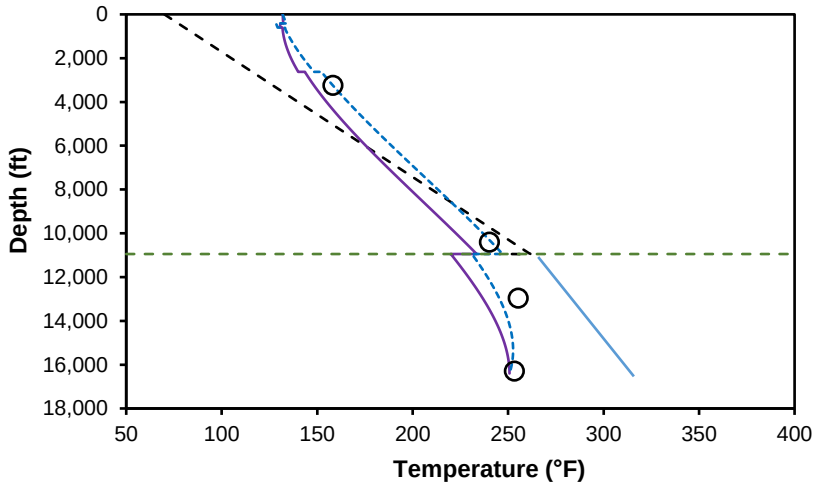


Figure 13. Performance of Model-1 for the change in geothermal gradient.

Table 2. Results of increased geothermal gradient.

| Model | $T_c$ at BTM, °F | $T_a$ at BTM, °F | $T_a$ at surface, °F |
|---|---|---|---|
| Model-1, single values of $U_a$, $U_t$. | 271.7 | 271.7 | 131.9 |
| Model-1, various values of $U_a$, $U_t$. | 271.6 | 271.6 | 126.5 |
| Model-2, single values of $U_a$, $U_t$. | 287.8 | 291.8 | 132 |
| Model-2, various values of $U_a$, $U_t$. | 296.9 | 319.2 | 126.7 |
| Model-3, various values of $U_a$, $U_t$. | 289.8 | 294.3 | 131.9 |
| Model-3, various values of $U_a$, $U_t$. | 270.3 | 269.3 | 126.5 |

# 6. DISCUSSION

The paper's central purpose was to present two new analytical models to extend the window of possible temperature profiles in wellbore fluid circulation. Given the paucity of field data in the open literature, verification of the new models became a daunting task. Our ardent hope is that the relative performance of all three models will shed some light on the viability of the proposed models.

We note that in Model-1, which has found widespread use over decades, we presuppose that the temperature at the well bottom, both in the annulus and the drill-pipe remains the same. This assumption holds well for a stable circulation rate. However, this BC does not appear reasonable for variable and high circulation rates. This reality prompted us to pursue two other BC's, such as those used for Models 2 and 3. Recent advances in the improved understanding of the physical aspects of drilling suggest that increased downhole wellbore temperature profiles are entirely feasible in forward-circulation cases. For instance, inclusion of frictional energy due to pressure losses or the contact area between the drill tool and the formation itself, as shown by Kumar and Samuel (2013), and the torque and drag forces originating from the drill string rotation as discussed by Mirhaj et al. (2016) are cases in point.

We attempt to validate the new models with the limited old data. Given the ability of all three models to handle changes in the geothermal gradient due to the characteristics of the sediments, salt domes, and gas hydrates, we explored the flexibility of their performances, wherein significant heat transfer occurs. The holistic approach pursued here provided the necessary insights into various temperature profiles in a given situation. This lesson prompted

us to explore items, such as uncertainty in geothermal gradient and its attendant consequence on its performance, abrupt changes in geothermal gradient arising from both the salt-dome and gas-hydrate intervals, and the shift in geothermal gradient itself stemming from the difference in sediments.

## 7. CONCLUSIONS

The following conclusions appear pertinent here:

1. This paper presents two new analytical solutions of the energy-balance equation for the fluid temperature during its circulation in the wellbore. The results of the proposed models suggest an increase in temperature profiles compared to the traditional Model-1. The increased temperature profiles may originate from the frictional energy and the rotational torque and drag forces.
2. These models can handle changes in wellbore diameter, geothermal gradient, and thermal properties throughout the wellbore in both forward and reverse circulation cases. Some of the field data tend to support the possible applications of the proposed models.
3. The results of Model-2 and -3 suggest that the maximum temperature occurs at the well bottom, in contrast to Model-1. In some cases, increasing or decreasing the geothermal gradient by 0.25% may cover all possible ranges of temperature measurements.

## NOMENCLATURE

$A$ = parameter defined by Eq. A-9, ft

$B$ = parameter defined by Eq. A-12, ft

$C_{fl}$ = heat capacity of mud, Btu/ $lb_m$-$^oF$

$g_G$ , $g_T$ = geothermal gradient, $^oF$ /ft

$k_e$ = conductivity of earth, Btu/hr-ft-$^oF$

$L$ = total depth, ft

$Q$ = heat flow from wellbore to the annulus, Btu/ $lb_m$

$Q_a$ = convection heat flow in annulus, Btu/ $lb_m$

$Q_F$ = heat flow from formation to annulus, Btu/ $lb_m$

$Q_t$ = convection heat flow in drill-pipe, Btu/ $lb_m$

$Q_{ta}$ = heat flow from annulus to drill-pipe fluid, Btu/ $lb_m$

$r_e$ , $r_w$ = wellbore radius, ft

$r_t$ = radius of drill-pipe, ft

$t$ = circulation time, hr

$T_a$ = mud temperature in annulus, $^oF$

$T_{as}$ = surface temperature of annular fluid, $^oF$

$t_D$ = dimensionless circulation time, $\alpha^* t/r_w^2$

$T_D$ = dimensionless temperature, define in Eqs. A-4 and 5

$T_{ei}$ = initial earth temperature, $^oF$

$T_{es}$ = surface temperature of earth, $^oF$

$T_t$, $T_{dp}$ = temperature of tubing or drill-pipe fluid, $^oF$

$T_{wb}$ = temperature at wellbore/formation interface, $^oF$

$T_c$ = temperature of casing fluid, $^oF$

$U$, $U_a$ = overall heat transfer coefficient across wellbore face, Btu/$ft^2$-$^oF$-hr

$U_t$ , $h_p$ = overall heat transfer coefficient across drill-pipe, Btu/$ft^2$-$^oF$-hr

$w$ = mass flow rate, $lb_m/hr$

$z$ = any vertical well depth, ft

$\alpha^*$ = heat diffusivity of formation (= $k_e/ c_e \rho_e$), $ft^2/hr$

$\lambda_1$ = parameter defined by Eq. B-6, dimensionless

$\lambda_1$ = parameter defined by Eq. B-7, dimensionless

$\xi_1$ = parameter defined by Eq. A-19, dimensionless

$\xi_2$ = parameter defined by Eq. A-20, dimensionless

$\rho_e$ = formation density, $lb_m/ft^3$

## ACKNOWLEDGMENT

The first author (A.Q.A. Al-Saedi) gratefully acknowledges the financial support provided by the Higher Committee for Education Development in Iraq (HCED) in pursuit of his Ph.D. study.

# APPENDIX A

# FORWARD CIRCULATION

This model involves energy balance between the formation and annulus, and the annulus to the drillpipe as presented in Figure 2. Computations of the temperature profile presuppose steady-state heat flow in the wellbore and transient heat conduction in the formation as shown earlier by Kabir et al. (1996). The energy balance for the steady-state condition for the forward circulation in the annulus is given by

$$\underset{z+dz}{Q_a} - \underset{z}{Q_a} = Q_{ta} - Q_F \tag{A-1}$$

or

$$C_{fl}\left[\underset{z+dz}{T_a} - \underset{z}{T_a}\right] = Q_{ta} - Q_F \tag{A-2}$$

where $Q_F$ refer to the heat flow form the formation to the wellbore, which can be written as

$$Q_F = \frac{2\pi k_e}{wT_D}\left(T_{ei} - T_{wb}\right)\mathrm{d}z \tag{A-3}$$

$T_D$ in Eq. A-3 represents the dimensionless temperature, which is defined by Hasan and Kabir (1994) for the constant heat flux, cylindrical-source well as

$$T_D = \left(1.1281\sqrt{t_D}\right)\left(1 - 0.3\sqrt{t_D}\right) \qquad \text{if} \quad 10^{-10} \le t_D \le 1.5 \tag{A-4}$$

$$T_D = \left(0.4063 + 0.5\ln t_D\right)\left(1 + \frac{0.6}{t_D}\right) \qquad \text{if} \quad t_D > 1.5 \tag{A-5}$$

where

$$t_D = \frac{\alpha^* t}{r_w^2} \tag{A-6}$$

Then, the heat losses from the wellbore to the annulus can be calculated by the overall-heat-transfer coefficient of the annulus system as given by

$$Q = \frac{2\pi r_e U_a}{w}\left(T_{wb} - T_a\right)\mathrm{d}z \tag{A-7}$$

The amount of heat flow from formation to the wellbore is equal to the heat flow from wellbore to annulus; therefore, by eliminating $T_{wb}$ from Eqs. A-3 and A-7 we obtained the following expression:

$$Q_F = \frac{C_{ft}}{A}\left(T_{ei} - T_a\right)\mathrm{d}z \tag{A-8}$$

where

$$A = \frac{C_{ft} w}{2\pi}\left(\frac{\left[k_e + r_e U_a T_D\right]}{r_e U_a k_e}\right) \tag{A-9}$$

Then, $Q_{ta}$ represent the heat losses from the annulus to the drilling string as

$$Q_{ta} = \frac{2\pi r_t U_t}{w}\left(T_a - T_t\right)\mathrm{d}z \tag{A-10}$$

Eq. A-10 can be simplified as

$$Q_{ta} = \frac{C_{ft}}{B}\left(T_a - T_t\right)\mathrm{d}z \tag{A-11}$$

where

$$B = \frac{w C_{ft}}{2\pi r_t U_t} \tag{A-12}$$

Substituting Eqs. A-8 and A-11 into Eq. A-2 and simplifying, we obtained the following expressions for the annulus

$$A\frac{\mathrm{d}T_a}{\mathrm{d}z} = \frac{A}{B}\left(T_a - T_t\right) - \left(T_{ei} - T_a\right) \tag{A-13}$$

and for the drill-pipe

$$T_a = T_t + B\frac{\mathrm{d}T_t}{\mathrm{d}z} \tag{A-14}$$

Differentiating Eq. A-14 with respect to depth, we obtain

$$\frac{dT_a}{dz} = \frac{dT_t}{dz} + B\frac{d^2T_t}{dz^2} \tag{A-15}$$

Substituting Eqs. A-14 and A-15 into Eq. A-13 and simplifying, and considering $T_f = T_s + g_G.z$, we obtained the following expression:

$$AB\frac{d^2T_t}{dz^2} - B\frac{dT_t}{dz} - T_t + T_{es} + g_G.z = 0 \tag{A-16}$$

The solution of the second-order ordinary differential equation above is obtained by the summation of solution for homogenous (complementary) equation and the particular solution of the inhomogeneous equation. The result for the tubular temperature is given by

$$T_t = \gamma e^{\xi_1 Z} + \delta e^{\xi_2 Z} + g_G Z - Bg_G + T_{es} \tag{A-17}$$

Applying Eq. A-17 into Eq. A-14, we get a mathematical form for the annular temperature, which is given by

$$T_a = (1 + \xi_1 B)\gamma e^{\xi_1 Z} + (1 + \xi_2 B)\delta e^{\xi_2 Z} + g_G Z + T_{es} \tag{A-18}$$

where

$$\xi_1 = \frac{\left[1 + \sqrt{1 + \left(\frac{4A}{B}\right)}\right]}{2A} \tag{A-19}$$

$$\xi_2 = \frac{\left[1 - \sqrt{1 + \left(\frac{4A}{B}\right)}\right]}{2A} \tag{A-20}$$

The constants $\gamma$ and $\delta$ of Eqs. A-17 and A-18 can be found by applying the proper boundary conditions. For the forward circulation in a vertical wellbore, BC's can be applied at two points; that is, at surface and bottomhole. Note that in forward circulation, all final solutions for all models depend on the tubular or drill-pipe temperature, while in reverse circulation the annular temperature is the key to our solutions. We note that the heat exchange

in all radial direction ends with the same mathematical formulation. The heat flow direction can occur from the tubular to the annular space and then to the formation and vice versa. The mathematical form of all models can be presented as follows:

## A.1. DIRICHLET BC OR MODEL-1

Both at surface and well bottom, the temperature of the annulus equal to that in the drill-pipe, which is given by

$$\text{At } Z = 0,\ T_t = T_{ti}, \text{and at Z} = L,\ T_t = T_a \tag{A-21}$$

Note that at total depth, the application of Eq. A-21 or $[(\mathrm{d}T_t/\mathrm{d}z)\big|_{Z=L} = 0]$ will give the same result due to Eq. A-14. Therefore, at surface depth, $T_t$=$T_{ti}$; hence, Eq. A-17 can be rewritten as

$$T_t = T_{ti} = \gamma e^{\xi_1 0} + \delta e^{\xi_2 0} + g_G 0 - Bg_G + T_{es}$$

$$\delta = T_{ti} + Bg_G - T_{es} - \gamma \tag{A-22}$$

and at the total depth or $Z$=$L$, $\left.\dfrac{\mathrm{d}T_t}{\mathrm{d}z}\right|_{Z=L} = 0$, $\left.\dfrac{\mathrm{d}T_t}{\mathrm{d}z}\right|_{Z=L} = 0 = \gamma\xi_1 e^{\xi_1 Z} + \delta\xi_2 e^{\xi_2 Z} + g_G$

$$\gamma\xi_1 e^{\xi_1 L} + \delta\xi_2 e^{\xi_2 L} + g_G = 0 \tag{A-23}$$

Substituting Eq. A-23 into Eq. A-22 and simplifying,

$$\gamma\xi_1 e^{\xi_1 L} + \left(T_{ti} + Bg_G - T_{es} - \gamma\right)\xi_2 e^{\xi_2 L} + g_G = 0$$

$$\gamma = \frac{-\left[\left(T_{ti} + Bg_G - T_{es}\right)\xi_2 e^{\xi_2 L} + g_G\right]}{\xi_1 e^{\xi_1 L} - \xi_2 e^{\xi_2 L}} \tag{A-24}$$

or

$$\gamma = \frac{\left[\left(T_{ti} + Bg_G - T_{es}\right)\xi_2 e^{\xi_2 L} + g_G\right]}{\left[\xi_2 e^{\xi_2 L} - \xi_1 e^{\xi_1 L}\right]} \tag{A-25}$$

and Eq. A-22 can be rewrite as

$$\delta = \frac{\left(T_{ti} + Bg_G - T_{es}\right)\xi_1 e^{\xi_1 L} + g_G}{\xi_1 e^{\xi_1 L} - \xi_2 e^{\xi_2 L}} \tag{A-26}$$

## A.2. NEUMANN BC'S OR MODEL-2

When $Z$=0, the tubular and the inlet tubular temperature are equal. At the well bottom, the derivative of the annular temperature with respect to depth equals to zero; that is,

$$\text{At Z} = 0,\ T_t = T_{ti}, \text{and at Z} = L,\ \left.\frac{\mathrm{d}T_a}{\mathrm{dz}}\right|_{Z=L} = 0 \tag{A-27}$$

Similar to Model-1, we can write

$$\delta = T_{ti} + Bg_G - T_{es} - \gamma \tag{A-28}$$

At the well bottom, Eq. A-18 becomes

$$\left.\frac{\mathrm{d}T_a}{\mathrm{dz}}\right|_{Z=L} = 0 = \left(1+\xi_1 B\right)\gamma\xi_1 e^{\xi_1 L} + \left(1+\xi_2 B\right)\delta\xi_2 e^{\xi_2 L} + g_G$$

$$\left(1+\xi_1 B\right)\gamma\xi_1 e^{\xi_1 L} + \left(1+\xi_2 B\right)\delta\xi_2 e^{\xi_2 L} + g_G = 0 \tag{A-29}$$

Using Eq. A-28 into Eq. A-29 and simplifying,

$$\gamma = \frac{\left[\left(T_{ti} + Bg_G - T_{es}\right)\xi_2\left(1+\xi_2 B\right)e^{\xi_2 L} + g_G\right]}{\left[\xi_2 e^{\xi_2 L}\left(1+\xi_2 B\right) - \xi_1 e^{\xi_1 L}\left(1+\xi_1 B\right)\right]} \tag{A-30}$$

## A.3. ROBIN BC'S OR MODEL-3

The tubular inlet temperature equal to the surface tubular temperature, and at bottom the derivative of tubular temperature with respect to the total depth equals the derivative of tubular temperature with respect to surface depth. That is,

$$\text{At Z} = 0,\ T_t = T_{ti}, \text{and at Z} = L,\ \left.\frac{\mathrm{d}T_t}{\mathrm{d}z}\right|_{Z=L} = \left.\frac{\mathrm{d}T_t}{\mathrm{d}z}\right|_{Z=0} \tag{A-31}$$

The application of first part of Eq. A-31 is given as

$$\delta = T_{ti} + Bg_G - T_{es} - \gamma \tag{A-32}$$

At total depth, or $Z=L$, we can write

$$\left.\frac{\mathrm{d}T_t}{\mathrm{d}z}\right|_{Z=0} = \left.\frac{\mathrm{d}T_t}{\mathrm{d}z}\right|_{Z=L}$$

$$\left.\frac{\mathrm{d}T_t}{\mathrm{d}z}\right|_{Z=0} = \xi_1\gamma + \xi_2\delta + g_G = \left.\frac{\mathrm{d}T_t}{\mathrm{d}z}\right|_{Z=L} = \xi_1\gamma e^{\xi_1 L} + \xi_2\delta e^{\xi_2 L} + g_G$$

$$\xi_1\gamma + \xi_2\delta = \xi_1\gamma e^{\xi_1 L} + \xi_2\delta e^{\xi_2 L} \tag{A-33}$$

Gathering Eq. A-32 with Eq. A-33 result in

$$\gamma = \frac{\left[\left(T_{ti} + Bg_G - T_{es}\right)\left(\xi_2 e^{\xi_2 L} - \xi_2\right)\right]}{\left[\xi_1 - \xi_1 e^{\xi_1 L} - \xi_2 + \xi_2 e^{\xi_2 L}\right]} \tag{A-34}$$

# APPENDIX B

# REVERSE CIRCULATION

Similar to the forward circulation, with the change in heat flow direction, the differential form of application of the energy balance for annulus given by

$$A\frac{\mathrm{d}T_a}{\mathrm{d}z}=\left(T_{ei}-T_a\right)-\frac{A}{B}\left(T_a-T_t\right) \tag{B-1}$$

and for tubular

$$T_a=T_t-B\frac{\mathrm{d}T_t}{\mathrm{d}z} \tag{B-2}$$

After diffrentiating Eq. B-2 and substituting in Eq. B-1, the ordinary diffrential equation is given by

$$AB\frac{\mathrm{d}^2T_t}{\mathrm{d}z^2}+B\frac{\mathrm{d}T_t}{\mathrm{d}z}-T_t+T_{es}+g_G.z=0 \tag{B-3}$$

Following the same logic of presentation in Appendix A, and by using the annular temperature as a solution reference, the final mathematical solutions for both the tubular and annular temperatures are given as

$$T_t=\alpha e^{\lambda_1 Z}+\beta e^{\lambda_2 Z}+g_G Z+T_{es}+Bg_G \tag{B-4}$$

$$T_a=\left(1-\lambda_1 B\right)\alpha e^{\lambda_1 Z}+\left(1-\lambda_2 B\right)\beta e^{\lambda_2 Z}+g_G Z+T_{es} \tag{B-5}$$

where the thermal properties constants *A*, *B*, $T_D$ are the same as in Appendix A.

The exponent coefficients $\lambda_1$ and $\lambda_2$ are given as

$$\lambda_1=\frac{\left[-1+\sqrt{1+\left(\frac{4A}{B}\right)}\right]}{2A} \tag{B-6}$$

and

$$\lambda_2=\frac{\left[-1-\sqrt{1+\left(\frac{4A}{B}\right)}\right]}{2A} \tag{B-7}$$

The solution constants $\alpha$ and $\beta$ can be found by applications of Model-1, Model-2, and Model-3.

## B.1. MODEL-1

At the position Z=0, $T_a = T_{as}$

$$T_a = T_{as} = \left(1-\lambda_1 B\right)\alpha e^{\lambda_1 0} + \left(1-\lambda_2 B\right)\beta e^{\lambda_2 0} + g_G 0 + T_{es}$$

$$\beta = \frac{T_{as} - T_{es} - \left(1-\lambda_1 B\right)\alpha}{\left(1-\lambda_2 B\right)} \tag{B-8}$$

and when Z=L, $T_t = T_a$.

$$T_t\big|_{Z=L} = \alpha e^{\lambda_1 L} + \beta e^{\lambda_2 L} + g_G L + T_{es} + B g_G$$

$$T_a\big|_{Z=L} = \left(1-\lambda_1 B\right)\alpha e^{\lambda_1 L} + \left(1-\lambda_2 B\right)\beta e^{\lambda_2 L} + g_G L + T_{es}$$

$$\left(1-\lambda_1 B\right)\alpha e^{\lambda_1 L} + \left(1-\lambda_2 B\right)\beta e^{\lambda_2 L} + g_G L + T_{es} = \alpha e^{\lambda_1 L} + \beta e^{\lambda_2 L} + g_G L + T_{es} + B g_G$$

$$\lambda_1 \alpha e^{\lambda_1 L} B + \beta e^{\lambda_2 L} \lambda_2 B = -B g_G \tag{B-9}$$

Substituting Eq. B-8 into Eq. B-9 and simplifying,

$$\alpha = \frac{\left[\left(T_{as} - T_{es}\right)\lambda_2 e^{\lambda_2 L} + \left(1-\lambda_2 B\right) g_G\right]}{\left[\left(1-\lambda_1 B\right)\lambda_2 e^{\lambda_2 L} - \left(1-\lambda_2 B\right)\lambda_1 e^{\lambda_1 L}\right]} \tag{B-10}$$

The first part of the boundary condition apply for all Models, so Eq. B-8 used to find the other constant, which are given below.

## B.2. MODEL-2

Applying the second BC for Model-2 as $\left.\frac{\mathrm{d}T_a}{\mathrm{d}z}\right|_{Z=L} = 0$, we obtain

$$\left(1-\lambda_1 B\right)\alpha\lambda_1 e^{\lambda_1 L} + \left(1-\lambda_2 B\right)\beta\lambda_2 e^{\lambda_2 L} + g_G = 0$$

$$\left.\frac{\mathrm{d}T_a}{\mathrm{d}z}\right|_{Z=L} = 0 = \left(1-\lambda_1 B\right)\alpha\lambda_1 e^{\lambda_1 L} + \left(1-\lambda_2 B\right)\beta\lambda_2 e^{\lambda_2 L} + g_G \tag{B-11}$$

Combining Eq. B-8 with Eq. B-11 results in

$$\alpha = \frac{\left[\left(T_{as} - T_{es}\right)\lambda_2 e^{\lambda_2 L} + g_G\right]}{\left[\left(1-\lambda_1 B\right)\left(\lambda_2 e^{\lambda_2 L} - \lambda_1 e^{\lambda_1 L}\right)\right]} \tag{B-12}$$

## B.3. MODEL-3

At total depth, we have the boundary condition: $\left.\frac{\mathrm{d}T_a}{\mathrm{d}z}\right|_{Z=0} = \left.\frac{\mathrm{d}T_a}{\mathrm{d}z}\right|_{Z=L}$

Therefore, we can write

$$\left.\frac{\mathrm{d}T_a}{\mathrm{d}z}\right|_{Z=0} = \left(1-\lambda_1 B\right)\alpha\lambda_1 + \left(1-\lambda_2 B\right)\beta\lambda_2 + g_G,$$

$$\left.\frac{\mathrm{d}T_a}{\mathrm{d}z}\right|_{Z=L} = \left(1-\lambda_1 B\right)\alpha\lambda_1 e^{\lambda_1 L} + \left(1-\lambda_2 B\right)\beta\lambda_2 e^{\lambda_2 L} + g_G$$

$$\left(1-\lambda_1 B\right)\alpha\lambda_1 e^{\lambda_1 L} + \left(1-\lambda_2 B\right)\beta\lambda_2 e^{\lambda_2 L} = \left(1-\lambda_1 B\right)\alpha\lambda_1 + \left(1-\lambda_2 B\right)\beta\lambda_2 \tag{B-13}$$

Gathering Eq. B-8 with Eq. B-13 yields the following expression:

$$\alpha = \frac{\left[\left(T_{as} - T_{es}\right)\left(\lambda_2 - \lambda_2 e^{\lambda_2 L}\right)\right]}{\left(1-\lambda_1 B\right)\left(\lambda_1 e^{\lambda_1 L} - \lambda_1 + \lambda_2 - \lambda_2 e^{\lambda_2 L}\right)} \tag{B-14}$$

## REFERENCES


Beirute, R. (1991). A circulating and shut-in well-temperature-profile simulator. *J Pet Technol* 43 (9), 1140-1146. http://dx.doi.org/10.2118/17591-PA.

Davies, S., Gunningham, M., Bittleston, S. (1994). Field studies of circulating temperatures under cementing conditions. *SPE Drill & Compl* 9 (1), 12-16. http://dx.doi.org/10.2118/21973-PA.

Edwardson, M., Girner, H., Parkison, H. (1962). Calculation of formation temperature disturbances caused by mud circulation. *J Pet Technol* 14 (4), 416-426. http://dx.doi.org/10.2118/124-PA.

Gao, Y., Sun, B., Xu, B. (2017). A wellbore/formation-coupled heat-transfer model in deepwater drilling and its application in the prediction of hydrate-reservoir dissociation. *SPE J.* 22 (3), 756-766. http://dx.doi.org/10.2118/184398-PA.

Guo, B., Li, G., Shan, L. (2016). Mathematical model provides annular temperature profile for thermal hydraulics in drilling gas hydrates. Paper SPE-180560-MS presented at the IADC/SPE Asia Pacific *Drill Technol Conf*, Singapore, 22-24 August. http://dx.doi.org/10.2118/180560-MS.

Hasan, A., & Kabir, C. (1994). Aspects of wellbore heat transfer during two-phase flow (includes associated papers 30226 and 30970). *SPE Prod & Facil* 9 (03), 211-216. http://dx.doi.org/10.2118/22948-PA.

Hasan, A., Kabir, C., & Ameen, M. (1996). A fluid circulating temperature model for workover operations. *SPE J* 1 (02), 133-144. http://dx.doi.org/10.2118/27848-PA.

Holmes, C. S., & Swift, S. C. (1970). Calculation of circulating mud temperatures. *J Pet Technol* 22 (6), 670-674. http://dx.doi.org/10.2118/2318-PA.

Kabir, C. S., Yi, X., Jakymec, M., & Hasan, A. R. (2014). Interpreting distributed-temperature measurements in deepwater gas-well testing: estimation of static and dynamic thermal gradients, and flow rates. *SPE Prod & Oper* 29 (02), 097-104. https://doi.org/10.2118/166333-PA.

Kabir, C., Hasan, A., Kouba, G., & Ameen, M. (1996). Determining circulating fluid temperature in drilling, workover, and well control operations. *SPE Drill & Compl* 11 (02), 74-79. http://dx.doi.org/10.2118/24581-PA.

Keller, H., Couch, E., and Berry, P. (1973). Temperature distribution in circulating mud columns. *SPE J.* 13 (1), 23-30. http://dx.doi.org/10.2118/3605-PA.

Kumar, A. and Samuel, R. (2013). Analytical model to predict the effect of pipe friction on downhole fluid temperatures. *SPE Drill & Compl* 28 (3), 270-277. http://dx.doi.org/10.2118/165934-PA.

Li, B., Li, H., Guo, B., Cai, X. et al. (2017). A new numerical solution to predict the temperature profile of gas-hydrate-well drilling. *SPE J.* 22 (4), 1201-1212. http://dx.doi.org/10.2118/185177-PA.

Mirhaj, S. A., Kaarstad, E., & Aadnoy, B. S. (2016). Torque and Drag Modeling; Soft-string versus Stiff-string Models. *SPE/IADC Middle East Drilling Technology Conference and Exhibition*. http://dx.doi.org/10.2118/178197-ms.

Powers, D. L. (2010). Boundary value problems: And partial differential equations. Amsterdam: Elsevier/Academic Press.

Ramey, H. (1962). Wellbore heat transmission. *J Pet Technol* 14 (04), 427-435. http://dx.doi.org/10.2118/96-pa.

Raymond, L. (1969). Temperature distribution in a circulating drilling fluid. *J Pet Technol* 21 (3), 333-341. http://dx.doi.org/10.2118/2320-PA.

Tragesser, A. F., Crawford, P. B., and Crawford, H. R. (1967). A method for calculating circulating temperatures. *J Pet Technol* 19 (11), 1507-1712. http://dx.doi.org/10.2118/1484-PA.

Willhite, G. (1967). Over-all heat transfer coefficients in steam and hot water injection wells. *J Pet Technol* 19 (5), 607-615. http://dx.doi.org/10.2118/1449-PA.

Wooley, G. R. (1980). Computing downhole temperatures in circulation, injection, and production wells. *J Pet Technol* 32 (9), 1509-1522. http://dx.doi.org/10.2118/8441-PA.

Yu, Z., Lerche, I., and Lowrie, A. (1992). Thermal impact of salt: Simulation of thermal anomalies in the Gulf of Mexico. *Pure and Applied Geophysics PAGEOPH* 138 (2): 181-192. http://dx.doi.org/10.1007/bf00878894.

# II. INFLUENCE OF FRICTIONAL OR ROTATIONAL KINETIC ENERGY ON WELLBORE FLUID-TEMPERATURE PROFILES DURING DRILLING OPERATIONS

A.Q. Al Saedi, R. E. Flori, and C. S. Kabir

Missouri University of Science and Technology

(Published in SPE Drilling & Completion (2019))

## ABSTRACT

Temperature-profile distributions in a wellbore during drilling operations might take different forms when applying the energy balance in the overall system. For steady-state conditions, wherein the wellbore is considered as a closed system, adding any source of additional energy to this system can influence the predicted temperature profiles. This study presents a new analytical model to investigate the influence of rotational energy arising from the drillstring on the wellbore-temperature behavior.

A significant part of drilling operation is the rotation of the drillstring. Depending on the drilling rig, various equipment provides this kind of energy, such as the rotary table or top drive. In addition, downhole motors or turbines can add additional rotation to the drill bit. This type of energy source may be construed as a supplemental heat source that can be added to the formulations of drillpipe-and annular-temperature profiles.

Overall, this study presents two models involving frictional and rotational energy. These models yield the same solution if we do not include the energy source, and they can apply equally well for any energy balance system. The proposed mathematical models provide

new insights into different energy terms that can be included to compute the temperature profiles in the drillpipe and annulus.

## 1. INTRODUCTION

The importance of temperature profiles for both tubular and annular conduits in wellbores underlies the influence of those temperatures on further operations and fluid properties. Moreover, an additional heat source may also influence the tools' longevity.

In drilling operations, the frictional forces originate from pressure losses or the contact area between the drilling tool and the drilled formation. Furthermore, the torque and drag forces result from rotating the drill string, such as those presented by Samuel (2007), Aadnoy and Djurhuus (2008), Aadnoy et al. (2010), and Mirhaj et al. (2016), among others. These factors may influence the drilling fluid temperature profiles by incorporating the necessary heat energy system model as presented by Kumar et al. (2012a, 2012b) for drilling operations, and for casing while drilling operations by including the plastering effect as in Kumar and Samuel (2012).

Historically, many studies provided the necessary mathematical tools to describe the temperature distribution inside the wellbore. Earlier studies presented the basic analytical models and provided the physical understanding of the steady-state and transient flow problems as those given by Edwardson et al. (1962) and Tragesser et al. (1967). Raymond (1969) provided the first numerical model for computing circulating-fluid temperatures during unsteady and pseudosteady-state conditions to handle multiple casing strings.

Furthermore, improvements to this model have been made by Keller et al. (1973) by adding new forms of energy as a result of frictional pressure losses throughout the drillpipe and annulus to the heat energy system with the limitations of the provided data. This model was further investigated by Marshall and Bentsen (1982) by using a full set of data. Subsequently, analytical solutions became feasible for less complicated systems, such as that for a single casing string. For example, Holmes and Swift (1970) presented a solution for the steady-state heat transfer in a drillpipe and annulus surrounded by the formation. In contrast, Kabir et al. (1996) and Hasan et al. (1996) obtained solutions for forward and reverse-circulation cases, for a variable mud-tank temperature of the circulating fluid. More recently, Kumar and Samuel (2013) expanded the scope of the previous models by including well deviation and heat generated by wellbore friction. They validated their fluid-temperature model with field data involving deviated and horizontal wellbores.

The primary aim of this study is to offer a comparison between two analytical fluid-temperature models with two sources of energy. Initially, we considered the frictional heat that has been available for some time, and, thereafter, one involving the rotational kinetic energy. Both these models may influence the drillpipe and annular temperature profiles during different wellbore operations. We used limited field data to validate the performance of both models.

## 2. MATHEMATICAL MODELS

For completeness, this section presents models for two sources of energy: frictional energy (FE) and rotational kinetic energy (RKE). However, to gain clarity in the difference between these two models, let us consider the schematic shown in Figure 1. The heat generated

from the RKE depends on the rotational speed of the drill string regardless of its physical contact with the wellbore. Consequently, the increase in fluid temperature will distribute gradually all around the drill string. In contrast, the heat generated by frictional energy is caused by the contact points between the drill string and the wellbore wall. Such contact may occur in some areas of the borehole in a vertical well, but more so when the well starts to deviate from vertical.

## 2.1. FRICTIONAL ENERGY

Keller et al. (1973) suggested an analytical model of the heat energy balance system for determining the temperature profiles for both drill string and annular temperature. The energy system performed for steady-state and transient conditions by using finite difference equations for eight solution points in the presence of multiple casing strings. The calculations begin with the energy balance inside the drill string and successively through the drill string, the flow annulus, the first casing string, the second annulus, the third annulus, the fourth annulus, and into the formation.

New energy sources added to the system involve the frictional flow in the drillpipe, wherein the shear work is done by rotating the drill string, and the frictional work at the drill bit. The validation of this model had been done by adopting the Holmes and Swift (1970) data.

Marshall and Bentsen (1982) further investigated the Keller et al. model using all the dataset required for the different casing size installed. More recently, Kumar and Samuel (2013) suggested a mathematical model for estimating the heat generated from the frictional forces of the drill string and incorporated this model into an energy system to find out the final mathematical form that represents the drillpipe and annular temperature profiles.

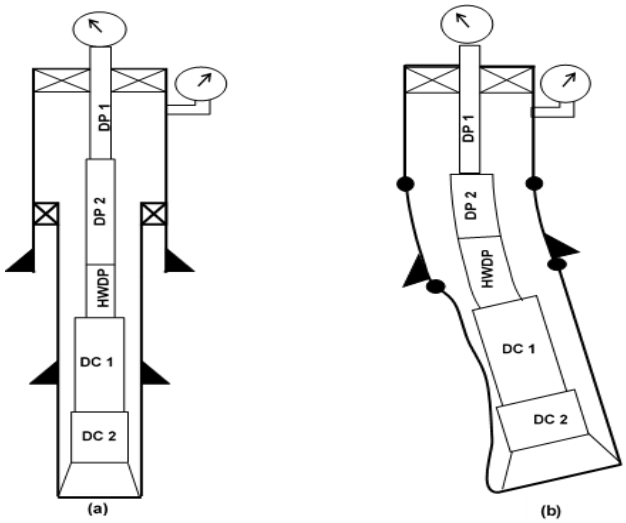


Figure 1. Wellbore schematics of a vertical (a) and a deviated well (b). DC = drill collar; DP = drillpipe; HWDP = heavy-weight drillpipe.

The energy system in this model was the same as that of Keller et al. (1973) and Marshall and Bentsen (1982) with one crucial difference. The Kumar and Samuel formulation presupposes that the steady-state heat-transfer occurs from the drillpipe to the annulus and from the annulus to the adjacent formation.

The complete mathematical model for the Kumar and Samuel (2013) study did not appear in the paper, presumably for brevity. We attempted to fill in that perceived void in this study. For the steady-state condition, the mathematical forms of the energy balance system for the annulus and the drillstring, respectively, can be expressed as:

$$\rho q C_p \frac{\mathrm{d}T_a}{\mathrm{d}z} + 2\pi r_p U \left(T_{dp} - T_a\right) + 2\pi r_w h_o \left(T_f - T_a\right) + Q_a = 0 \tag{1}$$

$$\rho q C_p \frac{\mathrm{d}T_{dp}}{\mathrm{d}z} + 2\pi r_p U \left(T_{dp} - T_a\right) = Q_p \tag{2}$$

Eq. 2 can be rewritten as

$$T_a = T_{dp} + \frac{\rho q C_p}{2\pi r_p U}\frac{\mathrm{d}T_{dp}}{\mathrm{d}z} - \frac{Q_p}{2\pi r_p U} \tag{3}$$

The solution of the ordinary-differential equations above for the drillpipe temperature can be written as

$$T_{dpFE} = C_1 e^{r_1 z} + C_2 e^{r_2 z} + g_T z + T_S + \frac{Q_p}{2\pi r_p U} + \frac{Q_a + Q_p}{2\pi r_w h_o} - A g_T \tag{4}$$

and the annular temperature by the following expression:

$$T_{aFE} = C_1 \left(1 + A r_1\right) e^{r_1 z} + C_2 \left(1 + A r_2\right) e^{r_2 z} + g_T z + T_S + \frac{Q_a + Q_p}{2\pi r_w h_o} \tag{5}$$

where

$$A = \frac{\rho q C_p}{2\pi r_p U} \tag{6}$$

The integration constants $C_1$ and $C_2$ can be found by applying the first kind of the boundary condition (BC) or Dirichlet BC. This boundary condition implies that at the surface the drillpipe temperature is the same as the inlet drillpipe temperature, whereas, the annular and the drillpipe temperatures are equal at total depth, as given in Powers (2010). We note that this boundary condition represents the industry standard. Prior studies of Raymond (1969), Holmes and Swift (1970), Keller et al. (1973), Marshall and Bentsen (1982), Arnold (1990), Kumar and Samuel (2013), and Gao et al. (2017) are cases in point. With the Dirichlet BC, the two constants can be written as:

$$C_2 = T_{dpi} - T_S - \frac{Q_p}{2\pi r_p U} - \frac{Q_a + Q_p}{2\pi r_w h_o} + A g_T - C_1 \tag{7}$$

$$C_1 = \frac{\left[\left(T_{dpi} - T_S - \frac{Q_p}{2\pi r_p U} - \frac{Q_a + Q_p}{2\pi r_w h_o} + Ag_T\right) Ar_2 e^{r_2 L} - \frac{Q_p}{2\pi r_p U} + Ag_T\right]}{\left[Ar_2 e^{r_2 L} - Ar_1 e^{r_1 L}\right]} \tag{8}$$

Appendix A provides the details of these derivations.

## 2.2. ROTATIONAL KINETIC ENERGY

Replacing the energy source in the proposed model above with the energy sources caused by the rotational kinetic energy for both the annular and drillpipe temperature can be presented as the following:

$$A\frac{\mathrm{d}T_a}{\mathrm{dz}} + \left(T_{dp} - T_a\right) + B\left(T_f - T_a\right) + R_{ra} = 0 \tag{9}$$

$$T_a = T_{dp} + A\frac{\mathrm{d}T_{dp}}{\mathrm{dz}} - R_{rp} \tag{10}$$

where *A* is given by Eq.6, and the definition of other symbols is as follows:

$$B = \frac{r_w h_o}{r_p U} \tag{11}$$

$$R_{ra} = \frac{1.75\text{E-}8\rho_p A_p \left(r_{po}^2 + r_{pi}^2\right).(R_s)^2}{r_p U t} \tag{12}$$

$$R_{rp} = \frac{3.48\text{E-}8\left(\rho_p A_{pi}\right)\left(r_{pi}^2\right).(R_s)^2}{r_p U t} \tag{13}$$

The final mathematical form for the drillpipe and annular temperature can be obtained from the solution of the ordinary differential equations (Eqs. 9 and 10) as the following expressions:

$$T_{dpRKE} = C_a e^{r_1 z} + C_b e^{r_2 z} + g_T Z + T_s + R_{rp} + \frac{R_{rp}}{B} + \frac{R_{ra}}{B} - Ag_T \tag{14}$$

$$T_{aRKE} = C_a e^{r_1 z}\left(1 + Ar_1\right) + C_b e^{r_2 z}\left(1 + Ar_2\right) + T_s + g_T Z + \frac{R_{rp}}{B} + \frac{R_{ra}}{B} \tag{15}$$

where

$$C_a = T_{dpi} - T_s - R_{rp} - \frac{R_{rp}}{B} - \frac{R_{ra}}{B} + Ag_T - C_b \tag{16}$$

$$C_b = \frac{\left[\left(T_{dpi} - T_s - R_{rp} - \frac{R_{rp}}{B} - \frac{R_{ra}}{B} + Ag_T\right) r_1 e^{r_1 L} - \frac{R_{rp}}{A} + g_T\right]}{\left[r_1 e^{r_1 L} - r_2 e^{r_2 L}\right]} \tag{17}$$

Appendix B presents the details of these derivations.

## 3. VERIFICATION OF MODELS

The original model proposed by Keller et al. (1973) used the dataset of a vertical wellbore presented earlier by Holmes and Swift (1970). Using those data, we applied both the frictional energy (FE) and rotational kinetic-energy (RKE) models with assumed $U$ and $h_o$ values of 3.2 and 1 Btu/ft$^2$-hr-$^o$F, respectively. The output of both models for the annular temperature, without including any bottomhole energy source, provides good agreement with that offered by Keller et al. (1973), as shown in Figure 2. In this example, the RKE model shows the annular temperature to be about 1 $^o$F higher than the FE model, at both well bottom and surface conditions, the distributed energy presented by this figure is referring to the dataset from Keller et al. (1973).

Although the Holmes and Swift (1970) data indicated that all the properties are applicable for the entire well depth, circulation is the only assumption that can trigger the RKE model. Usually, no or low-rotational speed of the drill string may be applied to avoid stuck pipe. Therefore, we assumed 5 rpm for 2 hours only.

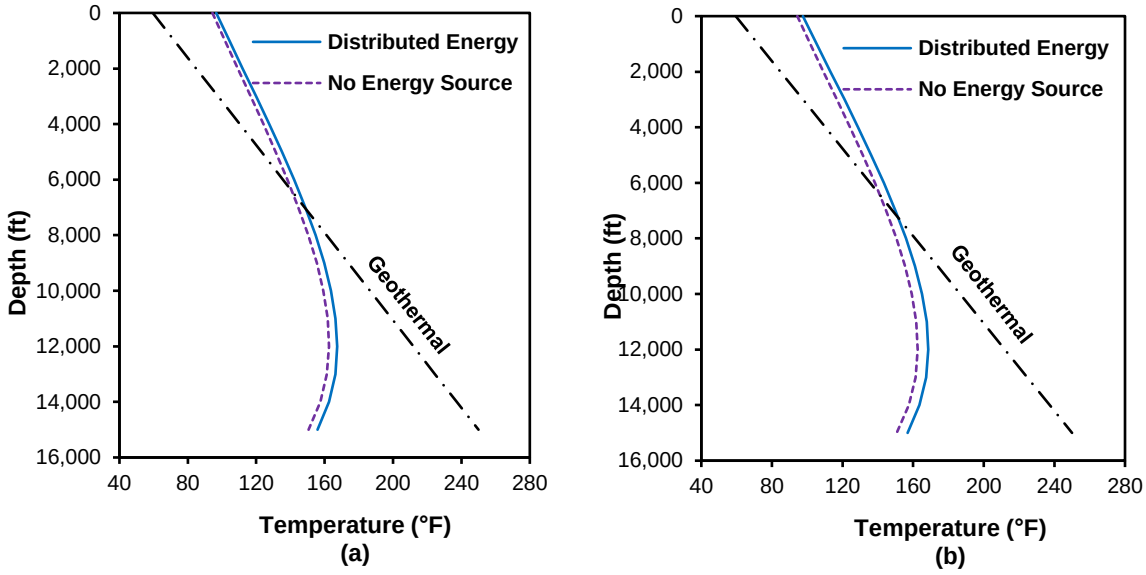


Figure 2. Calculated annular temperature, (a) FE model, (b) RKE model. The term "distributed energy" refers to data from Keller et al. (1973).

That is because, after tens of hours of mud circulation, the system will behave as though no energy source exists, thereby reflecting the steady-state circulation. Figure 2. Calculated annular temperature, (a) FE model, (b) RKE model. The term "distributed energy" refers to data from Keller et al. (1973).

To verify the proposed FE and RKE models, we adopted the data of Kumar and Samuel (2013) for the deviated well case, as shown in Table 1.

In this case, the drill-string stems from the bottom depth with an 8½ in. bit, MWD tool, reamers, stabilizer, a rotary-steerable system (RSS), and 5 in. HWDP. The kick-off depth was reported as true-vertical depth (TVD) of 7,685 ft, followed by the buildup section at measured depth (MD) of 4,149 ft, and then extended with a tangent section at MD of 2,431 ft.

The Kumar and Samuel (2013) model was applied for the long tangent section from 11,834 ft to 14,265 ft total depth by using 26 stands for 48 hrs. Based on these data, the length of each stand equals 93.5 ft, the rate of penetration occurred at 50.64 ft/hr and the time required to drill each stand equaled to 1.84 hr.

These considerations collectively led to a high rotational speed used to drill this section. We used the data in Table 1 and assumed other data, such as flow rate of 210 gal/min or 1,685 $ft^3$/hr, mud density of 10.015 lbm/gal or 74.81 lbm/$ft^3$, $T_{pi}$ of 102 $^oF$, $U$ of 2.5 Btu/$ft^2$-hr-$^oF$, and $h_o$=1.6 Btu/$ft^2$-hr-$^oF$. Some of these data came from the Marshall and Bentsen (1982) study. Figure 3 shows the results of the application of the FE model, the same output as from the Kumar and Samuel (2013) model. The variation in the geothermal gradient along with MD was assumed based on the formation temperature of offset wells. We emphasize that in all well-control calculations, especially for the pressure gradient, we used the TVD.

Therefore, we assumed a different value of geothermal gradient to match its variation after the kick-off point depth. An approximate linear expression of $T_f = T_s + g_T.z$ can represent the formation temperature of interest at a given depth.

Thereafter, calculations with the FE model followed at each stand, leading to an inlet temperature for Stand 1 at 80.33 $^oF$, and for Stand 26 at 107 $^oF$. Figure 4 presents these results. The bottomhole temperature was measured from the bottom by 37 ft for MWD2 and 95 ft for MWD1. Figure 5 represents the result of applying the FE model for the annular temperature to compare with the digitized temperature measurements for MWD1.

The agreement between the digitized Kumar and Samuel model results with that shown as the FE model, developed in this study, is reassuring. Now, let us consider two cases to verify the RKE model.

Table 1. Drilling parameters of a deviated well, Kumar and Samuel (2013).

| | |
|---|---|
| Bingham Plastic Mud | |
| Mud specific gravity | 1.2 |
| Plastic viscosity, cp | 20 |
| Yield stress, $lb_f/100\ ft^2$ | 15 |
| Inlet temperature at drill-pipe, ˚F | 80.33 |
| Coefficient of friction in open hole | 0.35 |
| Surface temperature, ˚F | 59 |
| Geothermal gradient, ˚F /ft | 0.013725 |
| Openhole ID, in. | 8.5 |
| Drill pipe outside diameter, in. | 5 |
| Drill pipe inside diameter, in. | 3 |
| Drill pipe weight, $lb_m/ft$ | 40 |
| Drill collar outside diameter, in. | 6.5 |
| Drill collar inside diameter, in. | 2.81 |
| Drill collar length, ft | 520 |
| Drill collar weight, $lb_m/ft$ | 100.8 |
| Bit nozzle total flow area, $in^2$ | 1.2 |
| Bit nozzle velocity constant, $C_d$ | 0.95 |
| Heat capacity of pipe/collar, Btu/lbm-°F | 0.0956 |
| Thermal conductivity of pipe/collar, Btu/ft-hr-˚F | 25.26 |

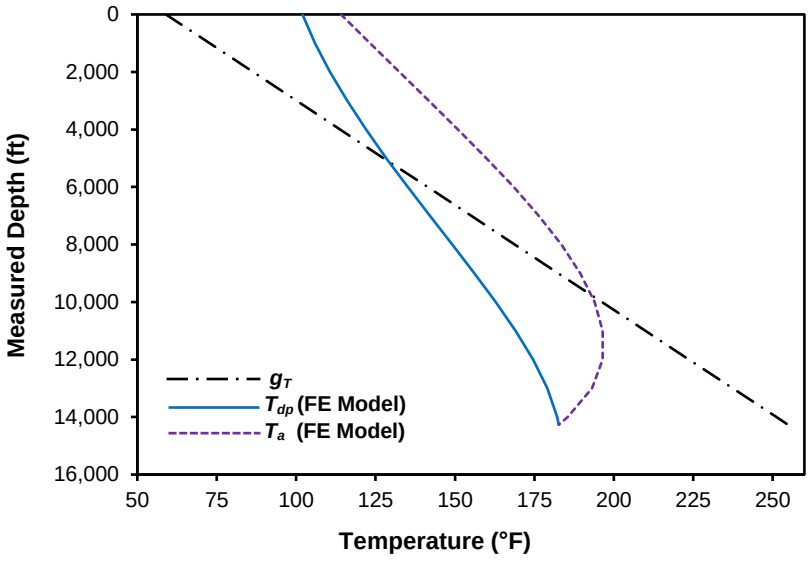


Figure 3. Application of the FE model for the total depth.

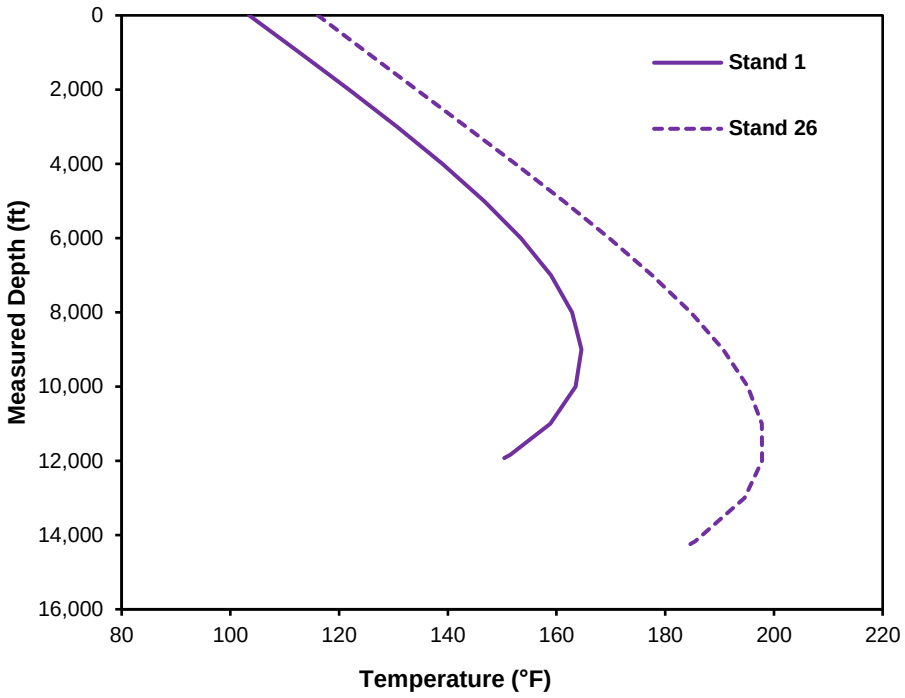


Figure 4. Annular temperature of FE model for Stand 1 and Stand 26.

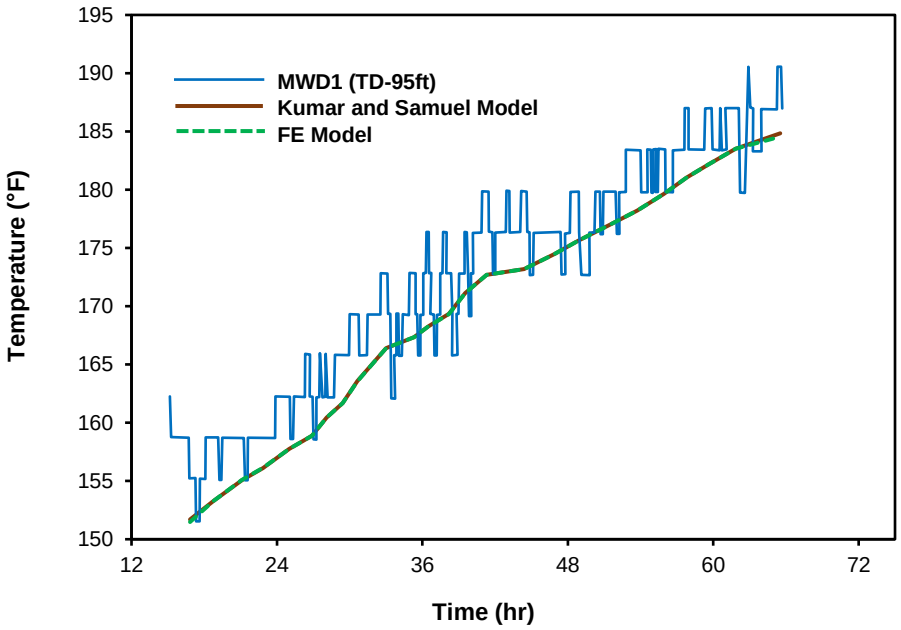


Figure 5. Comparison of FE model with the Kumar and Samuel (2013) model.

### 3.1. CASE-1

In this case, we assumed that the heat generated from the RKE is added to the annular temperature only; that is, Qrp equals to zero. We used the same data presented in Table 1, the same inlet temperature for the first and last stand at 80.33 °F and 107 °F, respectively, and used the same fluid properties with the constant rotational speed of 100 RPM from Kumar et al. (2012a). The heat transfer calculations from formation to the annulus and then to the drillpipe presupposed U = 3.6 Btu/ft2-hr-°F and ho=1.5 Btu/ft2-hr-°F. The reported time required to drill this section was 48 hr; therefore, we started at 110 hr in the first stand referring to all the previous operations until reaching this depth, then increased the time for each stand until reaching to 158 hr for Stand 26.

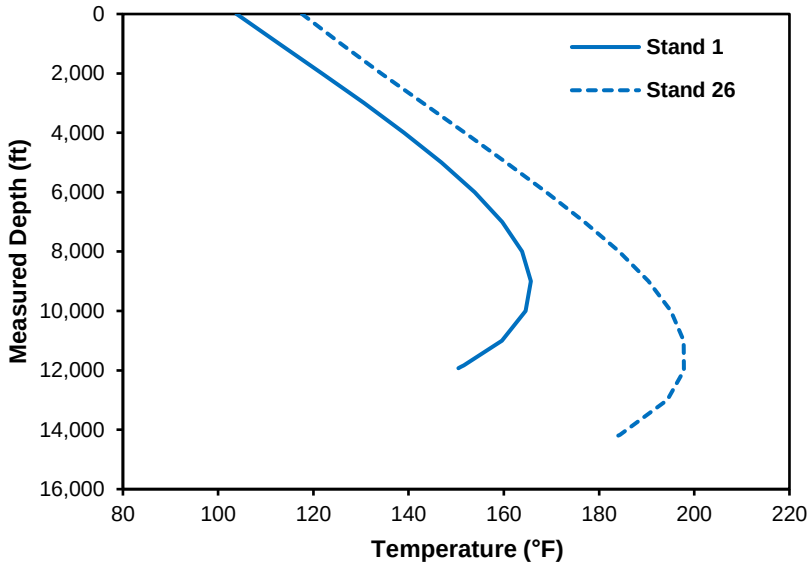


Figure 6. Annular temperature of the RKE model for Stands 1 and 26.

Figure 6 shows the two temperature profiles of interest for the two stands. Let us compare the results of the RKE model with the real-time temperature data while drilling. The

calculated temperature trend appeared less than the MWD1 and MWD2 measurements resulting from the RKE in the annulus not adequate to replace the FE sources as suggested by Kumar and Samuel (2013). Moreover, applying the heat energy model without accounting for the FE sources will result in a temperature, which is about 20 ˚F lower than with the inclusion of FE. Figure 7 presents the relevant results.

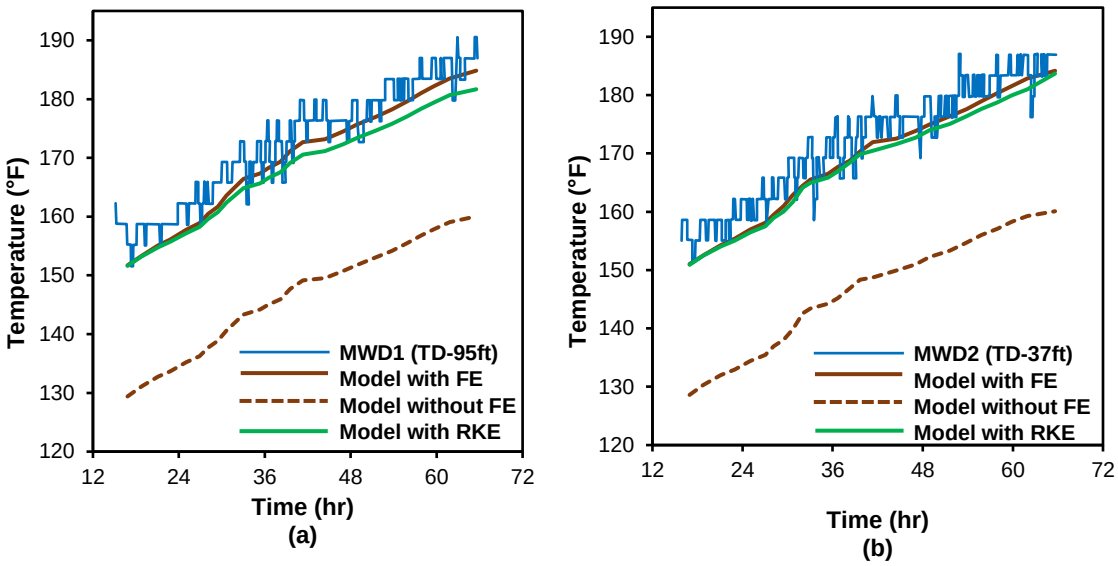


Figure 7. Adding RKE to annulus suggests a decent overall match with measured data, MWD1 (a), MWD2 (b).

The drilling process in a deviated well provides contact area of the drill string with the wellbore, which may affect the amount of overall heat-transfer coefficient from the annulus to the drillpipe *U*. The overall heat-transfer coefficient from the formation to the annulus $h_o$ remains constant with the steady-state assumption. Therefore, we retained the same data, and by changing *U* for each stand, we can get a good match with the measured data for MWD1,

and also for MWD2. As Figure 8 shows, by invoking the RKE model the temperature difference is about 15 ˚F.

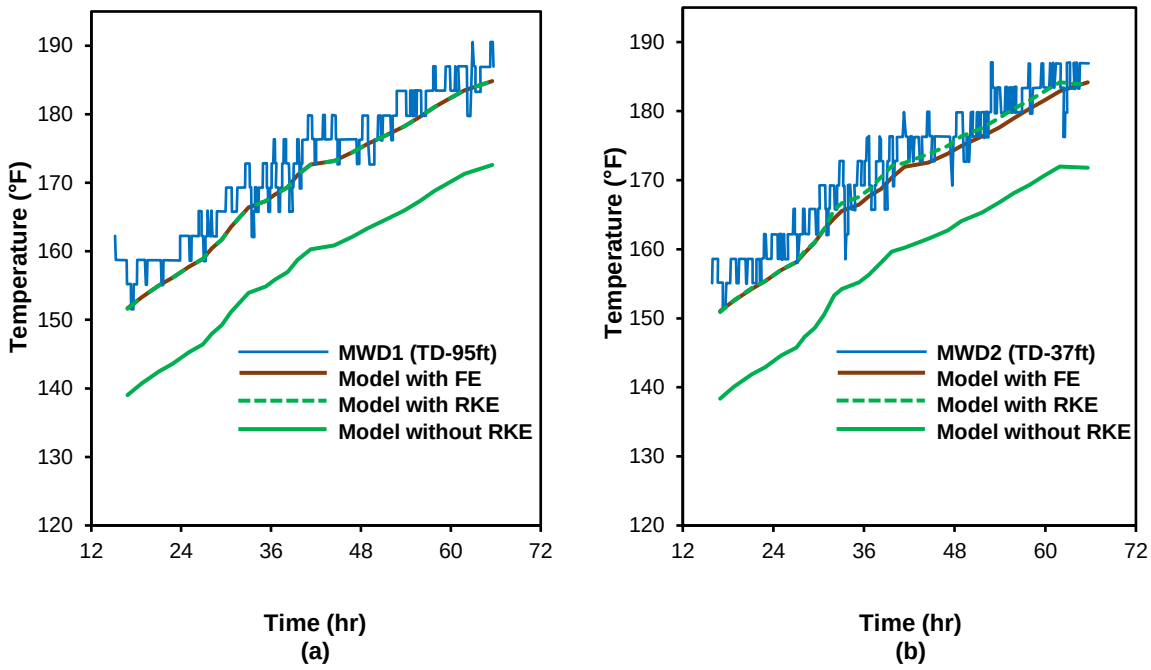


Figure 8. Adding RKE to the annulus vs. measured data by changing U: MWD1 (a); (b) MWD2.

We emphasize that the wellbore lacks uniformity as a result of deviated drilling operation with an average inclination of about 10˚ to 11˚ in the tangent section.Therefore, the heat generated by frictional energy owing to the contact between the drill string and the wellbore wall, as described by Kumar and Samuel (2013), may not occur uniformly on the inside area of the entire wellbore.In contrast, the application of RKE depends on the rotational speed of the drill string regardless of its contact with the wellbore. As a result, the temperature profiles from the RKE will be higher than the temperature profiles obtained by the FE model.

### 3.2. CASE-2

Here, the rotational energy working as the heat source may be added to the fluid both in the annulus $Q_{ra}$ and to the drillpipe $Q_{rp}$, as given by the RKE model. The same data assumed in Case-1 were used to obtain an increase in temperature profile for each stand as a result of the new source added to the fluid inside the drillpipe, as given in Figures 9 and 10.

Figures 9 and 10 suggest that the amount of heat generated from the rotational energy inside the drillpipe was fully accounted for, which we may refer to as the heat inside the drillpipe and from the drill bit.

Therefore, one can assume that the heat source inside the drillpipe takes only 60% of the total generated heat, and the remaining 40% goes to the bit. Keller et al. (1973) initially suggested this assumption, which Marshall and Bentsen (1982) used subsequently.

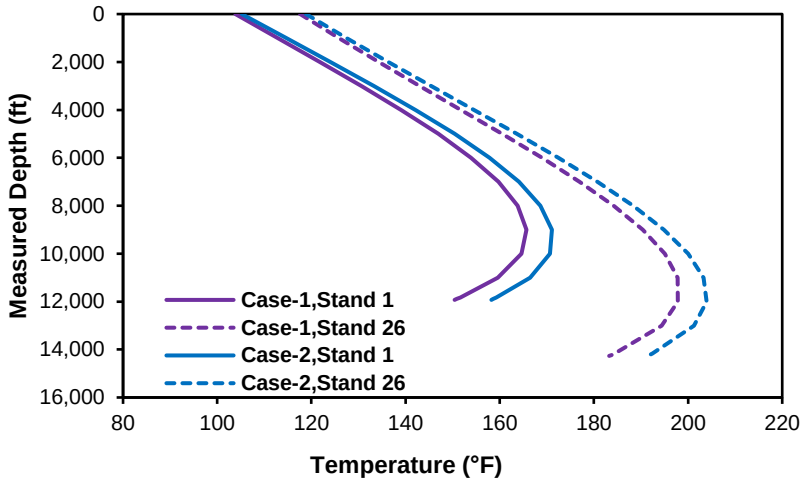


Figure 9. Annular-temperature profiles in two stands derived from the RKE model.

The use of this energy split will cause the annular temperature profile to increase more than that in Case-1, and the comparison with the measured data suggests even an improved match, as Figure 11 testifies.

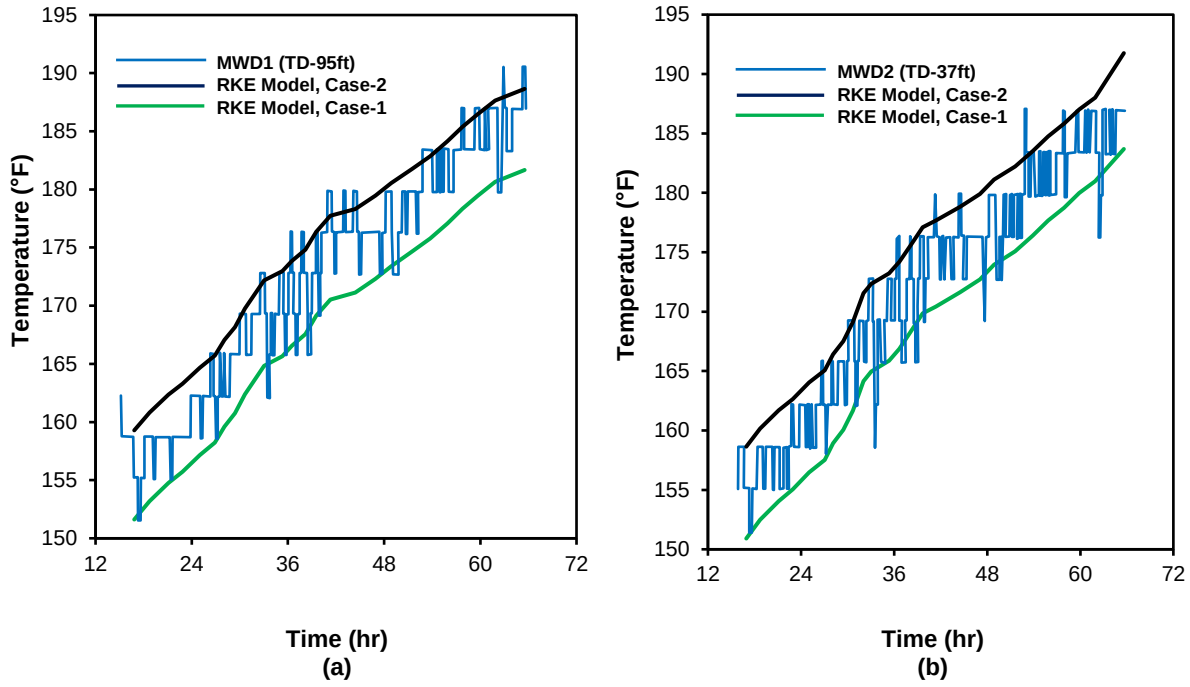


Figure 10. Adding RKE to the annulus and drillstring vs. measured data, MWD1 (a); (b) MWD2.

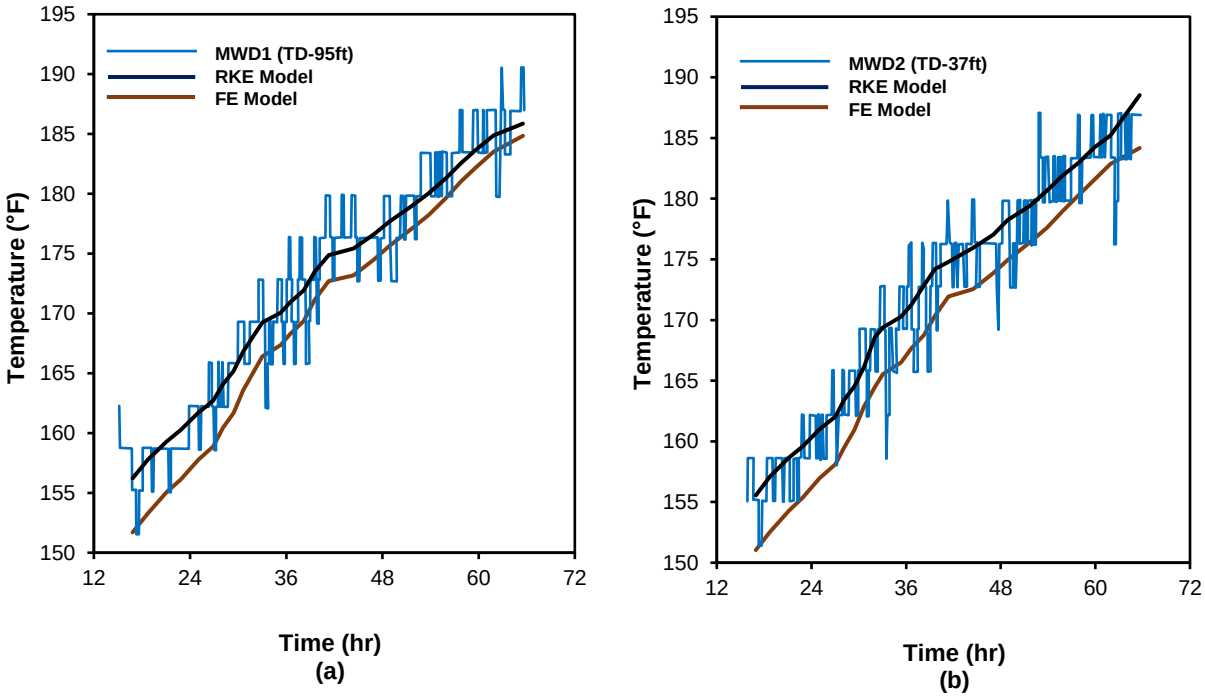


Figure 11. Adding 60% of RKE to the drill-string shows good agreement with measured data at MWD1 (a), MWD2 (b).

# 4. MODEL VALIDATION

We applied the proposed RKE model for 13 stands from 6,900 to 7,977 ft MD of a 12 ¼ in. hole buildup section in a recently drilled deviated well. The required drilling time involved 53 hrs with the bottomhole assembly consisting of a 12¼ in. PDC bit, rotary-steerable system, measurement-while-drilling or MWD tool, 1×5 in. HWDP, drilling jar, and 7×5 in. HWDP. The temperature measurement was obtained by using the MWD tool, located at 27 ft, which was the reference depth of measurement from the drill bit. Not all the required parameters for this field example were available; therefore, some required data were assumed from the literature. Table 2 presents the drilling and fluid parameters, and Table C-1 refers to drilling measurement data in Appendix C.

Table 2. Well and mud data.

| | |
|---|---|
| Section depth, ft | 7,977 |
| Drill bit size, in. | 12 1/4 |
| Drill stem OD, in. | 6 5/8 |
| Drill stem ID, in. | 3 |
| Mud viscosity, cp | 21 |
| Mud density, $lb_m$/gal | 10.8 |
| Circulation rate, gal/min | 750 |
| Inlet mud temperature, °F | 125 |
| Formation density, $lb_m$/gal | 20.86 |
| Rotational speed, rpm | 130 |
| Section length, ft | 1,077 |

We used the Hasan et al. (1996) model to estimate the required inlet temperature data for this field case, given their unavailability. Table C-2 presents those estimated temperatures at each stand. The MWD tool provided the measured temperature; the assumed geothermal

gradient of 0.013725 ˚F/ft allowed conversion to the measurement depth. Figure 12 presents the application of the proposed RKE model for both the drillpipe and annular temperatures.

All temperature measurements recorded by the MWD tool occurred at measured depths after the kick-off point. We may assume one value for the geothermal gradient for the vertical section only, although a variation in geothermal gradient may occur because of the change in sediments. Although not shown here, our findings suggest that the small differences in $g_T$ produce insignificant results given the short drilling intervals.

By using the same field data given in Table 2 and the calculated inlet temperatures given by Table C-2, the application of the FE model with $Q_a$ and $Q_p$ equals to 80 and 45 Btu/ft-hr, respectively.

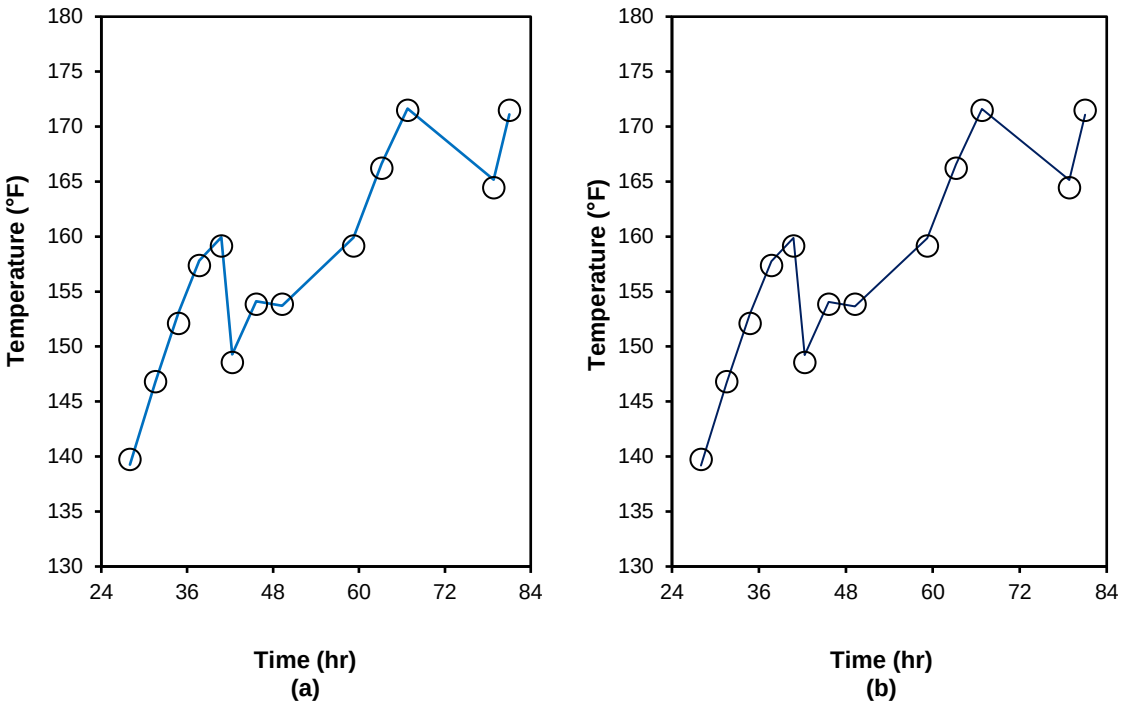


Figure 12. Validation of the RKE model with MWD, $T_a$ (a), $T_{dp}$ (b).

Figure 13 compares the model response with the measured temperature profiles for both in the annulus and drillpipe. Just as before, the variation of the geothermal gradient produced no perceptible change in the model performance.

The heat generated by FE relates to the contact area between the drill string and the wellbore, which depends on the survey measurement available at each depth. The inclination and azimuth gradually increase from the kick-off point depth to the target depth. Also, at early drilling time, the directional survey is relatively smaller than the late-time survey measurements. Therefore, heat generated at earlier times becomes insufficient to match the MWD measurements.

In contrast, at late drilling times, the drilling survey measurement will show more contact area required for generating the heat added to the drilling fluid, which could explain the improved match with the MWD measurements.

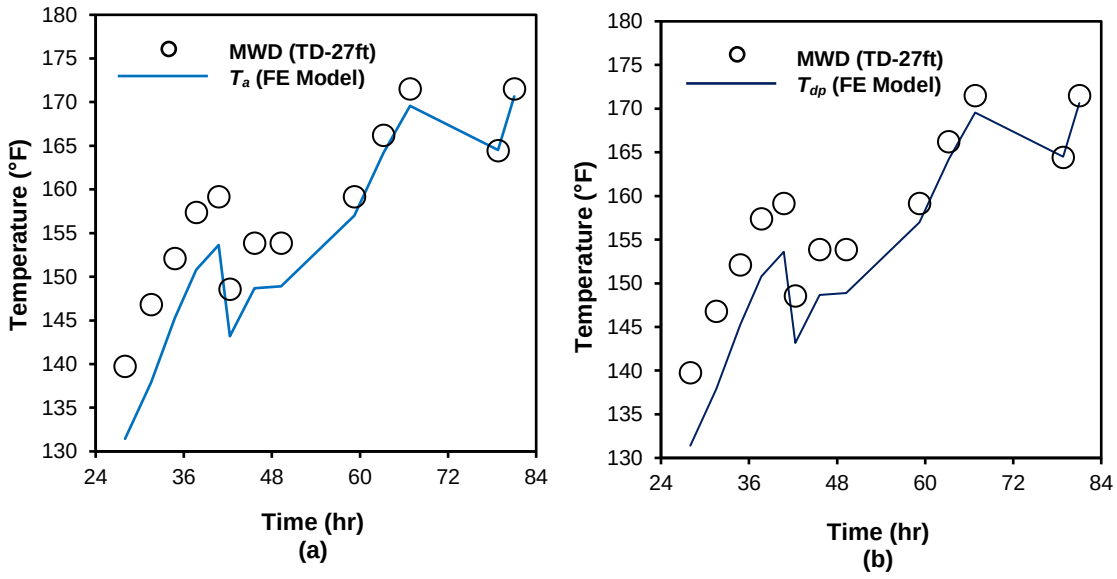


Figure 13. Validation of the FE model with MWD, $T_a$ (a), $T_{dp}$ (b).

# 5. DISCUSSION

The primary objective of this paper entailed investigation of the sources of energy that may impact temperature profiles in both mud conduits in a drilling operation. To that end, we have explored development and applications of both FE and RKE models. Analytical formulation underpins both models. The amount of rotational energy depends on the type of technology used in drilling. The prospect of these models provides some new insights that may be included in future studies in challenging environments.

The heat generated from the FE resulting from the frictional force contact between the drill string and the wellbore was assumed to be constant along all the wellbore depth. This underlying assumption may be open to debate because the actual contact occurs in some areas of the borehole in a vertical or near-vertical setting. However, in deviated wells, this assumption becomes a reality as high torque readings will suggest. In contrast, the RKE depends on the rotating speed of the drill string, regardless of the physical contact with the formation. Therefore, the temperature profiles generated with the RKE model will be higher than those produced with the FE model. We also note that the variation between TVD and MD as a result of directional drilling may lead to a change in geothermal gradient. However, this difference is likely to be small because of the short length of drilling interval.

Validation of the proposed models with field data supports the application of the rotating energy. The RKE caused by rotation of the drill string was assumed in two cases (Case-1 and Case-2) and presented previously to cover all possible temperature ranges in a typical drilling operation. The model's performance when compared with the drillpipe and annular temperature data provided confidence in the solution approach pursued in this study.

One may observe that the results of the two models (FE and RKE) appear similar for the problems discussed here despite their different formulations. During a drilling operation, temperature measurement can be obtained by the MWD sensor, which is usually located at least 30 ft above the drill bit followed by the BHA. Therefore, in a deviated well the contact area with the formation by the BHA promotes thermal energy caused by friction, leading to the proper application of the FE model; a similar situation may arise while encountering a tight spot in a vertical well. Of course, frictional energy becomes the prime driver while drilling a horizontal well. In contrast, the RKE model depends only on the rotation of the drillsting, which occurs continuously through all operations, regardless of the well deviation.

We note that the boundary condition (condition of the first kind or Dirichlet condition) used in the solution of the FE and RKE models leads to the reported results. However, a different set of results will appear when the boundary conditions differ. For instance, if we assume the Neumann condition; that is, $dT_a/dz = 0$ at $z = L$, or the Robin condition; that is, $dT_t/dz|_{z=0} = dT_t/dz|_{z=L} = 0$ to solve the fundamental equations, then increased temperature profiles occur in both conduits. Al Saedi et al. (2018) have recently made this point in another study.

## 6. CONCLUSIONS

The following conclusions appear pertinent here:

1. This study presents a new analytical model involving the rotational kinetic energy or RKE, which may be included in any energy-balance system of equations, for the fluid temperature profiles during drilling and fluid circulation operations in the wellbore.

2. This study also explored the development and use of the frictional energy or FE model (Kumar and Samuel 2013) to generate the temperature profiles in a drilling operation. In general, the RKE model tends to produce somewhat higher temperature profiles than the FE model, as field data suggest.
3. The maximum temperature occurs at a depth above the well bottom for both models. This outcome is a consequence of the use of the first kind of boundary condition or Dirichlet condition. Field examples suggested that both the FE and RKE models tend to produce the necessary energy needed to replicate the field measurements. They appear case dependent; therefore, both of them merit consideration while estimating temperature profiles.

## NOMENCLATURE

$A$ = parameter defined by Eq. 6, ft

$A_p$ = outer drillpipe area, $ft^2$

$A_{pi}$ = inner drillpipe area, $ft^2$

$B$ = parameter defined by Eq. B-20, dimensionless

$C_1$ = integration constant defined by Eq. A-18, $^oF$

$C_2$ = integration constant defined by Eq. A-16, $^oF$

$C_a$ = integration constant defined by Eq. B-28, $^oF$

$C_b$ = integration constant defined by Eq. B-30, $^oF$

$C_d$ = bit nozzle velocity constant

$C_p$ = heat capacity of mud, $Btu/lb_m$-$^oF$

$f$ = frequency, rev/sec

$g_T$ = geothermal gradient, $^oF/ft$

$h_o$ = overall heat transfer coefficient across wellbore wall, $Btu/ft^2\text{-}^oF\text{-}hr$

$I$ = moment of inertia, $lbm\text{-}ft^2$

$K_E$ = kinetic energy, $lbm\text{-}ft^2/sec^2$

$L$ = total depth (measured depth), ft

$m_p$ = tubular mass, lbm

$N$ = parameter defined by Eq. A-9, $^oF$

$q$ = mud flow rate $ft^3/hr$

$Q_a$ = heat source in annulus, Btu/ft.hr

$Q_{fa}$ = heat flow from formation to annular, Btu/ft.hr

$Q_p$ = heat source inside drill string, Btu/ft.hr

$Q_{pa}$ = heat flow from pipe to annular, Btu/ft.hr

$Q_{ra}$ = heat source in annulus caused by rotational energy, Btu/hr

$Q_{rp}$ = heat source inside drill string caused by rotational energy, Btu/hr

$r_1, r_2$ = exponent coefficients defined by Eq. A-10, $ft^{-1}$

$r_p, r_{po}$ = average outer radius of the drill string, ft

$r_{pi}$ = average inner radius of the drill string, ft

$R_{ra}$ = parameter defined by Eq. B-21, $^oF$

$R_{rp}$ = parameter defined by Eq. B-14, $^oF$

$R_s$ = rotating speed, revolution per min (RPM), rev/min

$r_w$ = wellbore radius, ft

$t$ = drilling or circulation time, hr

$T_a$ = mud temperature in annulus, $^oF$

$T_{dp}$ = temperature of drill string fluid, $^oF$

$T_f$ = formation temperature, $^oF$

$T_{pi}$ = inlet fluid temperature, $^oF$

$T_s$ = surface temperature of earth, $^oF$

$U$ = overall heat-transfer coefficient across drillpipe, Btu/ft$^2$-$^o$F-hr

$W$ = angular velocity, rad/sec

$z$ = any vertical well depth, ft

$\rho$ = drilling fluid density, lbm/ft$^3$

$\rho_p$ = drillpipe density, lbm/ft$^3$

## ACKNOWLEDGMENT

The first author (A.Q.A. Al-Saedi) gratefully acknowledges the financial support provided by the Higher Committee for Education Development in Iraq (HCED) in pursuit of his PhD study.

# APPENDIX A

# FRICTIONAL ENERGY MODEL

The assumptions and all the mathematical details of this model were presented earlier by Kumar and Samuel (2013). Application of the energy balance for the steady-state condition leads to the differential form of the forward circulation in a drillpipe, which is given by

$$\rho q C_p \frac{\mathrm{d}T_{dp}}{\mathrm{d}z} + 2\pi r_p U \left(T_{dp} - T_a\right) = Q_p \tag{A-1}$$

or

$$T_a = T_{dp} + \frac{\rho q C_p}{2\pi r_p U}\frac{\mathrm{d}T_{dp}}{\mathrm{d}z} - \frac{Q_p}{2\pi r_p U} \tag{A-2}$$

Differentiating Eq. A-2, we obtain

$$\frac{\mathrm{d}T_a}{\mathrm{d}z} = \frac{\mathrm{d}T_{dp}}{\mathrm{d}z} + \frac{\rho q C_p}{2\pi r_p U}\frac{\mathrm{d}^2 T_{dp}}{\mathrm{d}z^2} \tag{A-3}$$

and for the annulus

$$\rho q C_p \frac{\mathrm{d}T_a}{\mathrm{d}z} + 2\pi r_p U \left(T_{dp} - T_a\right) + 2\pi r_w h_o \left(T_f - T_a\right) + Q_a = 0 \tag{A-4}$$

Substituting Eqs. A-2 and A-3 into Eq. A-4 and simplifying, and considering $T_f = T_s + g_T.z$, we obtain the following expression:

$$\begin{aligned} &\frac{\left(\rho q C_p\right)^2}{2\pi r_p U}\frac{\mathrm{d}^2 T_{dp}}{\mathrm{d}z^2} - 2\pi r_w h_o \frac{\rho q C_p}{2\pi r_p U}\frac{\mathrm{d}T_{dp}}{\mathrm{d}z} - 2\pi r_w h_o T_{dp} = \\ &-2\pi r_w h_o T_s - 2\pi r_w h_o g_T Z - 2\pi r_w h_o \frac{Q_p}{2\pi r_p U} - Q_p - Q_a \end{aligned} \tag{A-5}$$

The solution of the left-hand side of Eq. A-5, which represents the homogenous (complementary) part, is given by

$$T_{dp}\underset{complementary}{} = C_1 e^{r_1 z} + C_2 e^{r_2 z} \tag{A-6}$$

and the right-hand side of Eq. A-5 refers to the particular part, and its solution is given by the following expression:

$$T_{\underset{particular}{dp}} = g_T z + N \tag{A-7}$$

Therefore, the final solution of Eq. A-5 can be obtained by summation of Eqs. A-6 and A-7, which is given by

$$T_{dp} = C_1 e^{r_1 z} + C_2 e^{r_2 z} + g_T z + N \tag{A-8}$$

where

$$N = T_S + \frac{Q_a + Q_p}{2\pi r_w h_o} + \frac{\left[ Q_p - \left( \rho q C_p \right) g_T \right]}{2\pi r_p U} \tag{A-9}$$

and

$$r_1, r_2 = \frac{\left(2\pi r_w h_o\right) \pm \sqrt{\left(2\pi r_w h_o\right)^2 + 4\left(2\pi r_p U\right)\left(2\pi r_w h_o\right)}}{2\rho q C_p} \tag{A-10}$$

Eq. A-8 can be rewritten as

$$T_{dpFE} = C_1 e^{r_1 z} + C_2 e^{r_2 z} + g_T z + T_S + \frac{Q_p}{2\pi r_p U} + \frac{Q_a + Q_p}{2\pi r_w h_o} - A g_T \tag{A-11}$$

$$A = \frac{\rho q C_p}{2\pi r_p U} \tag{A-12}$$

Differentiating Eq. A-11, we obtain

$$\frac{\mathrm{d}T_{dP}}{\mathrm{d}z} = r_1 C_1 e^{r_1 z} + r_2 C_2 e^{r_2 z} + g_T \tag{A-13}$$

Substituting Eqs. A-11 and A-13 into Eq. A-2 and simplifying,

$$T_{aFE} = C_1 \left(1 + A r_1\right) e^{r_1 z} + C_2 \left(1 + A r_2\right) e^{r_2 z} + g_T z + T_S + \frac{Q_a + Q_p}{2\pi r_w h_o} \tag{A-14}$$

To find the integration constants $C_1$ and $C_2$, we need to apply the first kind of the boundary condition or the Dirichlet BC, as discussed after Eq. 6 in the text, as follows:

At surface, $Z$=0, and $T_{dp}$=$T_{dpi}$, Eq. A-11 is given as

$$T_{dpi} = C_1 + C_2 + T_S + \frac{Q_p}{2\pi r_p U} + \frac{Q_a + Q_p}{2\pi r_w h_o} - Ag_T \tag{A-15}$$

$$C_2 = T_{dpi} - T_S - \frac{Q_p}{2\pi r_p U} - \frac{Q_a + Q_p}{2\pi r_w h_o} + Ag_T - C_1 \tag{A-16}$$

At total well depth or $Z=L$, $T_{dpL}=T_{aL}$, Eqs. A-11 and A-14 are given as

$$Ar_1 C_1 e^{r_1 L} + Ar_2 C_2 e^{r_2 L} = \frac{Q_p}{2\pi r_p U} - Ag_T \tag{A-17}$$

Substituting Eq. A-16 into Eq. A-17 and simplifying, we have

$$C_1 = \frac{\left[\left(T_{dpi} - T_S - \frac{Q_p}{2\pi r_p U} - \frac{Q_a + Q_p}{2\pi r_w h_o} + Ag_T\right) Ar_2 e^{r_2 L} - \frac{Q_p}{2\pi r_p U} + Ag_T\right]}{\left[Ar_2 e^{r_2 L} - Ar_1 e^{r_1 L}\right]} \tag{A-18}$$

# APPENDIX B

# ROTATIONAL KINETIC ENERGY MODEL

The kinetic energy of a rotating object is analogous to linear kinetic energy and can be expressed by the moment of inertia and angular velocity. During a drilling operation, the total kinetic energy resulting from the rotation of the drill string can be transferred to two kinds of heat source added to the drilling fluid inside the drill string $Q_{rp}$ and in the annulus $Q_{ra}$. Giancoli (2013) provides the rotational kinetic energy or RKE, which is given by

$$K_E = \frac{1}{2}.I.W^2 \tag{B-1}$$

where $I$ refers to the moment of inertia in lbm-ft$^2$, and $W$ is the angular velocity in rad/sec. Then, the moment of inertia can be calculated for the annulus as

$$I = \frac{m_p}{2}\left(r_{po}^2 + r_{pi}^2\right) \tag{B-2}$$

$$I = \frac{\rho_p.(A.dz)_p}{2}\left(r_{po}^2 + r_{pi}^2\right) \tag{B-3}$$

where $r_{po}$, $r_{pi}$ sequentially represents the outer and inner diameter of tubular in ft, and $m$ refers to the tubular mass in lbm. For the angular velocity, $W = cycle * f$ , where $f$ is the frequency or (revolution/min) in drilling, by converting the (revolution/min) to (revolution/sec).

$$f\big|_{\sec} = R_s = rpm = \frac{rev}{\min}.\frac{\min}{60\sec} = \frac{rev}{60\sec} \tag{B-4}$$

One cycle of any tubular will equal to ($2\pi/rev$). Thus, the angular velocity will equal to

$$W = \frac{2\pi.R_s}{60} \text{ in } \frac{Rad}{\sec} \tag{B-5}$$

Now, after calculating the angular velocity and moment of inertia, the kinetic energy in Eq. B-1 can be rewritten as

$$Q_{ra} = K_E = \frac{1}{2}.\frac{\rho_p.(A_p.dz)}{2}\left(r_{po}^2 + r_{pi}^2\right).\left(\frac{2\pi.R_s}{60}\right)^2 \tag{B-6}$$

Eq. B-6 represents the total RKE transferred to heat in the annulus in lbm-ft$^2$/sec$^2$. By converting this energy to Btu and dividing Eq. B-6 by the total time for drilling or circulating, we obtain the final mathematical form as

$$Q_{ra} = \frac{(1.098\text{E-}07)\rho_p.(A_p.dz)\left(r_{po}^2 + r_{pi}^2\right).(R_s)^2}{t} \tag{B-7}$$

In Eq. B-7, $Q_{ra}$ represents the amount of heat added to the inside of the annulus system as a result of rotation of the drill string in Btu/hr, and $t$ is the total drilling or circulating time in hr. The heat added to the inside of the drill string as a result of rotating the drill string $Q_{rp}$ is given by

$$Q_{rp} = \frac{(2.2\text{E-}07)\rho_p.(A_{pi}.dz)\left(r_{pi}^2\right).(R_s)^2}{t} \tag{B-8}$$

The difference between Eqs. B-7 and B-8 is because of the change in the moment of inertia for the inside of the drillstring given as $I = \rho_p.(A_p.dz)\left(r_{pi}^2\right)$.

Replacing the heat sources in the energy system in Appendix A, with the new heat source suggested by RKE, gives a new analytical model to determine the fluid temperature behavior in the drillpipe and annulus. The heat source added to the system by the RKE is $Q_{rp}$ and $Q_{ra}$ in Btu/hr. In contrast, the heat source in Keller et al. (1973), Marshall and Bentsen (1982), and Kumar and Samuel (2013) has the unit of Btu/ft-hr.

Therefore, we need to re-derive the energy system proposed in Appendix A in the following manner. The heat energy balance for the steady-state condition in the drillpipe is given by

$$Q_{p_z} - Q_{p_{z+dz}} - Q_{p.a} + Q_{rp} = 0 \tag{B-9}$$

Substituting each term in Eq. B-9, we obtain the following expression:

$$\rho q C_p \left( T_{\underset{z}{dp}} - T_{\underset{z+dz}{dp}} \right) - 2\pi r_p U \left( T_{dp} - T_a \right) \mathrm{d}z + \frac{2.2\text{E-}7 \left( \rho_p A_p \mathrm{d}z \right) \left( r_{pi}^2 \right) . (R_s)^2}{t} = 0 \tag{B-10}$$

Simplifying Eq. B-10 as

$$\frac{\rho q C_p}{2\pi r_p U} \frac{\mathrm{d}T_{dp}}{\mathrm{d}z} + \left( T_{dp} - T_a \right) - \frac{2.2\text{E-}7 \left( \rho_p A_p \right) \left( r_{pi}^2 \right) . (R_s)^2}{2\pi r_p U t} = 0 \tag{B-11}$$

or

$$T_a = T_{dp} + A \frac{\mathrm{d}T_{dp}}{\mathrm{d}z} - R_{rp} \tag{B-12}$$

where

$$A = \frac{\rho q C_p}{2\pi r_p U} \tag{B-13}$$

and

$$R_{rp} = \frac{3.48\text{E-}8 \left( \rho_p A_p \right) \left( r_{pi}^2 \right) . (R_s)^2}{r_p U t} \tag{B-14}$$

Differentiating Eq. B-12, we obtain

$$\frac{\mathrm{d}T_a}{\mathrm{d}z} = \frac{\mathrm{d}T_{dp}}{\mathrm{d}z} + A \frac{\mathrm{d}^2 T_{dp}}{\mathrm{d}z^2} \tag{B-15}$$

The mathematical form of the annular energy balance is given by the following expression:

$$Q_{\underset{z+dz}{a}} - Q_{\underset{z}{a}} + Q_{pa} + Q_{fa} + Q_{ra} = 0 \tag{B-16}$$

Eq. B-16 with the mathematical representation of each term can be written as

$$\rho q C_p (T_{\underset{z+dz}{a}} - T_{\underset{z}{a}}) + 2\pi r_p U \left( T_{dp} - T_a \right) \mathrm{d}z + 2\pi r_w h_o \left( T_f - T_a \right) \mathrm{d}z + \frac{1.098\text{E-}7 \rho_p . (A_p . \mathrm{d}z) \left( r_{po}^2 + r_{pi}^2 \right) . (R_s)^2}{t} = 0 \tag{B-17}$$

Rearranging Eq. B-17

$$\frac{\rho q C_p}{2\pi r_p U}\frac{(T_{a_{z+dz}} - T_{a_z})}{\mathrm{d}z} + \left(T_{dp} - T_a\right) + \frac{2\pi r_w h_o}{2\pi r_p U}\left(T_f - T_a\right) + \frac{1.098\text{E-}7\rho_p (A_p)\left(r_{po}^2 + r_{pi}^2\right).(R_s)^2}{2\pi r_p U t} = 0 \tag{B-18}$$

or $$A\frac{\mathrm{d}T_a}{\mathrm{d}z} + \left(T_{dp} - T_a\right) + B\left(T_f - T_a\right) + R_{ra} = 0 \tag{B-19}$$

where, $$B = \frac{r_w h_o}{r_p U} \tag{B-20}$$

and $$R_{ra} = \frac{1.75\text{E-}8\rho_p A_p \left(r_{po}^2 + r_{pi}^2\right).(R_s)^2}{r_p U t} \tag{B-21}$$

Substituting Eqs. B-12 and B-15 into Eq. B-19 and simplifying, and considering $T_f = T_s + g_T.z$, we obtain the following expression:

$$A^2\frac{\mathrm{d}^2 T_{dp}}{\mathrm{d}z^2} - AB\frac{\mathrm{d}T_{dp}}{\mathrm{d}z} - BT_{dp} = -BT_f - BR_{rp} - R_{rp} - R_{ra} \tag{B-22}$$

The summation of the homogenous and inhomogeneous solutions of the second-order ordinary differential equation above leads to the following expression:

$$T_{dpRE} = C_a e^{r_1 z} + C_b e^{r_2 z} + g_T Z + T_s + R_{rp} + \frac{R_{rp}}{B} + \frac{R_{ra}}{B} - Ag_T \tag{B-23}$$

where

$$r_1, r_2 = \frac{B}{2A}\left(1 \pm \sqrt{1 + \frac{4}{B}}\right) \tag{B-24}$$

Differentiating Eq. B-23, we obtain

$$\frac{\mathrm{d}T_{dP}}{\mathrm{d}z} = r_1 C_a e^{r_1 z} + r_2 C_b e^{r_2 z} + g_T \tag{B-25}$$

Substituting Eqs. B-24 and B-23 into Eq. B-12 and simplifying yields,

$$T_{aRE} = C_a e^{r_1 z}\left(1 + Ar_1\right) + C_b e^{r_2 z}\left(1 + Ar_2\right) + T_s + g_T Z + \frac{R_{rp}}{B} + \frac{R_{ra}}{B} \qquad \text{(B-26)}$$

and $C_a$ and $C_b$ depend on the BC of the Dirichlet condition, at surface depth or $Z$=0, and $T_{dp}$=$T_{dpi}$, justification of the Dirichlet BC is discussed after Eq. 6 in the text. Eq. B-23 can be written as

$$T_{dpi} = C_a + C_b + T_s + R_{rp} + \frac{R_{rp}}{B} + \frac{R_{ra}}{B} - Ag_T \qquad \text{(B-27)}$$

or

$$C_a = T_{dpi} - T_s - R_{rp} - \frac{R_{rp}}{B} - \frac{R_{ra}}{B} + Ag_T - C_b \qquad \text{(B-28)}$$

At total well depth or $Z$=$L$, $T_{dpL}$=$T_{aL}$, Eqs. B-23 and B-25 yields

$$Ar_1 C_a e^{r_1 L} + Ar_2 C_b e^{r_2 L} = R_{rp} - Ag_T \qquad \text{(B-29)}$$

Substituting Eq. B-28 into Eq. B-29 and simplifying we obtain,

$$C_b = \frac{\left[\left(T_{dpi} - T_s - R_{rp} - \frac{R_{rp}}{B} - \frac{R_{ra}}{B} + Ag_T\right) r_1 e^{r_1 L} - \frac{R_{rp}}{A} + g_T\right]}{\left[r_1 e^{r_1 L} - r_2 e^{r_2 L}\right]} \qquad \text{(B-30)}$$

# APPENDIX C

# RELEVANT DRILLING DATA OF A FIELD EXAMPLE

Table C.1. Measured drilling data.

| Stand | Depth (ft) | Drilling Time (hr) | Inclination (deg) | Azimuth (deg) | TVD (ft) | Dogleg (deg/100ft) | Vertical sect (ft) | Temperature (°F) |
|---|---|---|---|---|---|---|---|---|
| 1 | 6,900 | 28.00 | 2.81 | 171.24 | 6,899.16 | 1.18 | 38.97 | 139.75 |
| 2 | 6,994 | 31.55 | 4.47 | 165.39 | 6,992.96 | 1.81 | 44.87 | 146.80 |
| 3 | 7,089 | 34.78 | 6.92 | 163.11 | 7,087.49 | 2.59 | 54.28 | 152.10 |
| 4 | 7,183 | 37.70 | 9.29 | 161.85 | 7,180.54 | 2.53 | 67.52 | 157.39 |
| 5 | 7,277 | 40.75 | 11.44 | 160.78 | 7,273.00 | 2.30 | 84.42 | 159.15 |
| 6 | 7,371 | 42.30 | 13.42 | 162.97 | 7,364.79 | 2.16 | 104.64 | 148.57 |
| 7 | 7,464 | 45.63 | 15.46 | 164.87 | 7,454.85 | 2.25 | 127.77 | 153.86 |
| 8 | 7,571 | 49.25 | 17.97 | 163.28 | 7,557.32 | 2.38 | 158.46 | 153.86 |
| 9 | 7,663 | 59.23 | 20.48 | 161.81 | 7,644.19 | 2.78 | 188.72 | 159.15 |
| 10 | 7,759 | 63.18 | 23.11 | 162.34 | 7,733.32 | 2.75 | 224.34 | 166.21 |
| 11 | 7,853 | 66.80 | 25.79 | 162.48 | 7,818.88 | 2.85 | 263.21 | 171.50 |
| 12 | 7,946 | 78.82 | 27.99 | 161.14 | 7,901.82 | 2.45 | 305.24 | 164.44 |
| 13 | 7,977 | 81.02 | 28.01 | 160.71 | 7,929.19 | 0.65 | 319.79 | 171.50 |

Table C.2. Estimated inlet temperature.

| Stand | Depth (ft) | Inlet Temperature (°F) |
|---|---|---|
| 1 | 6,900 | 125 |
| 2 | 6,994 | 132 |
| 3 | 7,089 | 140 |
| 5 | 7,277 | 149 |
| 7 | 7,464 | 143 |
| 9 | 7,663 | 152 |
| 10 | 7,759 | 160 |
| 11 | 7,853 | 166 |
| 12 | 7,946 | 160 |
| 13 | 7,977 | 167 |

# REFERENCES


Aadnoy, B. S. and Djurhuus, J. (2008). Theory and Application of a New Generalized Model for Torque and Drag. *IADC/SPE Asia Pacific Drilling Technology Conference and Exhibition*, 25-27 August, Jakarta, Indonesia. http://dx.doi.org/10.2118/114684-MS.

Aadnoy, B. S., Fazaelizadeh, M., and Hareland, G. (2010). A 3D Analytical Model for Wellbore Friction. *J Can Pet Technol* 49 (10): 25-36. http://dx.doi.org/10.2118/141515-PA.

Al Saedi, A., Flori, R.E., and Kabir, C.S. (2018). New analytical solutions of wellbore fluid temperature profiles during drilling, circulating, and cementing operations. *J Pet Sci & Eng* 170: 206-217. http://dx.doi:10.1016/j.petrol.2018.06.027.

Arnold, F. C. (1990). Temperature Variation in a Circulating Wellbore Fluid. *J Energy Resour Tech*, 112 (2): 79-83. http://dx.doi.org/10.1115/1.2905726.

Edwardson, M., Girner, H., Parkison, H. (1962). Calculation of Formation Temperature Disturbances Caused by Mud Circulation. *J Pet Technol* 14 (4): 416-426. http://dx.doi.org/10.2118/124-PA.

Gao, Y., Sun, B., Xu, B. (2017). A Wellbore/Formation-Coupled Heat-Transfer Model in Deepwater Drilling and Its Application in the Prediction of Hydrate-Reservoir Dissociation. *SPE J*. 22 (3): 756-766. http://dx.doi.org/10.2118/184398-PA.

Giancoli, D. C. (2013). Physics for Scientists & Engineers with Modern Physics, Vol. 3 (Chs 36-44). Harlow: Pearson Education UK.

Hasan, A.R., Kabir, C.S., and Ameen, M. (1996). A Fluid Circulating Temperature Model for Workover Operations. *SPE J.* 1 (2): 133-144. http://dx.doi.org/10.2118/27848-PA.

Holmes, C. S., and Swift, S. C. (1970). Calculation of Circulating Mud Temperatures. *J Pet Techno*l 22 (6): 670-674. http://dx.doi.org/10.2118/2318-PA.

Kabir, C.S., Hasan, A.R., and Kouba, G. (1996). Determining Circulating Fluid Temperature in Drilling, Workover, and Well Control Operations. *SPE Drill & Compl* 11 (2): 74-79. http://dx.doi.org/10.2118/24581-PA.

Keller, H., Couch, E., and Berry, P. (1973). Temperature Distribution in Circulating Mud Columns. SPE J. 13 (1): 23-30. http://dx.doi.org/10.2118/3605-PA.

Kumar, A., and Samuel, R. (2012). Analytical Model to Estimate the Downhole Temperatures for Casing while *Drilling Operations. SPE Annual Technical Conference and Exhibition*, 8-10 October, San Antonio, Texas, USA. http://dx.doi.org/10.2118/159278-MS.

Kumar, A., Singh, A.P., and Samuel, R. (2012a). Analytical Model to Predict the Effect of Pipe Friction on Downhole Temperatures for Extended Reach Drilling (ERD). Paper SPE-151254-MS presented at the *IADC/SPE Drilling Conference and Exhibition*, 6-8 March, San Diego, California, USA. http://dx.doi.org/10.2118/151254-MS.

Kumar, A., Singh, A. P., and Samuel, R. (2012b). Field Application of an Analytical Model for Estimating the Downhole Temperatures due to Wellbore Friction. Paper SPE-156307-MS presented at the *IADC/SPE Asia Pacific Drilling Technology Conference and Exhibition*, 9-11 July, Tianjin, China. http://dx.doi.org/10.2118/156307-MS.

Kumar, A. and Samuel, R. (2013). Analytical Model to Predict the Effect of Pipe Friction on Downhole Fluid Temperatures. SPE *Drill & Compl* 28 (3): 270-277. http://dx.doi.org/10.2118/165934-PA.

Marshall, D. W. and Bentsen, R. G. (1982). A Computer Model to Determine the Temperature Distributions in a Wellbore. *J Can Pet Technol* 21 (1): 63-75. http://dx.doi.org/10.2118/82-01-05.

Mirhaj, S. A., Kaarstad, E., and Aadnoy, B. S. (2016). Torque and Drag Modeling; Soft-string versus Stiff-string Models. Paper-178197-MS presented at the *SPE/IADC Middle East Drilling Technology Conference and Exhibition*, 26-28 January, Abu Dhabi, UAE. http://dx.doi.org/10.2118/178197-MS.

Powers, D. L. (2010). Boundary Value Problems: and Partial Differential Equations. Amsterdam: Elsevier/Academic Press.

Raymond, L. (1969). Temperature Distribution in a Circulating Drilling Fluid. *J Pet Technol* 21 (3): 333-341. http://dx.doi.org/10.2118/2320-PA.

Samuel, G. R. (2007). Downhole Drilling Tools: Theory and Practice for Engineers and Students. Houston, TX: Gulf Pub.

Tragesser, A. F., Crawford, P. B., and Crawford, H. R. (1967). A Method for Calculating Circulating Temperatures. *J Pet Technol* 19 (11): 1507-1712. http://dx.doi.org/10.2118/1484-PA.

# III. EXPLORING ALTERATION OF NEAR-WELLBORE GEOTHERMAL GRADIENT DURING FLUID CIRCULATION AND PRODUCTION

A.Q. Al Saedi, R. E. Flori, and C. S. Kabir

Missouri University of Science and Technology

(Published in Journal of Petroleum Science and Engineering 177 (2019) 909-920)

## ABSTRACT

The constant undisturbed formation temperature profile controlling heat transfer into the wellbore appears counterintuitive in light of transient cooling of the formation that occurs upon fluid circulation in drilling and also heating during fluid production.

This study presents a mathematical model that shows that the heat transfer occurs from the wellbore/formation interface, not from some distance away from the wellbore wherein the initial formation temperature profile remains undisturbed. This new model allows investigation of heat transfer behavior from the formation into the wellbore during drilling or fluid circulation, and from the wellbore into the reservoir in the production mode.

Application of the line-source solution for the temperature diffusivity equation for a steady-state system provides the necessary ingredients for computing the temperature behaviors at different times and radii. This line-source solution can be used throughout the wellbore to determine the undisturbed formation temperature, which may be used to obtain the geothermal gradient dependent on the radius and fluid circulation time. Therefore, the initial geothermal gradient works as a time-dependent variable, and the resultant second-order polynomial relationships can describe the undisturbed formation temperature.

This study provides the required tools to assess the wellbore heat-transfer behavior and their effect on the wellbore temperature profiles. Also, the new mathematical model illuminates the impact of heat transfer by comparing its performance with the original formulations. Besides, this paper presents a complete derivation of the line-source solution of the temperature diffusivity equation to justify the proposed approach.

## 1. INTRODUCTION

Conservation of energy for both conductive and convective heat transfer underpins all studies while assessing the wellbore temperature profiles. When a temperature difference exists, conductive heat transfer occurs between the adjacent formation with the cooler wellbore, and between the outer and inner diameter of different tools inside the wellbore. In this context, the convective heat transfer occurs in the drilling or circulating fluid itself. In a drilling operation, the adjacent formation temperature remains higher than the wellbore fluid temperature, given the formation's geothermal gradient; therefore, the direction of heat flow will be from the reservoir toward the wellbore. This heat flow direction reverses itself during a well's production mode.

Two types of studies have emerged based on the direction of heat flow. In the first group the direction of heat flow occurs from the wellbore to the formation, such as those presented by Holmes and Swift (1970), Keller et al. (1973), Marshall and Bentsen (1982), Arnold (1990), Sagar et al. (1991), Kumar and Samuel (2013), Guo et al. (2016), and Gao et al. (2017), among others. The second group considered the heat flow direction from the initial formation temperature into the wellbore, such as those offered by Raymond (1969), Hasan

and Kabir (1994), Hasan et al. (1996), and Kabir et al. (1996). The difference between these two approaches is the amount of heat transfer that occurs after obtaining the wellbore temperature profile. For example, Holmes and Swift (1970) presented a solution for the steady-state heat transfer in a drillpipe and annulus surrounded by the formation. In contrast, Kabir et al. (1996) and Hasan et al. (1996) obtained solutions for forward and reverse-circulation cases for the variable mud-tank temperature of the circulating fluid.

Many studies also attempted to determine the formation temperature based on well logging measurements, such as those of Schoeppel and Gilarranz (1966), Prensky (1992), and Forrest and Scott (2007), among others. In contrast, others attempted to use the extrapolation of the bottomhole transient temperature for the static-formation temperature, as presented in Dowdle and Cobb (1975), Kritikos and Kutasov (1988). Moreover, Kutasov and Eppelbaum (2005) provided a mathematical model to determine the formation temperature from the bottom-hole logs by the generalized Horner method.

More recently, Kutasov and Eppelbaum (2018) presented a new approach to estimating the undisturbed formation temperature from shut-in temperature openhole logs for deep wells. They modified the Horner plot by adopting a new circulation and shut-in time concept to find the undisturbed formation temperature. Regardless of the methodology, once the formation temperature obtained, the geothermal gradient can be established.

For conservation of energy in any system, the formation temperature estimation largely depends on the type of boundary condition used in the solution of that system. We implemented two boundary conditions, the Dirichlet condition as the traditional one and the Robin condition as presented recently by Al Saedi et al. (2018), leading to different

geothermal gradients. The intrinsic idea was to cover a wide range of possible temperature profiles that may emerge due to operational considerations.

The purpose of this study is to offer a new analytical model to show the behavior of wellbore heat transfer after obtaining the wellbore fluid temperature for the normal or wellbore-to-formation heat flow directions. Application of the line-source solution for the temperature diffusivity equation allows us to investigate the appropriate radius and time of the undisturbed formation temperature from which the heat transfer occurs. The steady-state heat transfer model underpins these solutions for both fluid circulation and production.

## 2. MODEL DEVELOPMENT

### 2.1. FLUID CIRCULATION MODEL

For a steady-state system in radial coordinates, we assume that the heat transfer occurs from the initial formation temperature to some other formation close to the wellbore "invaded zone formation," and then to the outer wellbore radius, and finally to the annulus and by keeping the same assumption for inside the wellbore. Then by applying the heat energy balance for the suggested system presented by Figure 1.

Mathematically, for normal circulation of the fluid flow inside the drillpipe, we can represent the heat energy system by the following expression:

$$Q_{p_z} - Q_{p_{z+\mathrm{d}z}} + Q_{ap} = 0 \tag{1}$$

and heat transfer by applying the conservation of energy inside the annulus can be written as

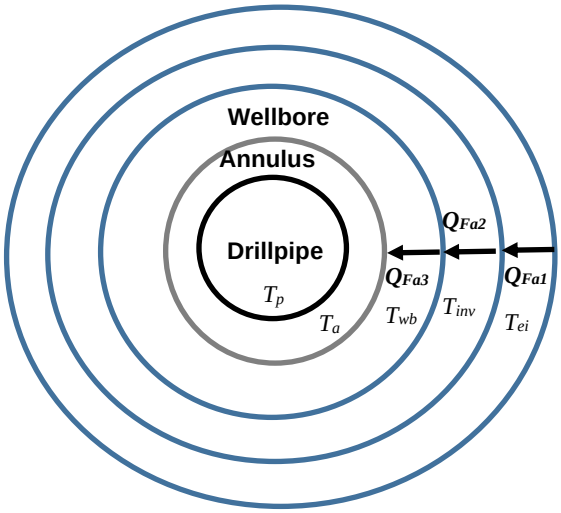


Figure 1. Heat transfer through different conduits.

$$Q_{a_{z+\mathrm{d}z}} - Q_{a_z} + Q_{Fa\mathrm{d}} - Q_{ap} = 0 \tag{2}$$

The solution of the energy system given by Eqs. 1 and 2 results in the final mathematical forms for drill-pipe and annular temperature as

$$T_P = K_1 e^{C_1 z} + K_2 e^{C_2 z} + g_T.z + T_S - g_T.A \tag{3}$$

$$T_a = K_1 C_3 e^{C_1 z} + K_2 C_4 e^{C_2 z} + g_T.z + T_S \tag{4}$$

where $C_1$ and $C_2$ refer to the thermal properties constants, and the $K_1$ and $K_2$ refer to the constants depends on the given boundary condition.

However, with the heat flow direction in our model starting from the formation toward the wellbore, we use more than one boundary condition to solve the system at total depth. This approach leads to the line-source solutions for investigating the formation temperature gradient. Appendix A presents the details of the solutions.

## 2.2. PRODUCTION MODEL

For the production model, the fluid flow from the sandface into the wellbore and then produced to surface by way of the tubing or annulus or both. Figure 2 depicts the production system of interest.

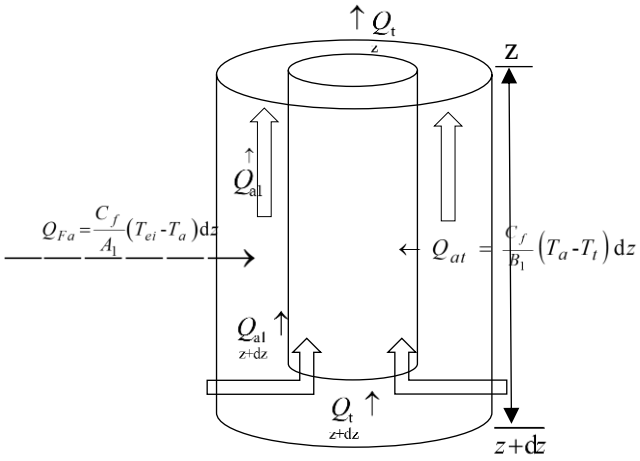


Figure 2. Schematic of a production system.

When the formation retains the highest energy source in the system, the direction of heat flow will be from the formation into the annulus and onto the tubing. The following expression describes the energy balance for the tubing:

$$\underset{z+dz}{Q_t} - \underset{z}{Q_t} + Q_{at} = 0 \tag{5}$$

and the annular energy balance can be written as

$$\underset{z+dz}{Q_{a1}} - \underset{z}{Q_{a1}} + Q_{Fa} - Q_{at} = 0 \tag{6}$$

Again, the solution for the system of equations described by Eqs. 5 and 6 are given by Eqs. 7 and 8

$$T_t = \alpha_1 e^{\lambda_1 z} + \alpha_2 e^{\lambda_2 z} + g_T z + T_s + 2A_1 g_T - B_1 g_T \quad (7)$$

$$T_a = \alpha_1 \lambda_3 e^{\lambda_1 z} + \alpha_2 \lambda_4 e^{\lambda_2 z} + T_s + g_T z + 2A_1 g_T - 2B_1 g_T \quad (8)$$

Appendix B presents the solution details.

## 2.3. LINE-SOURCE SOLUTION FOR THE TEMPERATURE DIFFUSIVITY EQUATION

Many authors have long recognized the analogy of the temperature diffusivity equation with that of the pressure diffusivity equation. Studies presenting the line-source solution for the pressure diffusivity equation include those offered by van Everdingen and Hurst (1949), Mathews and Russell (1967), and Dake (1978), among others. The analogy between the pressure and temperature diffusivity equations allows us to use the same procedure as presented by Dake (1978) to solve the temperature diffusivity equation. We can represent the formation temperature as a function of time and radius by adapting the line-source solution of the pressure diffusivity equation.

By adopting the same pressure line-source solution procedure presented by Dake (1978) for the temperature diffusivity equation given by Eq. C-1 in Appendix C, we obtained a line-source solution in field units as

$$T_{(r,t)} = T_{ei} + 0.68\left(\frac{Q_r}{hk_e}\right) E_i\left(\frac{-c_e \rho_e r^2}{4k_e t}\right) \quad (9)$$

where $E_i(-x)$ represent the exponential integral, which always results in a negative value resulting from the normal heat flow direction. Therefore, the temperature at any radius and time will be less than the initial temperature value ($T_{ei}$). Also, the approximation of the $E_i$ function to natural logarithm becomes feasible when the value of $x$ very small or time becomes

large. With this temperature line-source solution, other applications may be performed in the context of transient testing.

By knowing the bottomhole temperature, the initial formation temperature can be used to calculate the geothermal gradient as a function of radius and time by the following expression:

$$g_T = \frac{\left\{T_{wb} - \left[\left(\frac{0.68Q_r}{hk_e}\right)E_i\left(\frac{-c_e\rho_e {r_{wb}}^2}{4k_e t}\right)\right]\right\} - T_s}{D_{TV}} \tag{10}$$

Appendix C presents the details of the derivation.

## 3. MODEL VERIFICATION

### 3.1. FLUID CIRCULATION MODEL

To verify the drilling or circulation model, we used the dataset presented by Holmes and Swift (1970) for a steady-state system. Unlike the Holmes and Swift approach, the temperature profiles result from the heat transfer from the formation into the wellbore. By using the Dirichlet and Robin conditions, we obtained the drillpipe and annular temperature profiles as shown in Figure 3. Our goal was to investigate the heat-transfer behavior from the wellbore temperature profiles, which leads to an accurate formation temperature behavior estimation and, therefore, the geothermal gradient.

Figure 3a suggests that at the total depth (15,000 ft), the drillpipe and annular temperature are the same at 174.86 ˚F, which results by using the boundary condition of first kind or the Dirichlet condition. In contrast, Figure 3b shows different temperature behavior resulting from applying the Robin condition. The formation temperature will be equal to 250

˚F, which represents a linear relationship of $T_{ei} = g_T.z+T_s$. Where the geothermal gradient $g_T$ equal to 0.0127 ˚F/ft, as given in the Holmes and Swift (1970) dataset.

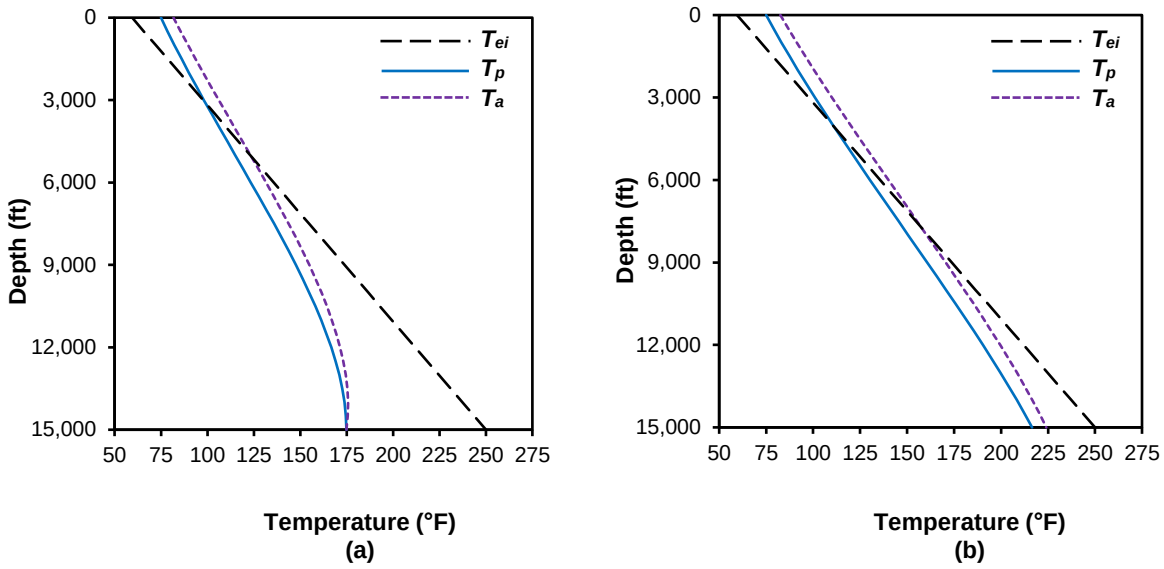


Figure 3. Wellbore temperature profiles, Dirichlet condition (a), Robin condition (b).

Note that the overall-heat-transfer coefficient across the drillpipe is 15 Btu/ft$^2$-˚F-hr, whereas that across the wellbore face is about 0.5 Btu/ft$^2$-˚F-hr. For the total depth at 15,000 ft, we have the drillpipe and annular temperatures. This information facilitates calculation of the amount of heat transfer from the formation into the annulus and then into the drillpipe based on heat flow equations used for this model, as given by Eqs. A-3, A-2, A-7, respectively. Tables 1 and 2 present the results obtained by the Dirichlet condition and by the Robin condition, respectively.

Table 1. Results by using the Dirichlet condition.

| Depth (ft) | $T_{ei}=g_T.z+T_s$ (°F) | $T_p$ (°F) | $T_a$ (°F) | $Q_{ap}$ (Btu/hr) | $mc_f(T_{az+dz}-T_{az})$ (Btu/hr) | $Q_{Fad}$ (Btu/hr) | $T_{ei,new}$ (°F) | $g_{T,new}$ (°F/ft) |
|---|---|---|---|---|---|---|---|---|
| 14,500 | 243.65 | 174.59 | 175.61 | 26,342.62 | -7,722.52 | 34,065.14 | 223.36 | 0.011301 |
| 15,000 | 250 | 174.86 | 174.86 | 0 | -37,643.09 | 37,643.09 | 227.63 | 0.011209 |

Table 2. Results by using the Robin condition.

| Depth (ft) | $T_{ei}=g_T.z+T_s$ (°F) | $T_p$ (°F) | $T_a$ (°F) | $Q_{ap}$ (Btu/hr) | $mc_f(T_{az+dz}-T_{az})$ (Btu/hr) | $Q_{Fad}$ (Btu/hr) | $T_{ei,new}$ (°F) | $g_{T,new}$ (°F/ft) |
|---|---|---|---|---|---|---|---|---|
| 14,500 | 243.65 | 212.51 | 220.43 | 206,041.21 | 194,495.82 | 11,545.39 | 236.61 | 0.012215 |
| 15,000 | 250 | 216.51 | 224.08 | 197,000.48 | 184,089.48 | 12,910.99 | 242.18 | 0.012179 |

From the tables above, we have two values for the formation temperature at the bottomhole. They include the old static formation temperature (dashed black) calculation based on the given geothermal gradient (0.0127 ˚F/ft) and the new formation temperature gradient (green) obtained as a result of the heat- transfer. As Figure 4 suggests, different model temperatures emerge, including that of the proposed model for drilling and fluid circulation. The temperatures of the drill-pipe and the annulus were calculated based on the old geothermal gradient value.

The new formation temperature calculated from the heat-transfer between the adjacent formation and the annulus may refer to the invaded zone temperature because of the direction of heat flow. Then, the new geothermal gradient may recalculate form the wellbore, invaded zone, and the new formation temperatures values.

Figure 5 presents the differences between the old geothermal gradient and the new geothermal gradient.

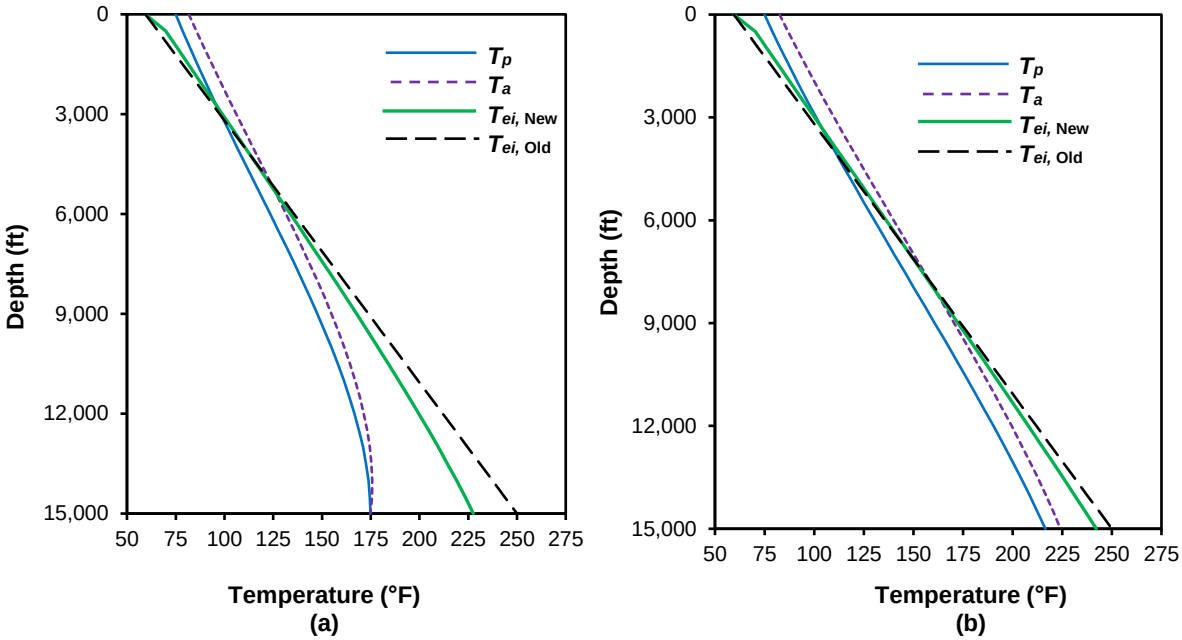


Figure 4. Wellbore temperature profiles based on Dirichlet condition (a), and Robin condition (b).

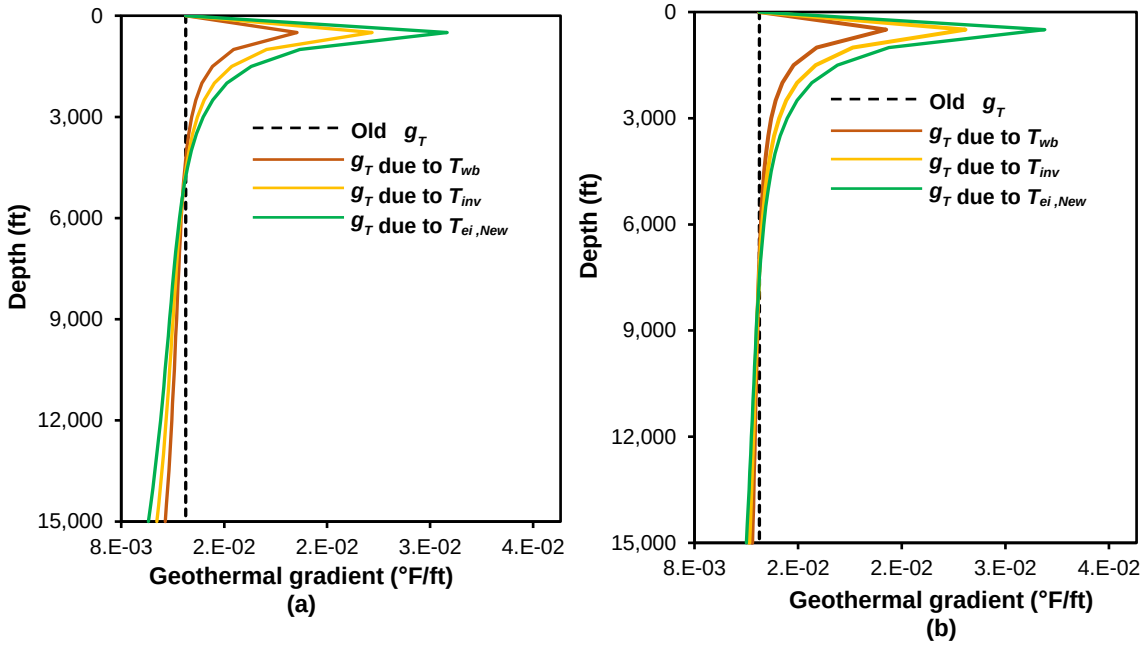


Figure 5. Comparison between the old and new geothermal gradients using the Dirichlet condition (a), and Robin condition (b).

## 3.2. PRODUCTION MODEL

Upon initiation of production, the producing fluid carries thermal energy into the wellbore. Therefore, the thermal energy generated by the production model will result in different temperature profiles in comparison to the drilling or circulation model. For simplicity, we presuppose that the Joule-Thomson heating or cooling due to fluid expansion in the reservoir does not occur in systems of interest. Table 3 presents a dataset that we used to verify the application of our proposed production model.

Table 3. The production model dataset.

| | |
|---|---|
| Vertical well depth, ft | 15,000 |
| Production casing OD, in. | 7 |
| Tubing OD, in. | 5 1/2 |
| Tubing ID, in. | 4 |
| Flow rate, STB/D | 5,000 |
| Production time, hr | 24 |
| Annular surface temperature, °F | 150 |
| Annular bottomhole temperature, °F | 209 |
| Oil specific heat, Btu/(lbm-°F) | 0.4 |
| Oil density, lbm/ $ft^3$ | 60 |
| Formation thermal conductivity, Btu/(ft-°F-hr) | 1.3 |
| Formation specific heat, Btu/(lbm-°F) | 0.2 |
| Formation density, lbm/ $ft^3$ | 165 |
| Surface earth temperature, °F | 59.5 |
| Geothermal gradient, °F/ft | 0.0127 |

Figure 6 shows the results of the application of the suggested system of equations (Eqs. 7 and 8) by using the Robin condition and that obtained from the Prosper solution. Figure 6a compares the model's solution for tubing flow with that of a commercial software package (Prosper).

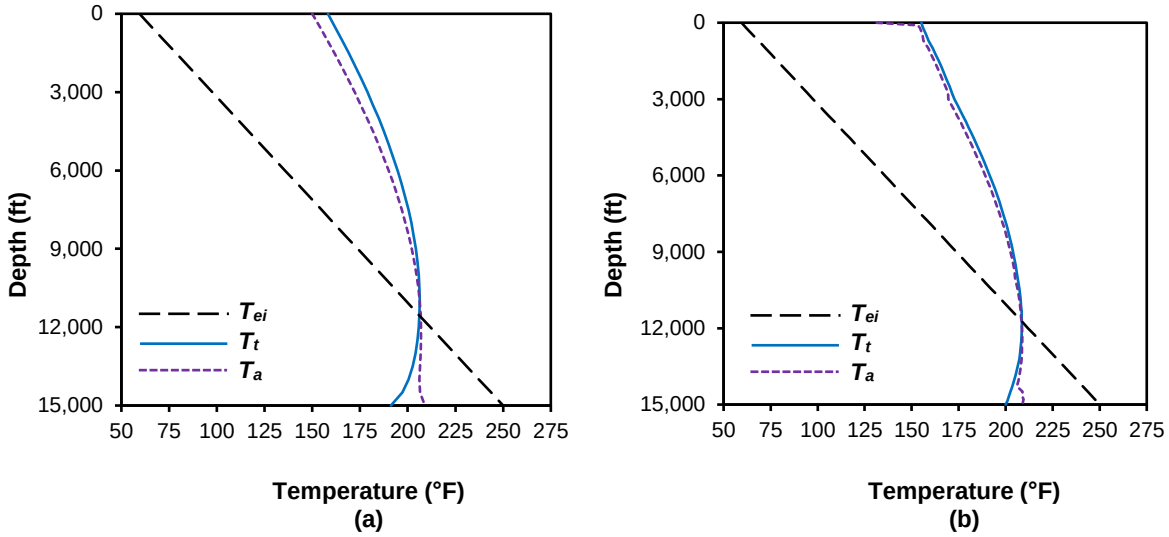


Figure 6. Wellbore temperature profile, proposed model (a), and Prosper solution (b).

In this case, we used the overall-heat-transfer coefficient across the wellbore face $U$ of 30.25 Btu/ft$^2$-hr-˚F and for the overall-heat-transfer coefficient across the tubing $U_t$ about 9 Btu/ft$^2$-hr-˚F. We generated another case wherein production occurs through the tubing and annulus for the same dataset given in Table 4.

Table 4. Results of Robin condition.

| Depth (ft) | $T_{ei}=g_T.z+T_s$ (°F) | $T_t$ (°F) | $T_a$ (°F) | $Q_{at}$ (Btu/lbm) | $wc_t(T_{az+dz}-T_{az})$ (Btu/lbm) | $Q_{Fa}$ (Btu/lbm) | $T_{ei,new}$ (°F) | $g_{T,new}$ (°F/ft) |
|---|---|---|---|---|---|---|---|---|
| 14,500 | 243.65 | 197.20 | 206.45 | 1.7 | 0.14 | 1.56 | 251.82 | 0.0133 |
| 15,000 | 250 | 191.26 | 209.26 | 3.27 | 1.01 | 2.25 | 274.39 | 0.0143 |

The software result for the wellbore temperature given by Figure 6b. As Figure 7 shows, the tubing and annular temperature profiles obtained by the application of our suggested model appear in good alignment with those obtained from Prosper.

Again, for the total depth or at (15,000 ft), we have the tubing and annular temperatures; then we can calculate the amount of heat transfer from the formation to the wellbore based on the heat flow equations used for this model, as given by Eqs. B-4, B-2, B-8, respectively, in Table 4. Figure 8 shows all the temperatures assumed in the production model and the geothermal gradient based on those temperatures.

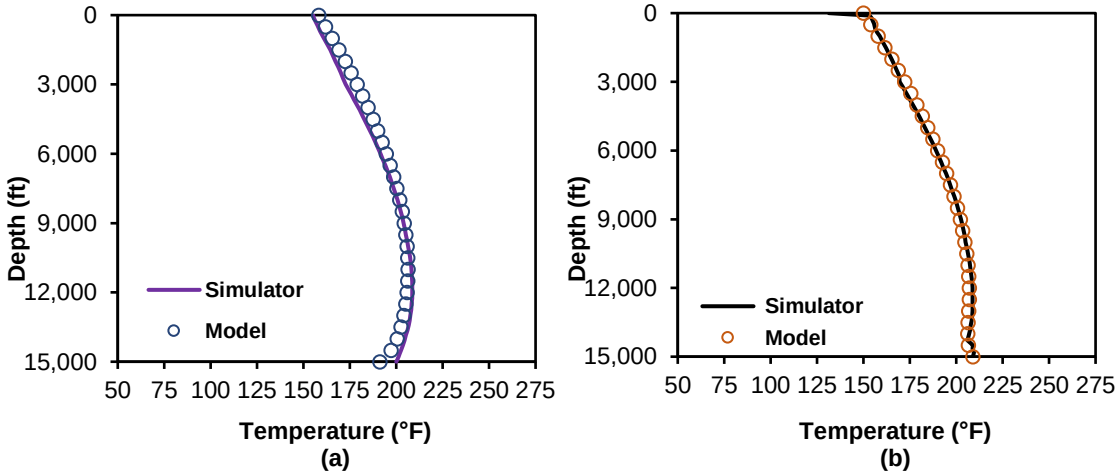


Figure 7. A comparison between the model and Prosper results, tubing profile (a), annular profile (b).

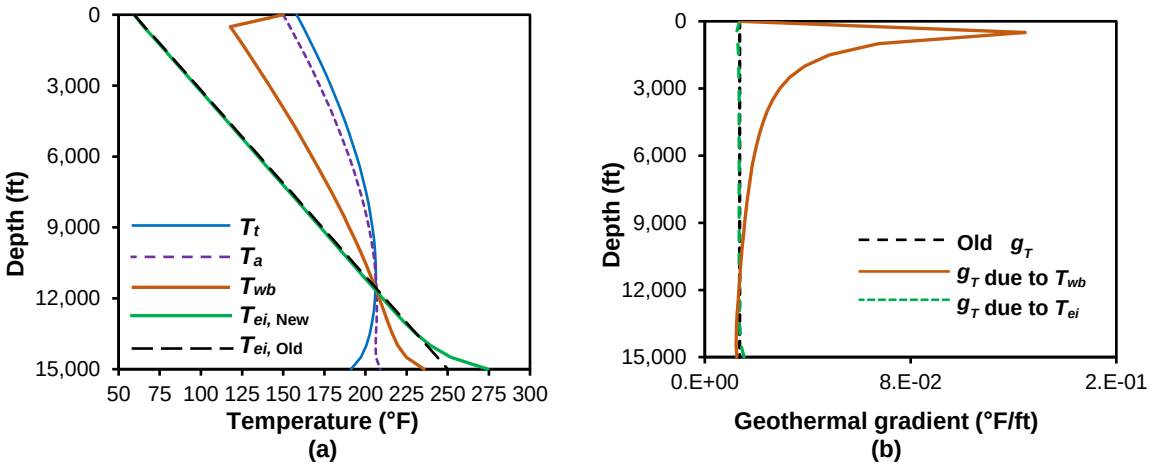


Figure 8. Results of the production model, temperature profile (a), and geothermal gradient (b).

# 4. APPLICATION OF MODELS

In this section, we present the formation temperature distributions by using the temperature line-source solution, as shown in Appendix C. Rewriting Eq. 9 in dimensionless form leads to the following expression:

$$T_{cD} = -E_i\left(\frac{-r_D^2}{4t_{cD}}\right) \tag{11}$$

Plotting the two variables of Eq. 11 on a semilog graph, as given by Figure 9, presents the expected straight-line signatures based on the log-approximation of the $E_i$ function.

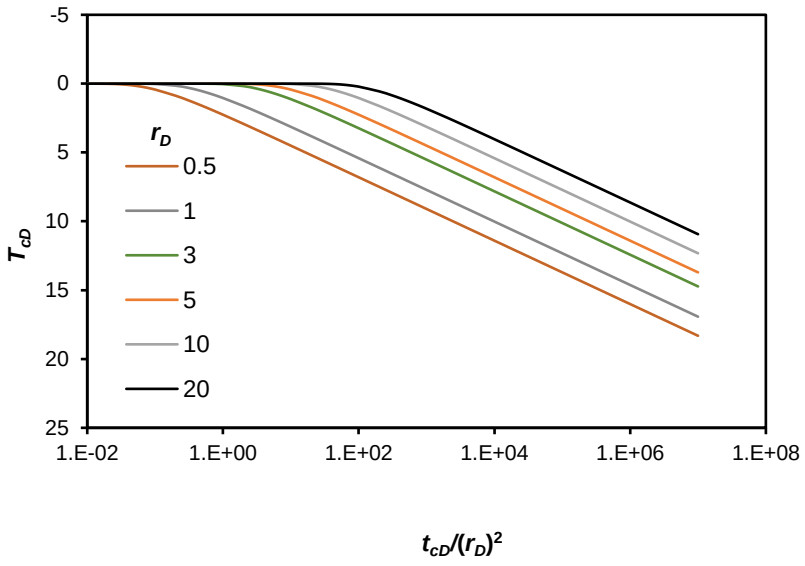


Figure 9. Dimensionless temperature profiles for different radii away from the wellbore.

At the total depth, the amount of heat transfer presented in Tables 1 and 2 for the drilling or circulation model result from the direction of heat flow; that is, from the formation to the wellbore. By knowing the amount of heat flow into the wellbore, and the initial formation

temperature which is about 250 °F, we can apply the line-source solution presented by Eq. 9 to determine temperature profile at any time and radius as given by Figure 10.

Figure 10 suggests that the temperature profiles will always be below the initial-formation temperature, and the effect of heat transfer will continue from the wellbore to 12 ft away from the wellbore. The same behavior occurs when the initial formation temperature set at 230 °F as opposed to 250 °F.

Some authors surmised that the effect of heat transfer would stop after 10 ft, given that the value of $E_i$ (-$x$) function becomes zero as long as (-$x$) equals to 10.

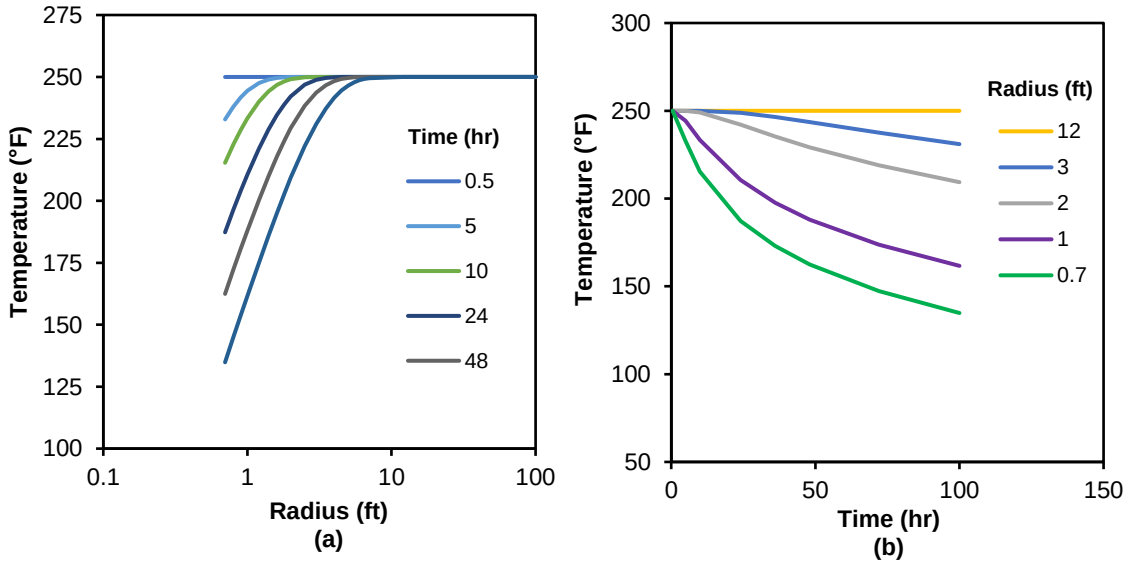


Figure 10. Application of the Ei solution at the total depth for different radii (a), and time domain (b).

However, heat transfer may continue beyond this radius until the transients reach the uninvaded zone wherein the initial formation temperature prevails. When the circulation stops, one can recalculate the wellbore temperature by applying the line-source solution at different times, as shown in Figure 11.

Note that Figure 11 shows various wellbore temperature profiles for the entire wellbore, but the critical reference temperature point occurs at the total depth, and it remains static. However, after 0.35 hr the wellbore temperature approximately equals the initial-formation temperature, then at 6.3 hr, the wellbore temperature will decrease to the new calculated formation temperature of about 226 $^{o}$F, and so on. Finally, it will be equal to the circulating temperature profile at 34.15 hr. The production model, when solved by using the Robin condition shows a similar effect of the radius which was about 12 ft from the wellbore, but it gives a different temperature behavior at total depth resulting from the use this boundary condition.

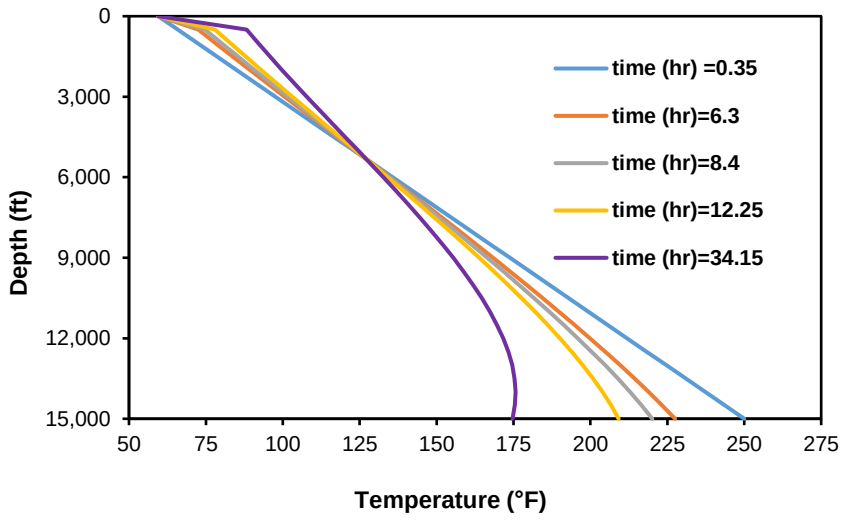


Figure 11. Wellbore temperature profile by applying Eq. 9 for Table 1 data.

The preceding discussion suggests that the formation temperature is 250 ˚F at the total depth, which was calculated based on the original geothermal gradient of 0.0127 ˚F/ft. Note that the wellbore temperature at the total depth is about 174.86 ˚F. After applying the steady-state circulation model, we obtained the temperature profile inside the wellbore that led us to

recalculate the heat-transfer rate from the adjacent formation to inside the wellbore. Based on the new calculations, the adjacent formation temperature of about 227.63 ˚F turned about to be the ‘new’ formation temperature, which prompted the actual heat-transfer toward the wellbore.

The well-known industry practice suggests that the geothermal gradient calculation result from the difference between the static or initial-formation temperature recorded at the well bottom and the constant surface temperature divided by the depth. Application of the line-source solution leads to the formation temperature; then the geothermal gradient will depend on time and radius as given by Eq. 10. Therefore, the new formation temperature will yield a new geothermal gradient of 0.0114 ˚F/ft for the drilling and circulation problem solved by the Dirichlet condition, and about 0.0122 ˚F/ft when solved by the Robin condition. As Figure 12 illustrates the new geothermal gradients precipitate the lowering of wellbore temperature profiles.

The preceding content suggests that the formation temperature gradient not only depends on time but also on depth and geothermal gradient. Figure 13 represents the geothermal and formation temperature behaviors for different times at total depth for the system of equations solved by the Dirichlet condition.

When the Robin condition applies, Figure 14 shows the corresponding results. Both figures suggest that the geothermal gradient and the formation temperature have a second-order polynomial relationship with time. We may logically infer that the heat transfer does not occur from the initial formation temperature per se due to the circulation of mud.

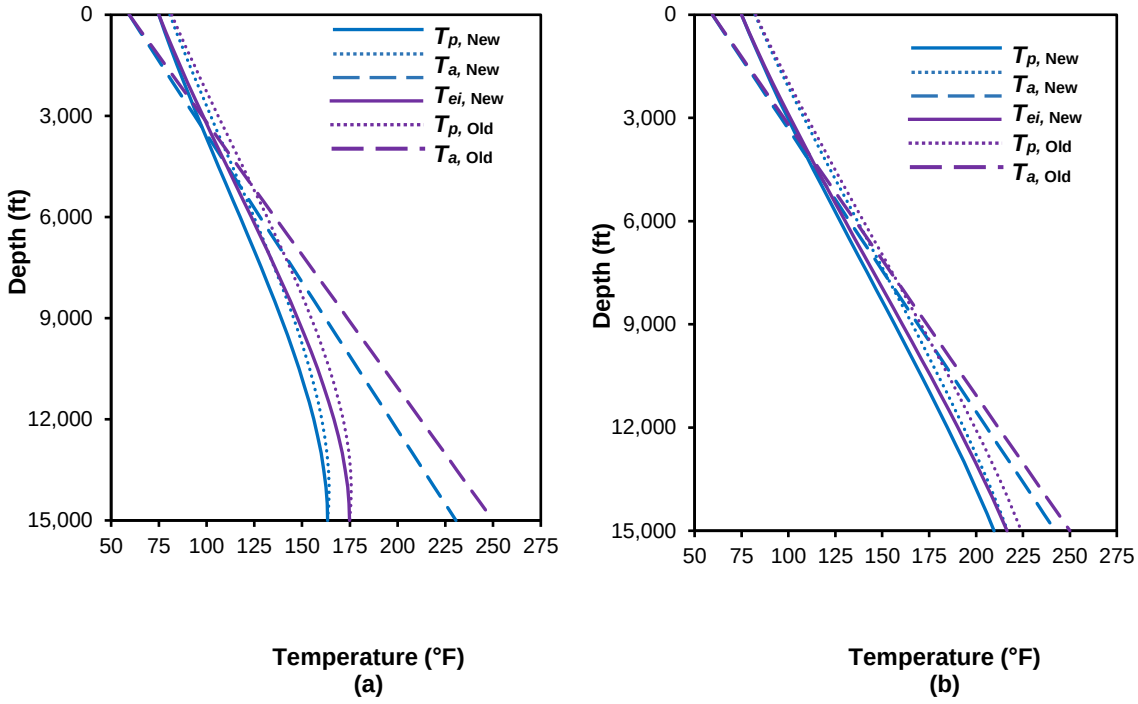


Figure 12. Total depth wellbore temperature due to the different geothermal gradient, Dirichlet condition (a), Robin condition (b).

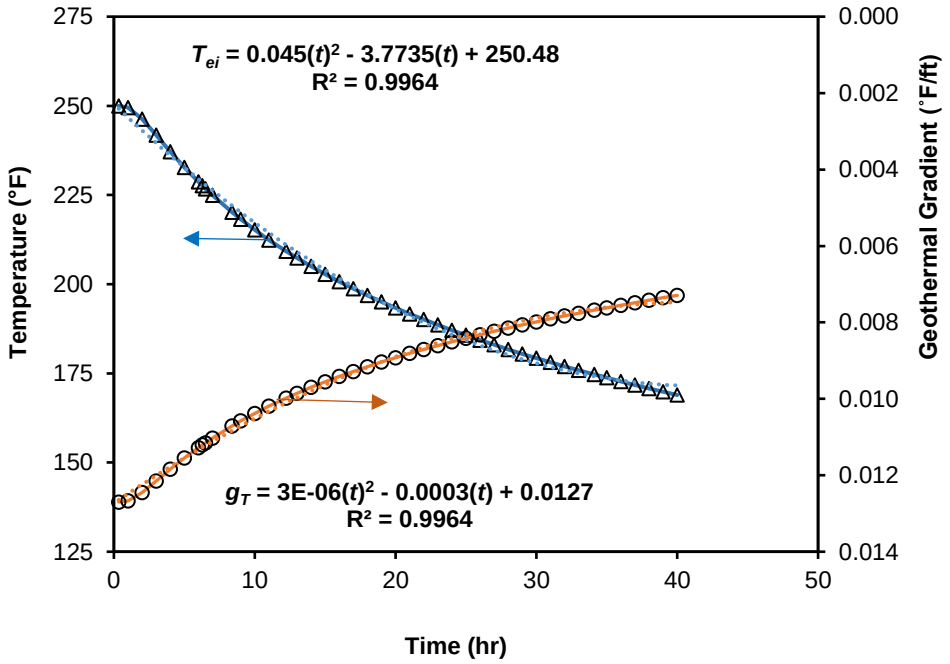


Figure 13. Geothermal gradient and formation temperature behavior with time.

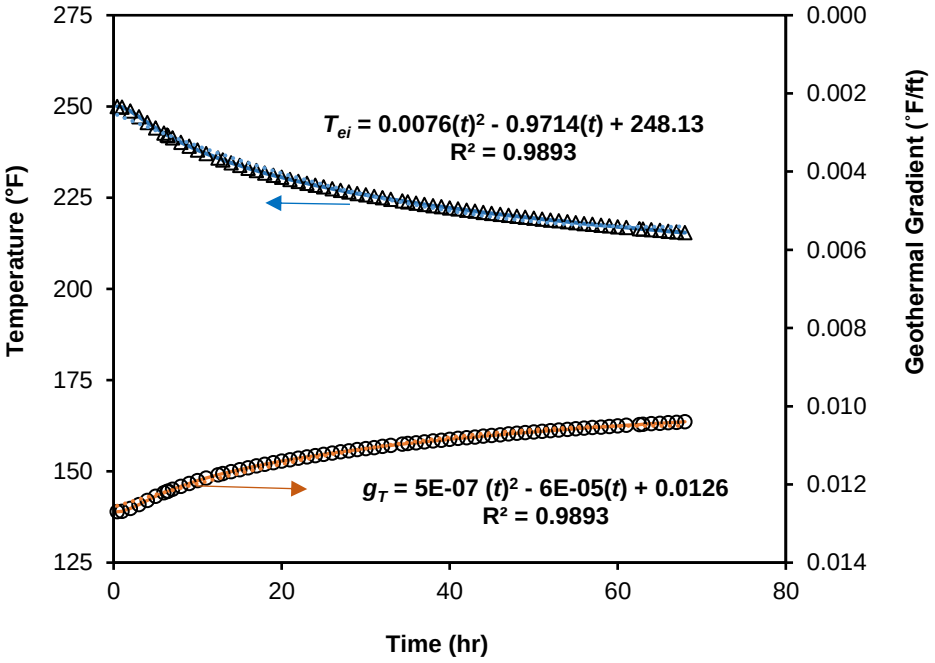


Figure 14. Geothermal gradient and formation temperature behavior with time.

## 5. DISCUSSION

This study proposes new mathematical models to determine the rate of heat transfer involving the entire wellbore profile during fluid circulation and production. Both models show that the temperature gradient is time-dependent and that the initial-formation temperature neither at the well bottom nor in the entire profile remains static. The amount of the thermal energy transferred into the wellbore during fluid circulation and away from it during fluid production affect the wellbore temperature profiles. In other words, the transient nature of the temperature profile associated with heat flow in either direction precipitates this movable boundary condition, which requires appropriate treatment before initiating any computations.

The calculated heat flow from the wellbore temperatures depends on the assumed heat flow direction as discussed in the Introduction. For instance, if the direction of heat flow occurs from the wellbore to the formation during fluid circulation, then the heat flow will have a negative value, which leads to higher wellbore temperature than the initial-formation temperature. In many cases, the amount of heat flow data required for the application of the line-source solution may be unavailable, but we may have just the time-dependent wellbore temperature data. Therefore, the use of the dimensionless line-source solution provides us with the proper procedure to determine the initial-formation temperature, as the field example illustrates.

Application of the line-source solution of the temperature diffusivity equation allows estimation of the wellbore temperature profiles at total depth regardless of the direction of heat flow. Both the initial-formation temperature and geothermal gradient are time-dependent that affect the wellbore temperature behavior. Verification of the proposed fluid-circulation model with the widely used data of Holmes and Swift (1970) and the fluid production model results with a commercial software Prosper instills confidence. Furthermore, we validated the fluid-circulation model with a field data set. Note that in fluid flow modeling in the reservoir we assumed the isothermal response, meaning Joule-Thompson heating or cooling is negligible.

Our perception is that recognition of the changing initial condition will result in more accurate heat transfer calculations, leading to improved tubular design and operational management. For instance, the annular-pressure buildup arising from excessive heating of the trapped annular fluid that adversely impacts the fluid withdrawal rate is a case in point.

Similarly, issues arising from the sustained casing pressure due to leakage of the tubular fluid into the annulus may also be very relevant.

## 6. CONCLUSIONS

The following conclusions appear pertinent here:

1. The proposed analytical models are rooted in the line-source solution of the temperature diffusivity equation. These models address heat flow during steady-state fluid circulation or fluid production in a wellbore.
2. The model results suggest that the heat transfer depends largely on the altered initial-formation temperature distribution at the sandface. A constant temperature gradient occurs some distance away from the wellbore (about 10 ft), regardless of the heat flow direction during either fluid circulation or production.
3. The initial formation temperature at the well bottom and the geothermal gradient depend on time, and second-order polynomial expressions can describe their nonlinearity.

## NOMENCLATURE

$\alpha_1$ = parameter defined by Eq. B-21, ˚F

$\alpha_2$ = parameter defined by Eq. B-22, ˚F

$\lambda_1$ = parameter defined by Eq. B-17, 1/ft

$\lambda_2$ = parameter defined by Eq. B-18, 1/ft

$\lambda_3$ = parameter defined by Eq. B-19, dimensionless

$\lambda_4$ = parameter defined by Eq. B-20, dimensionless

$A$ = parameter defined by Eq. A-10, ft

$A_1$ = parameter defined by Eq. B-9, ft

$B$ = parameter defined by Eq. A-10, ft

$B_1$ = parameter defined by Eq. B-5, ft

$C_1$ = parameter defined by Eq. A-19, dimensionless

$C_2$ = parameter defined by Eq. A-20, dimensionless

$C_3$ = parameter defined by Eq. A-21, dimensionless

$C_4$ = parameter defined by Eq. A-22, dimensionless

$C_f$ = heat capacity of fluid (mud or oil), Btu/ $lb_m$-˚F

$D_{TV}$ = true vertical depth, ft

$g_T$ = geothermal gradient, ˚F/ft

$h_p$ = overall heat transfer coefficient across the drillpipe, Btu/$ft^2$-˚F-hr

$K_1$ = parameter defined by Eq. A-23, ˚F

$K_2$ = parameter defined by Eq. A-24 or 25, ˚F

$k_e$ = formation thermal conductivity, Btu/hr-ft-˚F

$L$ = total measured depth, ft

$Q_a$ = heat flow in annulus, Btu/hr

$Q_{a1}$ = heat flow in annulus, Btu/lbm

$Q_{ap}$ = heat flow across drillpipe, Btu/hr

$Q_{at}$ = heat flow across drillpipe, Btu/lbm

$Q_{Fa}$ = heat flow from formation to annulus, Btu/lbm

$Q_{Fad}$= heat flow from formation to annulus, Btu/hr

$Q_p$ = heat source inside drillpipe, Btu/hr

$Q_r$ = radial heat flow, Btu/hr

$R$ = parameter defined by Eq. A-8, dimensionless

$r_D$ = dimensionless radius

$r_p$ = radius of drillpipe, (= $r/ r_{wb}$), ft

$r_t$ = radius of tubing, ft

$r_{wb,}\ r$ = wellbore radius, ft

$t$ = drilling or circulation time, hr

$T_a$ = fluid temperature in annulus, ˚F

$T_{as}$ = annular surface measurement, ˚F

$T_{cD}$ = dimensionless circulating temperature, defined by Eq. C-25

$t_{cD}$ = parameter defined by Eq. C-27, dimensionless

$T_{ei}$ = formation temperature, ˚F

$T_{inv}$ = invaded zone temperature, ˚F

$T_p$ = temperature of drillpipe fluid, ˚F

$T_{pi}$ = inlet temperature of drillstring fluid, ˚F

$T_s$ = surface temperature of earth, ˚F

$T_t$ = temperature of tubing fluid, ˚F

$T_{wb}$ = wellbore temperature, ˚F

$U$ = overall heat transfer coefficient across the wellbore face, Btu/ft$^2$-˚F-hr

$U_t$ = overall heat transfer coefficient across the tubing, Btu/ft$^2$-˚F-hr

$w$ , $m$ = mass flow rate, $lb_m$/hr

$z$ = any vertical well depth, ft

$\rho_f$ = formation density, lbm/ft$^3$

$\alpha$ = heat diffusivity of formation (= $k_e/ c_e \rho_e$), ft$^2$/hr

## ACKNOWLEDGMENT

The first author (A.Q.A. Al-Saedi) gratefully acknowledges the financial support provided by the Higher Committee for Education Development in Iraq (HCED) in pursuit of his Ph.D. study.

# APPENDIX A

# MODEL FOR FLUID CIRCULATION

The proposed model development starts by considering the following assumptions:

1. For a steady-state system, the heat flow direction starts from the formation to the wellbore.
2. The heat transfer occurs from different segments as shown in Figure 1. Incorporation of the new relaxation parameter *R* alters the temperature behavior.
3. Using more than one boundary condition to solve the energy system allows us to cover new possible temperature behavior.

Then for the steady-state system, the application of the conservation of energy inside the annulus can be written as

$$Q_{a_{z+dz}} - Q_{a_z} + Q_{Fad} - Q_{ap} = 0 \tag{A-1}$$

where

$$Q_{a_{z+dz}} - Q_{a_z} = mC_f (T_{a_{z+dz}} - T_{a_z}) \tag{A-2}$$

and

$$Q_{ap} = 2\pi r_p h_p \left(T_a - T_p\right) \mathrm{dz} \tag{A-3}$$

The heat flow from the formation into the annulus $Q_{Fa}$ can be written as

$$Q_{Fa1} = 2\pi k_e \left(T_{ei} - T_{inv}\right) \mathrm{dz} \tag{A-4}$$

Similarly, from the invasion zone to the wellbore radius as

$$Q_{Fa2} = 2\pi k_e \left(T_{inv} - T_{wb}\right) \mathrm{dz} \tag{A-5}$$

and from the wellbore to the annulus as

$$Q_{Fa3} = 2\pi r_{wb} U \left(T_{wb} - T_a\right) \mathrm{d}z \tag{A-6}$$

Given that we do not have the exact radius of the different heat transfer segments, we assume that the conductive heat transfer depends on the temperature difference, formation thermal conductivity, and the vertical drilled section.

At steady-state condition, $Q_{Fa1}$, $Q_{Fa2}$, and $Q_{Fa3}$ are equal, and by substituting the wellbore temperature ($T_{wb}$) from Eq. A-6 into Eq. A-5, and then the invaded zone temperature ($T_{inv}$) from Eq. A-5 into Eq. A-4, we can obtain the heat transfer from the formation into the annulus by the following expression:

$$Q_{Fad} = 2\pi k_e R \left(T_{ei} - T_a\right) \mathrm{d}z \tag{A-7}$$

where

$$R = \frac{r_{wb} U}{2 r_{wb} U + k_e} \tag{A-8}$$

We can write the differential form of the forward circulation in the annulus by substituting Eqs. A-7, A-3, and A-2 into Eq. A-1, leading to the following expression:

$$A \frac{\mathrm{d}T_a}{\mathrm{d}z} = \left(T_a - T_p\right) - B\left(T_{ei} - T_a\right) \tag{A-9}$$

where

$$A = \frac{mC_f}{2\pi r_p h_p}, \quad B = \frac{k_e R}{r_p h_p} \tag{A-10}$$

and the heat transfer inside the drillpipe is given by

$$Q_{p_z} - Q_{p_{z+\mathrm{d}z}} + Q_{ap} = 0 \tag{A-11}$$

where

$$Q_{p_z} - Q_{p_{z+\mathrm{d}z}} = mC_f \left(T_{p_z} - T_{p_{z+\mathrm{d}z}}\right) \tag{A-12}$$

and $Q_{ap}$ is given by Eq. A-3. Then, we can rewrite Eq. A-11 as

$$T_a = T_p + A\frac{\mathrm{d}T_p}{\mathrm{d}z} \tag{A-13}$$

Differentiating Eq. A-13, we obtain

$$\frac{\mathrm{d}T_a}{\mathrm{d}z} = \frac{\mathrm{d}T_p}{\mathrm{d}z} + A\frac{\mathrm{d}^2T_p}{\mathrm{d}z^2} \tag{A-14}$$

Substituting Eqs. A-13 and A-14 into Eq. A-9 and simplifying, we obtain the following expression:

$$A^2\frac{\mathrm{d}^2T_p}{\mathrm{d}z^2} - AB\frac{\mathrm{d}T_p}{\mathrm{d}z} - BT_p = -BT_{ei} \tag{A-15}$$

The formation temperature can be expressed by a linear equation, given by $T_{ei} = g_T.z+T_s$. The summation of solutions for the homogeneous and inhomogeneous equations results in the solution of the second-order ordinary differential equation given by Eq. A-15. The result for the tubular temperature can be written as

$$T_p = K_1e^{C_1z} + K_2e^{C_2z} + g_T.z + T_S - g_T.A \tag{A-16}$$

Differentiating Eq. A-16 with respect to $z$ results in the following expression:

$$\frac{\mathrm{d}T_p}{\mathrm{d}z} = C_1K_1e^{C_1z} + C_2K_2e^{C_2z} + g_T \tag{A-17}$$

Then, the annular temperature can be obtained by combining Eqs. A-16 and A-17 with Eq. A-13 as

$$T_a = K_1C_3e^{C_1z} + K_2C_4e^{C_2z} + g_T.z + T_S \tag{A-18}$$

where the constants, $C_1$, $C_2$, $C_3$, and $C_4$ depend on thermal properties and are given as

$$C_1 = \frac{B}{2A}\left[1+\sqrt{1+\frac{4}{B}}\right] \tag{A-19}$$

$$C_2 = \frac{B}{2A}\left[1-\sqrt{1+\frac{4}{B}}\right] \tag{A-20}$$

$$C_3 = (1+AC_1) \tag{A-21}$$

$$C_4 = (1+AC_2) \tag{A-22}$$

and $K_1$ and $K_2$ depend on the first kind or Dirichlet boundary conditions that are given by the following expressions:

$$K_1 = T_{Pi} - T_S + g_T.A - K_2 \tag{A-23}$$

$$K_2 = \frac{g_T.A - \left[(T_{Pi} - T_S + g_T.A)e^{C_1L}(1-C_3)\right]}{\left[e^{C_2L}(1-C_4) - e^{C_1L}(1-C_3)\right]} \tag{A-24}$$

In contrast, $K_2$ takes a different form when the Robin condition is applied

$$K_2 = \frac{\left[\left(T_{pi} - T_S + g_T.A\right)C_1\left(1-e^{C_1L}\right)\right]}{\left[\left(C_2e^{C_2L} - C_1e^{C_1L}\right) - \left(C_2 - C_1\right)\right]} \tag{A-25}$$

# APPENDIX B

# MODEL FOR FLUID PRODUCTION

Application of the conservation of energy for the production case entails the flow path from the sandface into the wellbore and then to surface by way of the tubing or annulus or both, as depicted in Figure 2. The resulting expressions in a mathematical form represent the temperature profiles in both tubing and annulus. Given that the flowing fluid carries energy from the formation, the direction of heat flow occurs from the formation into the annulus and the tubing. The annular energy balance can be described by the following expression:

$$\underset{z+\mathrm{d}z}{Q_{a1}} - \underset{z}{Q_{a1}} + Q_{Fa} - Q_{at} = 0 \tag{B-1}$$

where the heat flow $Q$ at any element is given by Btu/lbm. The heat flow across the control volume $z$ to d$z$ can be written as

$$\underset{z+\mathrm{d}z}{Q_{a1}} - \underset{z}{Q_{a1}} = c_f \left( \underset{z+\mathrm{d}z}{T_a} - \underset{z}{T_a} \right) \tag{B-2}$$

The heat flow from the annulus to the tubing $Q_{at}$ can be presented as

$$Q_{at} = \frac{2\pi r_t U_t}{w} \left( T_a - T_t \right) \mathrm{d}z \tag{B-3}$$

which can be represented by

$$Q_{at} = \frac{c_f}{B_1} \left( T_a - T_t \right) \mathrm{d}z \tag{B-4}$$

where

$$B_1 = \frac{c_f w}{2\pi r_t U_t} \tag{B-5}$$

The amount of heat flow from the formation into the wellbore can be described by Fourier's law, given by the following expression:

$$Q = \frac{2\pi k_e}{w} \left( T_{ei} - T_{wb} \right) \mathrm{d}z \tag{B-6}$$

and the amount of heat transfer from the wellbore into the tubing or casing is given by Newton's law for cooling as

$$Q = \frac{2\pi r_{wb} U}{w}\left(T_{wb} - T_a\right)\mathrm{d}z \tag{B-7}$$

By assuming that the heat flow rates given by Eqs. B-6 and B-7 are equal; we can eliminate the wellbore temperature from both equations and can represent the heat flow from the formation to the annulus as

$$Q_{Fa} = \frac{c_f}{A_1}\left(T_{ei} - T_a\right)\mathrm{d}z \tag{B-8}$$

where

$$A_1 = \frac{c_f w\left(k_e + r_{wb} U\right)}{2\pi r_{wb} U k_e} \tag{B-9}$$

Substituting Eqs. B-2, B-3, and B-8 into Eq. B-1, and rearranging, we have

$$\frac{\mathrm{d}T_a}{\mathrm{d}z} = \frac{1}{B_1}\left(T_a - T_t\right) - \frac{1}{A_1}\left(T_{ei} - T_a\right) \tag{B-10}$$

To solve Eq. B-10, we need to find the heat-flow model for the tubing, which is given by

$$\underset{z+\mathrm{d}z}{Q_t} - \underset{z}{Q_t} + Q_{at} = 0 \tag{B-11}$$

Eq. B-11 can be rewritten as

$$T_a = T_t - B_1 \frac{\mathrm{d}T_t}{\mathrm{d}z} \tag{B-12}$$

Differentiation Eq. B-12 with respect to *z*, we have

$$\frac{\mathrm{d}T_a}{\mathrm{d}z} = \frac{\mathrm{d}T_t}{\mathrm{d}z} - B_1 \frac{\mathrm{d}^2 T_t}{\mathrm{d}z^2} \tag{B-13}$$

Substituting Eqs. B-12 and B-13 into Eq. B-10, and rearranging, we have the following second-order equation:

$$A_1 B_1 \frac{\mathrm{d}^2 T_t}{\mathrm{d}z^2} - \left(2A_1 + B_1\right)\frac{\mathrm{d}T_t}{\mathrm{d}z} + T_t = T_{ei} \tag{B-14}$$

Where the initial-formation temperature is given by $T_{ei} = T_s + zg_T$. By finding the complementary and the particular solutions for the system described by Eq. B-14, the tubing and annular temperature relations can be written as

$$T_t = \alpha_1 e^{\lambda_1 z} + \alpha_2 e^{\lambda_2 z} + g_T z + T_s + 2A_1 g_T - B_1 g_T \tag{B-15}$$

$$T_a = \alpha_1 \lambda_3 e^{\lambda_1 z} + \alpha_2 \lambda_4 e^{\lambda_2 z} + T_s + g_T z + 2A_1 g_T - 2B_1 g_T \tag{B-16}$$

where

$$\lambda_1 = \frac{\dfrac{\left(2A_1 + B_1\right)}{A_1 B_1} + \sqrt{\left(\dfrac{\left(2A_1 + B_1\right)}{A_1 B_1}\right)^2 - \left(\dfrac{4}{A_1 B_1}\right)}}{2} \tag{B-17}$$

$$\lambda_2 = \frac{\dfrac{\left(2A_1 + B_1\right)}{A_1 B_1} - \sqrt{\left(\dfrac{\left(2A_1 + B_1\right)}{A_1 B_1}\right)^2 - \left(\dfrac{4}{A_1 B_1}\right)}}{2} \tag{B-18}$$

$$\lambda_3 = \left(1 - B_1 \lambda_1\right) \tag{B-19}$$

$$\lambda_4 = \left(1 - B_1 \lambda_2\right) \tag{B-20}$$

The boundary condition constants $\alpha_1$ and $\alpha_2$ can be found by practicing different boundary conditions, as presented by Al Saedi et al. (2018). The third kind or Robin condition provides the best fit of data in when compared with the results obtained from the commercial software package, Prosper. As shown by Figure 2, at surface depth when $z = 0$, the annular temperature equals the fluid surface temperature, then the constant $\alpha_1$ is given as

$$\alpha_1 = \frac{T_{as} - T_s - 2A_1 g_T - \alpha_2 \lambda_4}{\lambda_3} \tag{B-21}$$

and at the bottomhole as per the Robin condition ( $\left.\frac{\mathrm{d}T_a}{\mathrm{d}z}\right|_{Z=0} = \left.\frac{\mathrm{d}T_a}{\mathrm{d}z}\right|_{Z=L}$ ), the constant $\alpha_2$ is given by the following expression:

$$\alpha_2 = \frac{\left[\left(T_{as} - T_s - 2A_1 g_T\right)\left(\lambda_1 - \lambda_1 e^{\lambda_1 L}\right)\right]}{\left(\lambda_2 \lambda_4 e^{\lambda_2 L} - \lambda_2 \lambda_4 + \lambda_1 \lambda_4 - \lambda_4 \lambda_1 e^{\lambda_1 L}\right)} \tag{B-22}$$

# APPENDIX C

# LINE-SOURCE SOLUTION OF THE TEMPERATURE DIFFUSIVITY EQUATION

Many studies presented the line-source solution for the pressure diffusivity equation, such as those given by Mathews and Russell (1967) and Dake (1978), among others. The analogy between the pressure and temperature diffusivity equations allows us to use the same procedure presented by Dake (1978) to solve the temperature diffusivity equation. We can represent the temperature as a function of time and radius inside the reservoir by adapting the line-source solution of the pressure-diffusivity equation. Imposition of the following initial and boundary conditions,

1. $T=T_{ei}$ at $t = 0$, for all $r$
2. $T=T_{ei}$ at $r$ = infinity, for all $t$
3. $\lim_{r\to 0} r\frac{\mathrm{d}T}{\mathrm{d}r} = \frac{-Q_r}{2\pi k_e h}$

Lead to the final form of the temperature diffusivity equation given by

$$\frac{\partial^2 T}{\partial r^2} + \frac{1}{r}\frac{\partial T}{\partial r} = \frac{c_e \rho_e}{k_e}\frac{\partial T}{\partial t} \tag{C-1}$$

or in the differential form as

$$\frac{1}{r}\frac{\partial}{\partial r}\left(r\frac{\partial T}{\partial r}\right) = \frac{c_e \rho_e}{k_e}\frac{\partial T}{\partial t} \tag{C-2}$$

where the diffusivity constant given by ($\alpha = k_e/c_e.\rho_e$), and by introducing the Boltzmann's transformation with symbol $s$, we can write

$$s = \frac{r^2}{4(\alpha)t} \tag{C-3}$$

Substituting the diffusivity constant into Eq. C-3 will result in

$$s = \frac{c_e \rho_e r^2}{4k_e t} \tag{C-4}$$

Differentiating Eq. C-4 with respect to the radius and time result in the following expressions:

$$\frac{\partial s}{\partial r} = \frac{c_e \rho_e r}{2 k_e t} \tag{C-5}$$

$$\frac{\partial s}{\partial t} = \frac{-c_e \rho_e r^2}{4 k_e t^2} \tag{C-6}$$

Then by using the chain rule, Eq. C-2 can be rewritten as

$$\frac{1}{r}\frac{\partial}{\partial s}\left( r \frac{\partial T}{\partial s}\frac{\partial s}{\partial r}\right)\frac{\partial s}{\partial r} = \frac{c_e \rho_e}{k_e}\frac{\partial T}{\partial s}\frac{\partial s}{\partial t} \tag{C-7}$$

Substituting Eqs. C-5 and C-6 into Eq. C-7 will result

$$\frac{1}{r}\frac{\partial}{\partial s}\left( r \frac{\partial T}{\partial s}\frac{c_e \rho_e r}{2 k_e t}\right)\frac{c_e \rho_e r}{2 k_e t} = \frac{c_e \rho_e}{k_e}\frac{\partial T}{\partial s}\frac{-c_e \rho_e r^2}{4 k_e t^2} \tag{C-8}$$

or

$$\frac{r}{r}\frac{\partial}{\partial s}\left( \frac{\partial T}{\partial s}\left( \frac{c_e \rho_e r^2}{4 k_e t}\right)\right)\frac{c_e \rho_e}{k_e t} = \frac{-c_e \rho_e}{k_e t}\left( \frac{c_e \rho_e r^2}{4 k_e t}\right)\frac{\partial T}{\partial s} \tag{C-9}$$

By using the Boltzmann's transformation term given by Eq. C-4, then Eq. C-9 can be rewritten as

$$\frac{\partial}{\partial s}\left( \frac{\partial T}{\partial s} s\right) = -s\frac{\partial T}{\partial s} \tag{C-10}$$

Eq. C-10 shows that temperature change only with variable *s*, which is a function of radius and time. Therefore, we can change Eq. C-10 from PDE to ODE in the following manner:

$$\frac{\mathrm{d}}{\mathrm{d}s}\left( \frac{\mathrm{d}T}{\mathrm{d}s} s\right) = -s\frac{\mathrm{d}T}{\mathrm{d}s} \tag{C-11}$$

Eq. C-11 can be simplified as

$$s\frac{\mathrm{d}^2 T}{\mathrm{d}s^2} + \frac{\mathrm{d}T}{\mathrm{d}s} = -s\frac{\mathrm{d}T}{\mathrm{d}s} \tag{C-12}$$

Now, let us consider

$$\frac{\mathrm{d}T}{\mathrm{d}s} = T' \text{ and } \frac{\mathrm{d}^2T}{\mathrm{d}s^2} = \frac{\mathrm{d}T'}{\mathrm{d}s} = T'' \tag{C-13}$$

Then, Eq. C-12 becomes

$$s\frac{\mathrm{d}T'}{\mathrm{d}s} + T'(1+s) = 0 \tag{C-14}$$

By integrating Eq. C-14, we have

$$\ln|T'| = -\ln|s| - s + c_1$$

or

$$\frac{\mathrm{d}T}{\mathrm{d}s} = T' = \frac{e^{-s}.c_2}{s} \tag{C-15}$$

where $C_1$ and $C_2$ are the constants of integration and $C_2$ can be evaluated using the line-source boundary condition. The heat transfer from the formation into the wellbore by conduction in radial coordinates can be written as (Fourier's law):

$$\lim_{r\to 0} r\frac{\mathrm{d}T}{\mathrm{d}r} = \frac{-Q_r}{2\pi k_e h} = r\frac{\mathrm{d}T}{\mathrm{d}s}.\frac{\mathrm{d}s}{\mathrm{d}r} = \frac{4k_e t}{c_e\rho_e r}s\frac{\mathrm{d}T}{\mathrm{d}s}\frac{c_e\rho_e r}{2k_e t} = 2s\frac{\mathrm{d}T}{\mathrm{d}s} \tag{C-16}$$

Therefore,

$$2\left(s.\frac{\mathrm{d}T}{\mathrm{d}s}\right) = \frac{-Q_r}{2\pi h k_e} \tag{C-17}$$

Substituting Eqs. C-15 into Eq. C-17, and considering when $r$ goes to zero and $s$ equals to zero, we can write

$$C_2 = \frac{-Q_r}{4\pi h k_e} \tag{C-18}$$

Then, Eq. C-15 can be rewritten as

$$T' = \frac{\mathrm{d}T}{\mathrm{d}s} = \frac{-Q_r}{4\pi h k_e} . \frac{e^{-s}}{s} \tag{C-19}$$

or

$$\mathrm{d}T = \frac{-Q_r}{4\pi h k_e} . \frac{e^{-s}}{s} \mathrm{d}s \tag{C-20}$$

Integration of Eq. C-20 with the limit of *s* up to infinity, and the current value of *t*, for which *s* = *x*; the current temperature *T* leads to the following expression:

$$\int_{T_{ei}}^{T} \mathrm{d}T = \frac{-Q_r}{4\pi h k_e} \int_{\infty}^{x} \frac{e^{-s}}{s} \mathrm{d}s \tag{C-21}$$

which yields

$$\left(T - T_{ei}\right) = \frac{Q_r}{4\pi h k_e} \int_{x=\frac{c_e \rho_e r^2}{4 k_e t}}^{\infty} \frac{e^{-s}}{s} \mathrm{d}s \tag{C-22}$$

By introducing the exponential integral, denoted by $E_i(-X)$, which is defined by the following expression:

$$\int_{x}^{\infty} \frac{e^{-s}}{s} \mathrm{d}s = \int_{x=\frac{c_e \rho_e r^2}{4 k_e t}}^{\infty} \frac{e^{-s}}{s} \mathrm{d}s \tag{C-23}$$

we can rewrite Eq. C-22 as follows:

$$T_{(r,t)} = T_{ei} + \frac{Q_r}{4\pi h k_e} E_i \left[ \frac{-c_e \rho_e r^2}{4 k_e t} \right] \tag{C-24}$$

Eq. C-24 represents the line-source solution of the temperature diffusivity equation that expresses temperature as a function of position and time. In field units, Eq. C-24 can be rewritten as

$$T_{(r,t)} = T_{ei} + 0.68\frac{Q_r}{hk_e}E_i\left[\frac{-r^2}{4\alpha t}\right] \tag{C-25}$$

And by introducing the following dimensionless parameters as

$$T_{cD} = \frac{\left(T_{ei} - T_{(r,t)}\right)hk_e}{0.68Q_r} \tag{C-26}$$

$$r_D = \frac{r}{r_{wb}} \tag{C-27}$$

$$t_{cD} = \frac{\alpha t}{r_{wb}^2} \tag{C-28}$$

Then, Eq. C-24 can be rewritten in dimensionless form as

$$T_{cD} = -E_i\left(\frac{-r_D^2}{4t_{cD}}\right) \tag{C-29}$$

The formation geothermal gradient reflects the difference between the undisturbed formation temperature at the bottomhole and surface divided by the true vertical depth interval with the following expression:

$$g_T = \frac{T_{ei} - T_s}{D_{TV}} \tag{C-30}$$

By using the initial-formation temperature from Eq. C-30 for a given wellbore radius, the formation geothermal gradient can be express as

$$g_T = \frac{\left\{T_{wb} - \left[\left(\frac{0.68Q_r}{hk_e}\right)E_i\left(\frac{-c_e\rho_e r_{wb}{}^2}{4k_e t}\right)\right]\right\} - T_s}{D_{TV}} \tag{C-31}$$

# REFERENCES


Al Saedi, A., Flori, R.E., and Kabir, C.S. (2018). New analytical solutions of wellbore fluid temperature profiles during drilling, circulating and cementing operations. *J. Pet. Sci. & Eng*. 170 (2018), 206-217. http://dx.doi:10.1016/j.petrol.2018.06.027.

Arnold, F. C. (1990). Temperature variation in a circulating wellbore fluid. *J. Energy Resour. Technol*. 112 (2), 79. http://dx.doi.org/10.1115/1.2905726.

Dake, L. P. (1978). Fundamentals of Reservoir Engineering. Elsevier Scientific Publishing Company, vol. 8.

Dowdle, W. L., and Cobb, W. M. (1975). Static formation temperature from well logs ─ An empirical method. *J. Petrol. Technol*. 27 (11), 1326-1330. http://dx.doi.org/10.2118/5036-PA.

Forrest, J., Marcucci, E., and Scott, P. (2007). Geothermal gradients and subsurface temperatures in the Northern Gulf of Mexico. Trans. GCAGS.55: 233–248.

Gao, Y., Sun, B., and Xu, B. (2017). A wellbore/formation-coupled heat-transfer model in deepwater drilling and its application in the prediction of hydrate-reservoir dissociation. *SPE J.* 22 (3), 756-766. http://dx.doi.org/10.2118/184398-PA.

Guo, B., Li, G., and Shan, L. (2016). Mathematical model provides annular temperature profile for thermal hydraulics in drilling gas hydrates. *IADC/SPE* Asia-Pacific Drill. Technol. Conf. http://dx.doi.org/10.2118/180560-MS.

Hasan, A.R., and Kabir, C.S. (1994). Aspects of wellbore heat transfer during two-phase flow (includes associated papers 30226 and 30970). *SPE Prod. & Facil*. 9 (03), 211-216. http://dx.doi.org/10.2118/22948-PA.

Hasan, A.R., Kabir, C.S., and Ameen, M. (1996). A fluid circulating temperature model for workover operations. *SPE J*. 1 (02), 133-144. http://dx.doi.org/10.2118/27848-PA.

Holmes, C. S., and Swift, S. C. (1970). Calculation of circulating mud temperatures. *J. Petrol. Technol*. 22 (6), 670-674. http://dx.doi.org/10.2118/2318-PA.

Kabir, C.S., Hasan, A.R., Kouba, G., and Ameen, M. (1996). Determining circulating fluid temperature in drilling, workover, and well control operations. *SPE Drill. & Complet*. 11 (02), 74-79. http://dx.doi.org/10.2118/24581-PA.

Keller, H., Couch, E., and Berry, P. (1973). Temperature Distribution in Circulating Mud Columns. *SPE J*. 13 (1): 23-30. http://dx.doi.org/10.2118/3605-PA.

Kritikos, W.R., and Kutasov, I. M. (1988). Two-point method for determination of undisturbed reservoir temperature. *SPE Form. Eval*. 3 (1), 222-226. http://dx.doi.org/10.2118/15204-PA.

Kumar, A. and Samuel, R. (2013). Analytical model to predict the effect of pipe friction on downhole fluid temperatures. *SPE Drill. & Complet*. 28 (3), 270-277. http://dx.doi.org/10.2118/165934-PA.

Kutasov, I. M., and Eppelbaum, L. V. (2005). Determination of formation temperature from bottom-hole temperature logs—a generalized Horner method. *J. Geophys. & Eng*. 2 (2), 90-96. https://doi.org/10.1088/1742-2132/2/2/002.

Kutasov, I. M., and Eppelbaum, L. V. (2018). Utilization of the Horner plot for determining the temperature of frozen formations — A novel approach. *Geothermics* 71, 259-263. https://doi.org/10.1016/j.geothermics.2017.10.005.

Marshall, D. W. and Bentsen, R. G. (1982). A Computer Model to Determine the Temperature Distributions in a Wellbore. *J. Can. Petrol. Technol*. 21 (1): 63-75. http://dx.doi.org/10.2118/82-01-05.

Matthews, C. S., Russell, D. G. (1967). Pressure buildup and flow tests in wells. *SPE Monograph*, vol. 1.

Prensky, S., (1992). Temperature Measurements in Boreholes ─ An overview of engineering and scientific applications. *Society of Petrophysicists and Well-Log Analysts*.

Prosper, (2018). http://www.petex.com/media/2272/prosper-brochure.pdf.

Raymond, L., (1969). Temperature distribution in a circulating drilling fluid. *J. Petrol. Technol*. 21 (3), 333-341. http://dx.doi.org/10.2118/2320-PA.

Sagar, R., Doty, D., & Schmidt, Z., (1991). Predicting temperature profiles in a flowing well. *SPE Prod. Eng*. 6 (04), 441-448. http://dx.doi.org/10.2118/19702-PA.

Schoeppel, R., & Gilarranz, S., (1966). Use of well log temperatures to evaluate regional geothermal gradients. *J. Petrol. Technol*. 18 (06), 667-673. http://dx.doi.org/10.2118/1297-PA.

Van Everdingen, A., and Hurst, W., (1949). The application of the Laplace transformation to flow problems in reservoirs. *J. Petrol. Technol*. 1 (12), 305-324. https://doi.org/10.2118/949305-g.

# IV. ESTIMATING THE INITIAL-FORMATION TEMPERATURE AND FLOWING-TEMPERATURE GRADIENT WITH TRANSIENT-TEMPERATURE ANALYSIS: APPLICATIONS IN GAS RESERVOIRS

A.Q. Al Saedi, R. E. Flori, and C. S. Kabir

Missouri University of Science and Technology

(Published in Journal of Natural Gas Science and Engineering 66 (2019) 126-137)

## ABSTRACT

The formation temperature constitutes one of the essential factors that affect the wellbore fluid temperature behavior in production mode. The amount and direction of the radial heat transfer between the surrounding formation and the wellbore depend on the temperature differential and thermal properties of the media.

Traditional studies probing geothermal gradients depended principally on extrapolating the transient bottomhole temperature to infinite shut-in time for obtaining the undisturbed formation temperature. After that, a straight line from the surface to the bottomhole condition constituted the geothermal gradient. Of course, the implicit assumption in this approach is that a linear geothermal gradient exists in light of unavailability of depth-wise temperature measurements.

This study presents a new transient-temperature analysis approach to determine the undisturbed formation temperature. Specifically, we show the application of the line-source solution that has roots in the temperature-diffusivity equation. Secondly, using the distributed temperature measurements associated with transient-pressure testing, we proved that the

bottomhole or static temperature is time-dependent, leading to alteration of the geothermal gradient in a well's proximity. Finally, the lowering of the temperature-derivative plateau with increasing depth during well shut-in periods indicated an increase in thermal conductivity, resulting in a nonlinear geothermal gradient.

## 1. INTRODUCTION

The similarity between the pressure diffusivity equation presented by van Everdingen and Hurst (1949) and the temperature diffusivity equation given by Carslaw and Jaeger (1959) allowed many authors to adopt the same solution methods for the pressure diffusivity equation for its temperature counterpart.

The temperature diffusivity equation allows to describe the heat transfer and to find the undisturbed radial formation temperature distribution. In general, the undisturbed formation temperature for the wellbore can be characterized by a linear relationship including the geothermal gradient which required a knowledge of the bottomhole and surface temperatures.

Many studies presented the line-source solution for pressure diffusivity equation, such as those given by Mathews et al. (1967) and Dake (1978). Horner (1951) presented an analytical study to find the initial reservoir pressure involving flow and shut-in periods. The study was based on the line-source solution of the pressure diffusivity equation. His solution approach known as the Horner method has served the industry well as documented in many textbooks, such as that in Lee et al. (2003). Many studies followed to find the static formation

temperature by adopting the Horner method or superposition in time, but the derivation details for its temperature counterpart are a few.

A comparison between the temperature and pressure buildup study was presented by Dowdle and Cobb (1975); however, no mathematical details appeared. The authors suggested the buildup temperature equation based on the similarities with the pressure buildup equation obtained by Horner (1951). Nonetheless, Dowdle and Cobb (1975) showed that Horner-type analysis could be used to find the static formation temperature under the assumption of short fluid circulation times. However, this method was more investigated to estimate the initial formation temperature as presented by Roux et al. (1980), Hasan and Kabir (1994a), among others. Furthermore, the flowing fluid temperature of two-phase flow for a complex well demands the application of an energy balance including pressure gradient was presented by Hasan et al. (2009), which expand the window of fluid temperature calculation by depth steps covering the possible variety of the heat loss and geothermal gradient throughout the well path.

Earlier, Kutasov and Eppelbaum (2005) provided a mathematical model to determine the formation temperature from bottomhole logs by generalized Horner method. More recently, Kutasov and Eppelbaum (2018) presented a new approach to estimate the undisturbed formation temperature from shut-in temperature data gathered in openhole systems. They modified the Horner method by adopting a new circulation and shut-in time concept to find the undisturbed formation temperature.

Studying flowing fluid temperature behavior by using the distributed temperature measurements in gas wells inspired us to investigate different aspects of temperature behavior to elicit more information beyond those reported recently by Hashmi et al. (2015).

Specifically, we offer a new application of the temperature analysis method to determine the initial-formation temperature from transient-temperature data. We also applied the superposition principle to estimate the behavior of fluid temperature profiles for transient tests involving multiple flow and shut-in periods. Finally, we obtained two slightly different formation temperature profiles by implementing the new methods.

## 2. MATHEMATICAL MODELS

Production initiation from the deepest interval serves as a heat source to the entire wellbore and the associated formation. By assuming the reservoir around the wellbore as a homogenous system and applying the energy balance on the formation for the 1D cylindrical coordinate system, one can obtain the appropriate working equations. Appendix A presents the relevant formulations as a function of production time and radial distance.

The temperature diffusivity equation used to describe the temperature behavior outside the wellbore to the reservoir boundary, and the solution of temperature diffusivity equation in field units is given by Eq. 1, which was obtained by using the boundary condition presented by Hasan and Kabir (1994b), as follows:

$$T_{(r,t)} = T_{ei} + 0.68\left(\frac{Q}{hk_e}\right)E_i\left(\frac{-c_e\rho_e r^2}{4k_e t}\right) \tag{1}$$

For a steady-state system, we can determine the amount of heat transfer and the initial-formation temperature by having the well shut-in temperature as follows:

$$T_{ws} = T_{ei} + 1.566\left(\frac{Q}{hk_e}\right)\left[\log\left(\frac{r_w^2}{\alpha\Delta t}\right) + \log(0.445)\right] \tag{2}$$

In Eq. 2, $T_{ws}$ is the shut-in wellbore temperature measurement at test time $t$, and $T_{ei}$ refers to the initial formation temperature, and $\alpha$ represents the diffusivity constant, which is given by $k_e/\rho_e c_e$. However, Eq. 2 can be rewritten as:

$$T_{ws} = b - m\log(\Delta t) \tag{3}$$

where

$$m = \left(\frac{1.566Q}{hk_e}\right), \qquad b = T_{ei} - m\left[\log\left(\frac{\alpha}{r_w^2}\right) + 0.352\right] \tag{4}$$

By applying the result of Eq. 3 on a semilog plot, one can obtain the initial-formation temperature from parameter $b$, which refers to the intercept, and the slope $m$ that allows estimation of heat flow. When flow rate changes, such as in flow-after-flow situation, the fluid flow rate ordinarily stabilizes soon after its change. However, the corresponding heat flow rate from or to the formation takes much longer to stabilize. In this transient heat flow environment, we can estimate the fluid temperature behavior by using the superposition principle associated with varying fluid flow rates corresponding to each period. The following expression, whose derivation is detailed in Appendix A, presents the relevant superposition solution:

$$T_{ei} - T_f = \left(\frac{-0.68}{hk_e}\right)\sum_{j=0}^{N}\left[\left(Q_{j+1} - Q_j\right)E_i\left(\frac{-c_e\rho_e r_w{}^2}{4k_e\left(t_N - t_j\right)}\right)\right] \tag{5}$$

## 3. MODEL APPLICATIONS FOR THE SHUT-IN PERIODS

To validate our proposed technique, we used the transient-temperature data for a multipoint-temperature sensor (MTS) of Well 4 for dry-gas production in a deepwater setting

in West Australia presented earlier by Hashmi et al. (2015). The measurements were taken at 11 different depth locations shown schematically in Figure 1a, and temperature responses in five of those stations appear in Figure 1b. These relay stations transmit real-time pressure and temperature data to surface during drillstem testing.

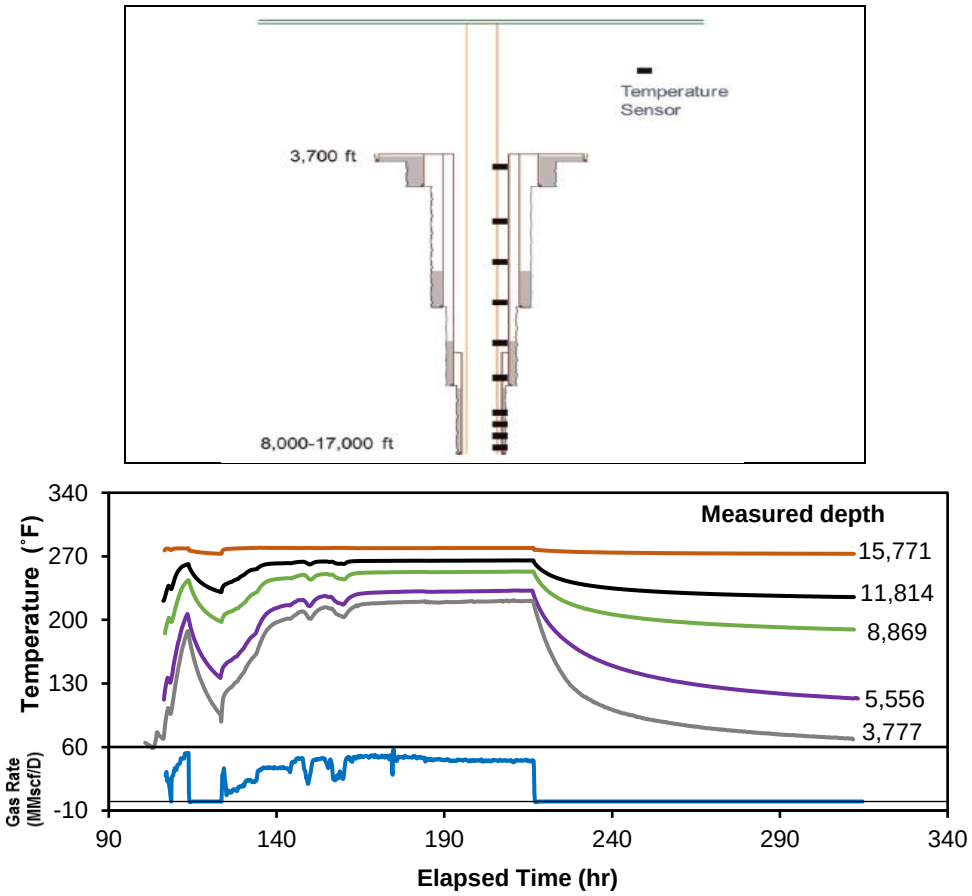


Figure 1. (a) Schematic of multipoint temperature measurements at relay stations in Well 4, (b). Depth-dependent measurements of transient temperature responses in Well 4.

Figure 1b indicates three shut-in periods: the first shut-in period of about 0.83 hr, 9.81 hr for the second one, and 98 hr recorded for the third buildup test. We used our proposed method presented by Eq. 3 to find the undisturbed formation temperature for each shut-in

period. By estimation the intercept and slope we can determine the undisturbed formation temperature and the heat flow for each station depth. The result of application Eq. 3 given by Figure 2 and Table 1.

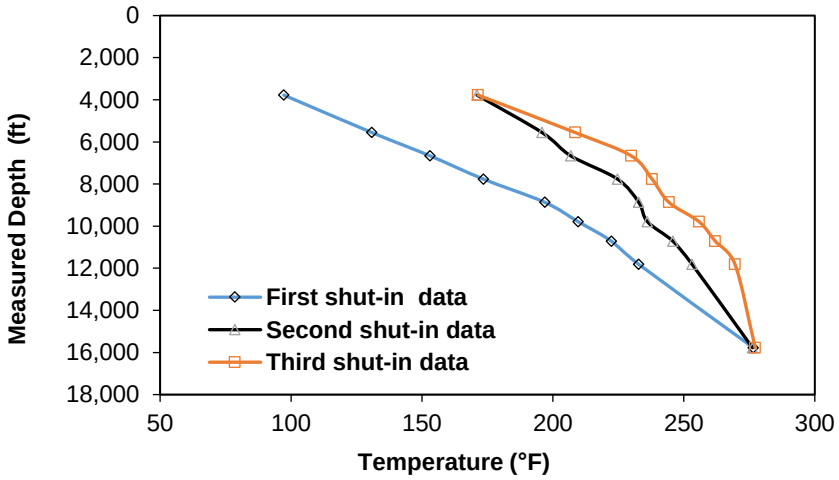


Figure 2. Estimated formation temperature for all shut-in periods.

Table 1. Results of application of Eq. 3.

| | First shut-in | | Second shut-in | | Third shut-in | |
|---|---|---|---|---|---|---|
| Measured Depth, ft | $T_{ei}$, °F | $Q$, Btu/hr | $T_{ei}$, °F | $Q$, Btu/hr | $T_{ei}$, °F | $Q$, Btu/hr |
| 3,777 | 97.26 | 78.69 | 171.02 | 1912.77 | 171.42 | 1324.01 |
| 5,556 | 130.88 | 36.62 | 195.87 | 1617.68 | 208.53 | 1230.95 |
| 6,661 | 153.03 | 90.91 | 206.82 | 1210.38 | 229.88 | 1118.07 |
| 7,765 | 173.44 | 199.35 | 224.67 | 1102.16 | 237.85 | 898.93 |
| 8,869 | 196.91 | 220.60 | 232.76 | 934.55 | 244.30 | 710.61 |
| 9,789 | 209.63 | 143.48 | 236.08 | 725.92 | 255.80 | 689.74 |
| 10,710 | 222.29 | 101.13 | 245.77 | 688.13 | 261.95 | 635.91 |
| 11,814 | 232.77 | 129.36 | 253.14 | 604.89 | 269.53 | 597.01 |
| 15,771 | 276.53 | 63.49 | 276.18 | 92.82 | 277.25 | 59.32 |

Both Figure 2 and Table 1 suggest that the formation temperature increased for each shut-in period throughout the well path resulting from the amount of heat gain precipitated by

the significant temperature difference, except at the bottomhole where the temperature difference is the least. We note that the conventional approach of geothermal gradient estimation depends on the bottomhole temperature only, leading to a straight-line behavior because the other point occurs either at the surface or near the mudline. However, whenever the distributed formation temperature becomes available, we typically observe a nonlinear geothermal gradient due to different thermal conductivity of the sediments at each point of measurement.

After obtaining the initial formation temperature ($T_{ei}$) and the amount of heat flow from the formation to the wellbore ($Q$), we can apply Eq. 1 to find the radius and time required to attain the equilibrium status. Figure 3 presented the results of application Eq. 1 at 3,777 ft of the first shut-in period for different radii and time domains.

Figure 3 suggests that the temperature transients will travel about 28 ft or take 720 hr to reach equilibrium. Adopting the same approach, calculations for all other shut-ins periods at four different depth points appear in Table 2.

Given sufficient durations, both the second and third shut-in periods allowed us to study the thermal conductivity behavior of the formation at three different depths.

In analogy to the pressure-transient signature, Figure 4 shows that the three distinct derivative plateaus indicate increasing thermal conductivity with increasing depth. In other words, the geothermal gradient increases with depth. We validate this point in subsequent sections. Figure 5 illustrates how the variable thermal conductivity influences the shut-in temperature profiles with the time that results from the variation of the amount of heat-

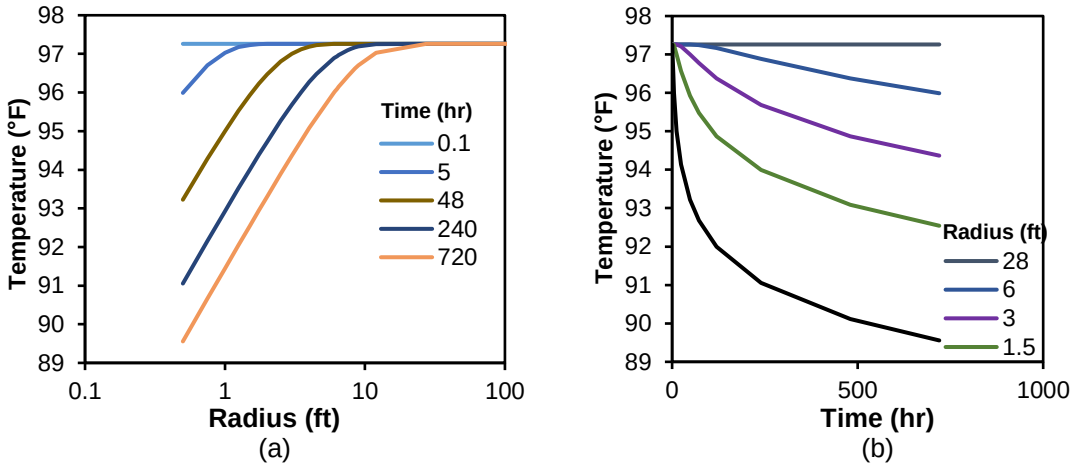


Figure 3. Application of Ei solution at 3,777 ft showing different radii (a), and different time domain (b).

Table 2. Influence of thermal radius at different depths.

| | First shut-in | Second shut-in | Third shut-in |
|---|---|---|---|
| Measured Depth, ft | Radius, ft | Radius, ft | Radius, ft |
| 3,777 | 27.5 | 34.0 | 33.25 |
| 8,869 | 34.0 | 33.0 | 35.40 |
| 10,709 | 40.0 | 30.5 | 30.00 |
| 15,771 | 27.0 | 27.0 | 26.20 |

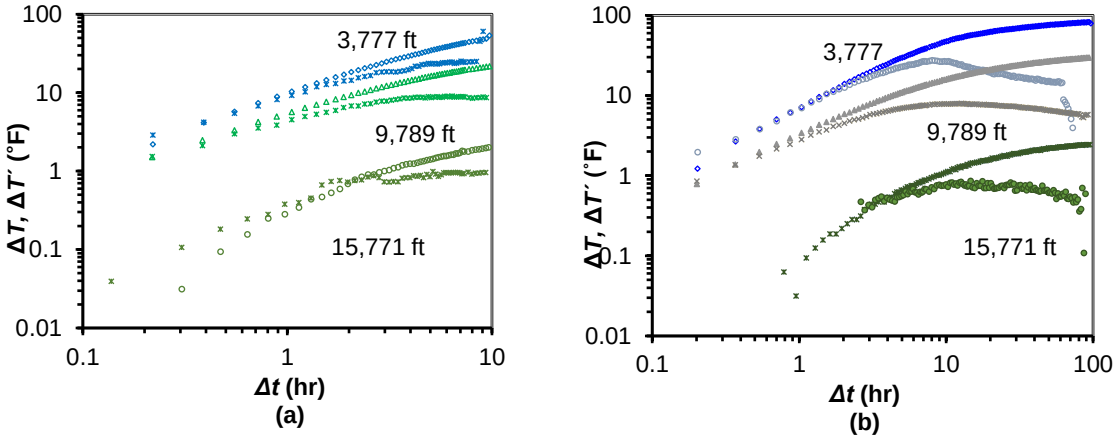


Figure 4. Log-log temperature signatures, second shut-in period (a), third shut-in period (b).

transfer over each shut-in period. we can apply the principle of superposition (Eq. 5) to check the validity of our contention. Figure 5a presents the result of the application of the superposition principle for the second shut-in period, whereas that for the third shut-in appears in Figure 5b. Appendix B shows the calculation procedure in Example-1.

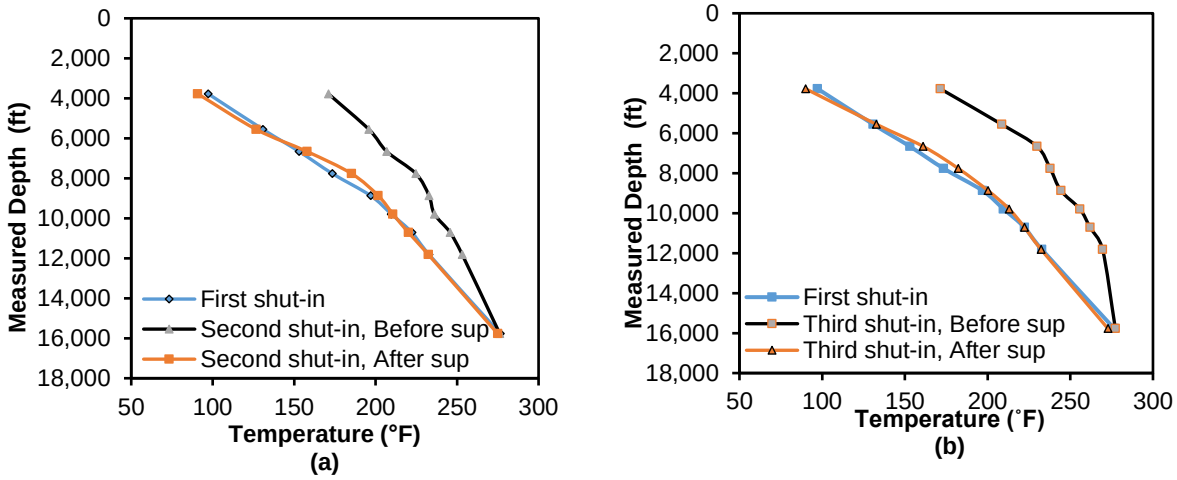


Figure 5. Wellbore temperature behavior before and after applying superposition: second shut-in (a), third shut-in (b).

## 4. UNDERSTANDING FLOWING-FLUID TEMPERATURE GRADIENT BEHAVIOR

The formation temperature is considered an essential key to studying the fluid temperature distribution. Usually, a linear relationship between the surface and the bottomhole temperature constitutes the geothermal gradient. The bottomhole temperature can be obtained by different measurements depending on the open or cased-hole environment, such as well logging as shown by Schoeppel and Gilarranz (1966), formation tester, and drillstem test. Considering the calculated initial formation temperature as shown in Table 1 for the three

shut-in periods, and 85 °F as the surface temperature, we observed that the geothermal gradient is about 0.013 °F /ft.

Kabir et al. (2014) presented an analytical model for calculating the flow rate by using the transient temperature measurement for a dry-gas well. They determined an accurate geothermal gradient by calculating the static temperature by analysis of the transient temperature at different stations. To apply their model, we needed the initial-formation temperature $T_{ei}$, which one can establish from the estimated geothermal gradient. We used two values of the geothermal gradient; the first one is the geothermal gradient created from the bottomhole temperature ($g_{G.TD}$), which is about 0.013 °F /ft and is used for the entire well depth. The second one involves the formation temperature ($g_{G.VD}$) estimated at each depth, as shown in Table-1.

Therefore, for the initial formation temperature calculation based on the geothermal gradient from the bottomhole, we can determine the flowing-fluid temperature by adopting the Hasan and Kabir (2018) model for single-phase gas flow. Figure 6a presents such a solution. In contrast, if we use the initial formation temperature of the second shut-in period as shown in Table 1, and calculate the geothermal gradient for each depth point ($g_{G.VD}$), Figure 6b emerges. The flowing fluid temperature presented by Figure 6 were calculated by using the annular thermal conductivity of 0.1 Btu/ft.hr.˚F, and the fluid thermal conductivity of 0.2 Btu/ft.hr.˚F. We obtained Figure 7 following the same approach for the third shut-in period.

Figure 8 compares the results of the two solution approaches involving both the second and third shut-in periods. The traditional method of estimating the initial-formation temperature depends on the geothermal gradient and the static-bottomhole temperature obtained from a routine transient-well test.

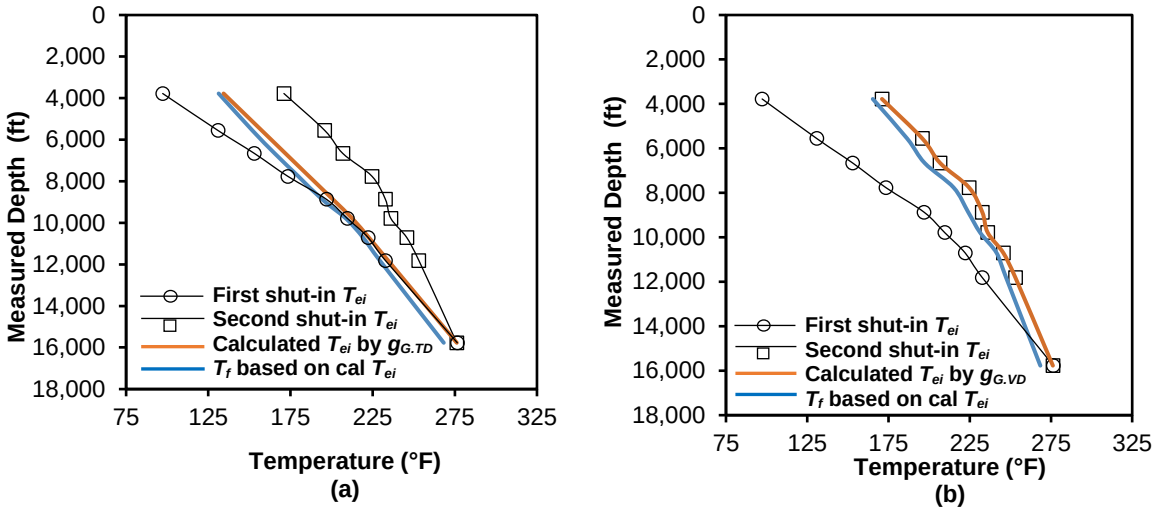


Figure 6. Fluid temperature profile after the second shut-in period based on: geothermal from bottomhole ($g_{G.TD}$) (a), geothermal from each depth ($g_{G.VD}$) (b).

As Figure 8 shows, two different flowing-fluid temperature profiles may emerge to illuminate possible range of flowing fluid temperature profiles compared to those that may be used commonly.

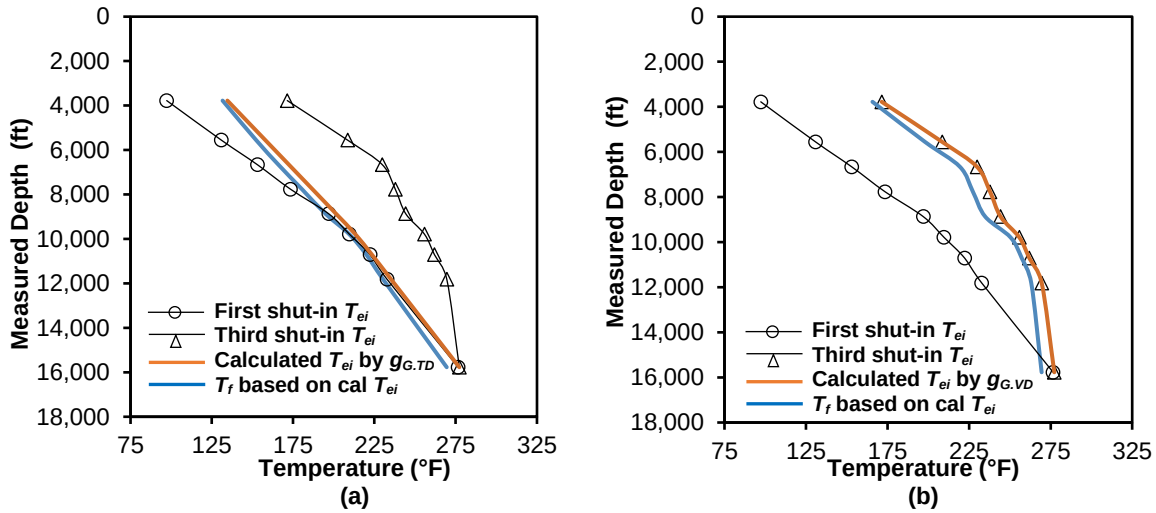


Figure 7. Fluid temperature profile after the third shut-in period based on: Geothermal from bottomhole ($g_{G.TD}$) (a), Geothermal from each depth ($g_{G.VD}$) (b).

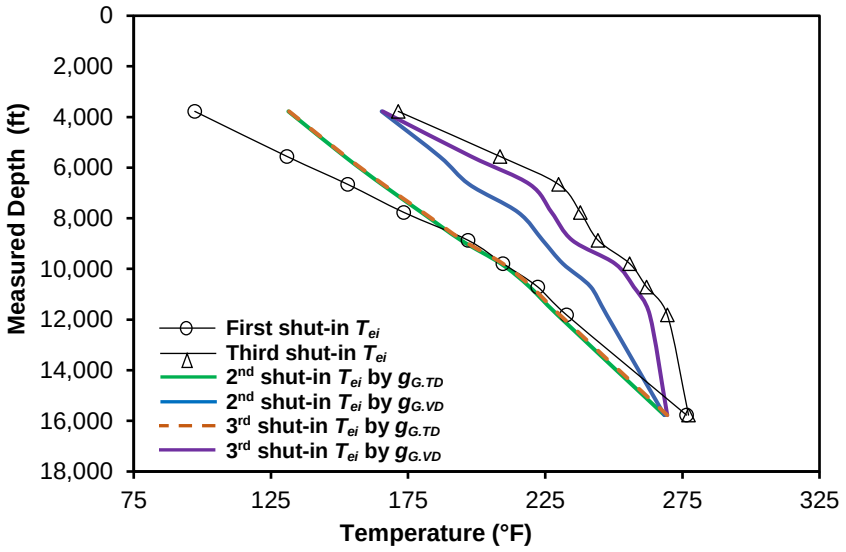


Figure 8. A comparison between the fluid temperature profiles for second and third shut-in data.

## 5. VERIFICATION OF THE PROPOSED METHOD

Kutasov and Eppelbaum (2018) presented a new iterative approach for estimating the undisturbed formation temperature from the shut-in temperature logs. They modified the 'Horner plot method' by adopting a new circulation and shut-in time concept to calculate the formation temperature. They used four depths for a field example to demonstrate the procedure for determining the formation temperature of frozen formations.

The authors used some iterations to show the accuracy in estimation of the formation temperature, which provides us with options to select the proper range to match the estimated formation temperature. The result obtained by our suggested model was verified by using the Kutasov and Eppelbaum (2018) or K-E model for the three shut-in periods. Example 2 in Appendix B presents the calculation approach.

Table 3. Application of Eq. 3 for the first shut-in period involving different iterations.

| Measured Depth, ft | Iteration | $T_{ei}$, ˚F | $B$ |
|---|---|---|---|
| 3,777 | 4 — 5 | 99.32 | 1.755 |
| 5,556 | 3 — 5 | 130.08 | 0.835 |
| 6,661 | 3 — 6 | 153.28 | 0.510 |
| 7,765 | 3 — 5 | 173.22 | 2.374 |
| 8,869 | 2 — 6 | 195.78 | 2.915 |
| 9,789 | 3 — 6 | 207.84 | 2.803 |
| 10,710 | 4 — 5 | 220.41 | 2.515 |
| 11,814 | 2 — 5 | 231.74 | 2.253 |
| 15,771 | 3 — 6 | 275.55 | 2.080 |

For the 3,777 ft of the first shut-in period, and by choosing the proper iteration, which is in this case from (4 —5), the formation temperature obtained by the intercept equals to 99.32 ˚F. As Table 1 shows, this value is the closest to that obtained by application Eq. 3. The corresponding B value is 1.755. Table 3 presents the results by applying the same procedure for all data points for the first shut-in period.

Figure 9 shows a good match between the results obtained by applying our method presented by Eq. 3 to determine the undisturbed formation temperature with the result obtained by using the K-E model for each station depth of the same first shut-in period. Table 4 presents the result for the second shut-in period.

Again, by using K-E model with the second shut-in dataset and by choosing the suitable iteration as shown by Table 4. We got a good match with the calculated formation temperature from the first shut-in, and another match with the fluid temperature after applying the superposition principle for the second shut-in period which is the same line presented by Figure 5a.

Results are given by Figure 10. Finally, the result of the third shut-in period is given by Table 5. Figure 11 shows a good agreement with the calculated formation temperature from the first shut-in, and another match with the fluid temperature after applying the superposition principle for the third shut-in period.

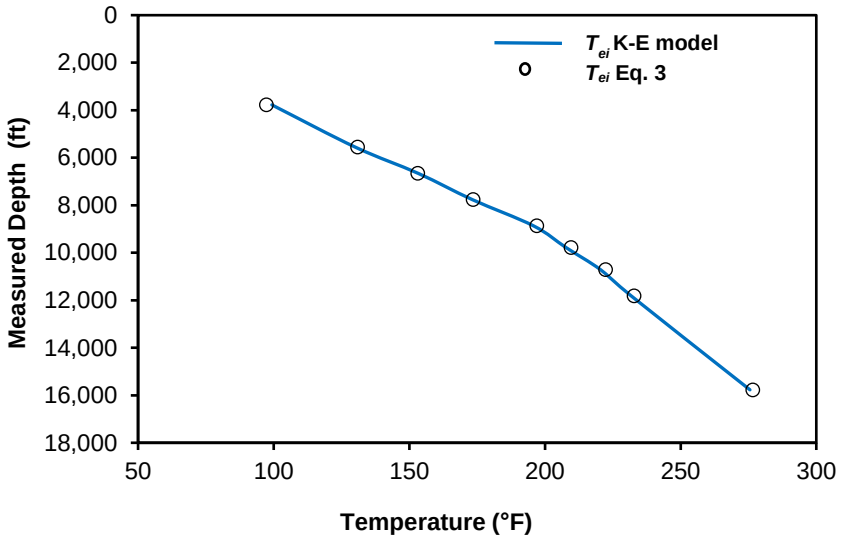


Figure 9. Formation temperature obtained from Eq. 3 and K-E model, first-shut-in data.

Table 4. Results of application Eq. 3 for the 2nd shut-in and for different iterations.

| Match with first shut-in | | | After Superposition value match | | |
|---|---|---|---|---|---|
| Iteration | $T_{ei}$, ˚F | $B$ | Iteration | $T_{ei}$, ˚F | $B$ |
| 8 — 14 | 97.10 | 24.28 | 8 — 19 | 89.17 | 27.50 |
| 8 — 20 | 130.52 | 20.34 | 8 — 25 | 126.24 | 22.25 |
| 12 — 29 | 153.77 | 16.68 | 8 — 25 | 158.56 | 13.99 |
| 11 — 35 | 173.02 | 18.20 | 5 — 18 | 185.34 | 11.72 |
| 6 — 19 | 195.98 | 13.97 | 5 — 14 | 201.33 | 11.60 |
| 6 — 19 | 209.72 | 9.27 | 5 — 20 | 210.32 | 8.89 |
| 6 — 17 | 220.12 | 10.55 | 5 — 15 | 222.53 | 9.38 |
| 5 — 18 | 232.10 | 8.46 | 5 — 18 | 232.10 | 8.46 |
| 2 — 5 | 275.33 | 0.28 | 2 — 16 | 274.17 | 0.72 |

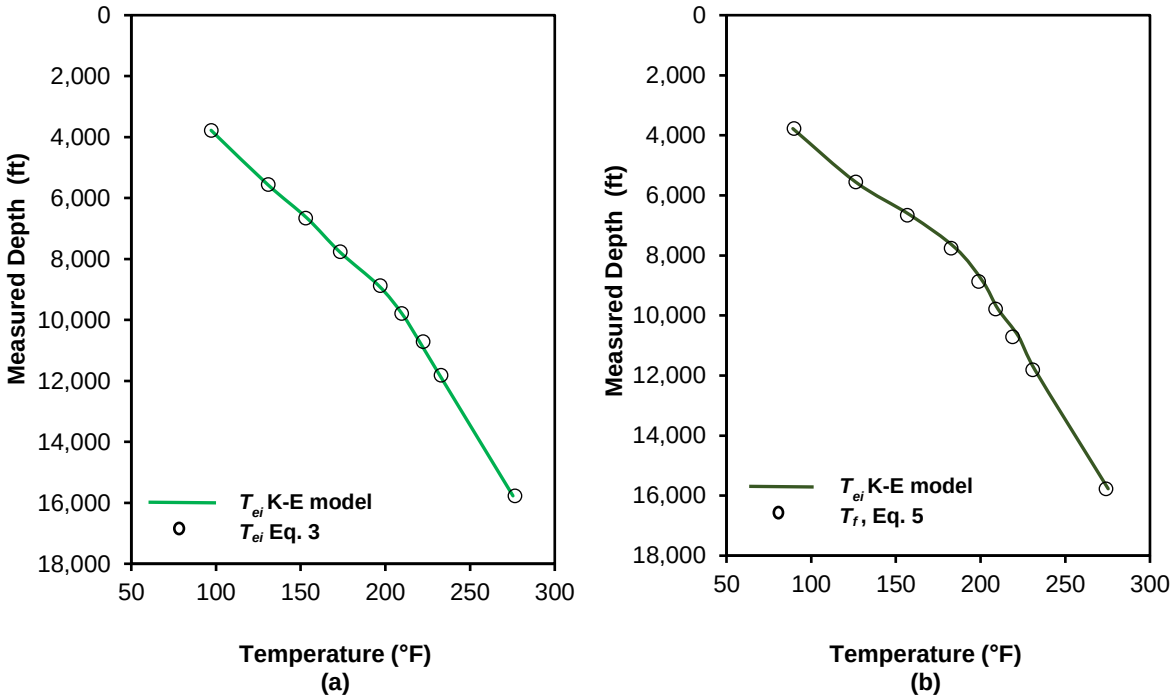


Figure 10. The K-E model for the second shut-in data: match with Tei from first shut-in (a), match with fluid temperature after superposition (b).

Table 5. Results of application Eq. 3 for the 3rd shut-in and for different iterations.

| Match with first shut-in | | | After Superposition value match | | |
|---|---|---|---|---|---|
| Iteration | $T_{ei}$, ˚F | $B$ | Iteration | $T_{ei}$, ˚F | $B$ |
| 3—29 | 96.96 | 19.13 | 3—12 | 144.38 | 10.70 |
| 10—28 | 130.73 | 16.76 | 3—14 | 173.20 | 7.95 |
| 10—46 | 152.94 | 14.99 | 3—17 | 189.73 | 6.96 |
| 10—58 | 173.66 | 13.31 | 3—9 | 216.23 | 4.19 |
| 3—42 | 196.05 | 9.29 | 2—6 | 231.52 | 2.73 |
| 3—40 | 209.00 | 7.88 | 2—10 | 233.23 | 3.22 |
| 3—24 | 222.38 | 6.09 | 2—8 | 239.59 | 2.88 |
| 3—30 | 232.84 | 5.13 | 2—7 | 249.43 | 1.97 |
| 2—15 | 275.94 | 0.22 | 2—5 | 276.82 | 0.06 |

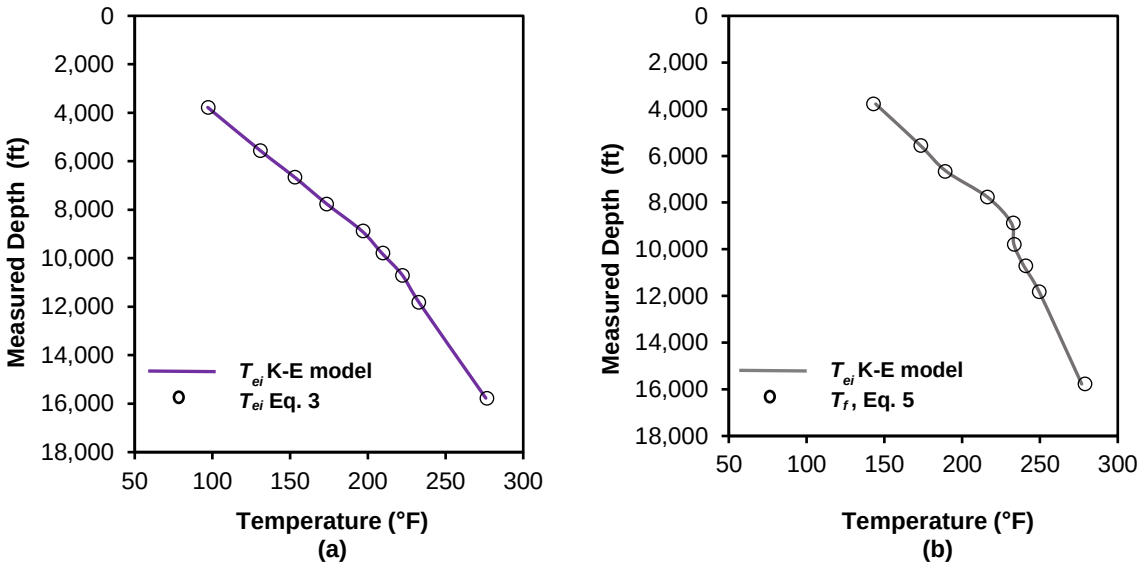


Figure 11. Performance of the K-E model for the third shut-in data: match with Tei from first shut-in (a), match with fluid temperature after superposition (b).

Despite the good agreement between the K-E model and those resented here, we found that the K-E model does not always provide desirable solutions. In particular, we noted that the formation temperature estimation depends on the suitable iteration range involving either early or late-time measurements. In contrast, the traditional Horner-type methods deal with the late-time shut-in data.

Let us point out the K-E model has been applied in the open borehole situations, which we surmised from the circulation and drilling times used. In such an environment, the thermal storage is very small or negligible. Therefore, the application of the K-E model for the late-time measurement of the first shut-in period, which is about 0.83 hr, results in an acceptable match when compared with the proposed model. However, application of the K-E model for the late-time temperature data measurements, such as those for the second and third shut-in periods, will not result in a good match as shown in Figure 12. Here, Figure 12a, b represents the second and third shut-in period, respectively.

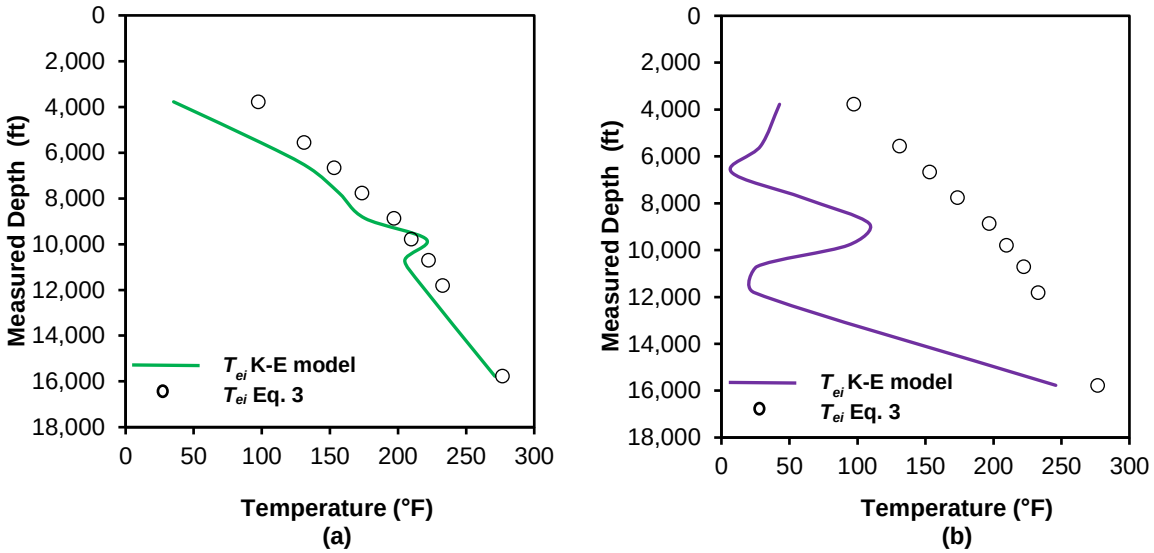


Figure 12. Application of the K-E model for late-time data only: second shut-in (a), third shut-in (b).

## 6. DISCUSSION

Previously, all the heat flow and temperature-transient analyses depended on the analogy between the pressure and temperature-diffusivity equations. Consequently, temperature-transient analyses were performed by adopting the pressure line-source solution, without accounting for the heat flow behavior. In contrast, this study provides a complete derivation of the temperature line-source solution from the temperature-diffusivity equation. Therefore, we can introduce the temperature superposition principle to study the temperature behavior for different flow and shut-in periods.

In this context, this study presents two new analytical approaches for estimating the fluid temperature in the formation. Eq. 3 showing the first approach helped determine the initial-formation temperature and heat-flow rate for three different shut-in periods of transient temperature data for a day-gas well. The second one presented by Eq. 5 helped to investigate

the temperature profiles for the multirate flow situations by application of the superposition principle. Moreover, the radius of the thermal influence was determined by the line-source solution derived from the temperature-diffusivity equation.

Depending on the loss or gain of heat, the behavior of the fluid temperature will change. The undisturbed formation temperature decreases with decreasing depth. Therefore, the temperature of the produced fluid will be higher than the adjacent formation throughout its journey to the surface, which leads to the nonlinear geothermal gradient. Of course, the variation of sediments' thermal conductivity largely contributes to this nonlinearity.

The Kabir et al. (2014) model allowed us to study the two different flowing-fluid temperature profiles by using two different initial formation temperature gradients, one from the traditional calculation of the geothermal gradient, and the other obtained from our suggested method. To ensure the application of our purposed methods, validation with field data helped instill confidence in our holistic modeling approach.

## 7. CONCLUSIONS

This paper presents a new analytical method to determine the heat-flow rate and the initial-formation temperature profiles during well shut-ins. The following conclusions appear relevant:

1. The line-source solution enabled investigation of the radius of thermal influence. Multiple sequential flow rates lead to a corresponding change in heat flow rates from or to the wellbore; the use of the superposition principle reaffirmed the rationality of fluid temperature profiles.

2. The continuous gas production results in increased flowing-fluid temperature profiles that originate from the near-wellbore-altered geothermal gradient.
3. Interpreting the transient-temperature measurements at about every 1,000 ft for the dry-gas production well allowed us to obtain a nonlinear geothermal gradient; increasing bed conductivity with increasing depth triggered this nonlinearity.

## NOMENCLATURE

$\Delta t$ = shut-in time, hr

$b$ = parameter defined by Eq. A-30, ˚F/cycle

$c_e$ = formation heat capacity, Btu/ $lb_m$-˚F

$g_G$ = formation geothermal gradient, ˚F/ft

$g_{G\text{-}TD}$ = formation geothermal gradient at total depth, ˚F/ft

$g_{G\text{-}VD}$ = formation geothermal gradient at each depth point, ˚F/ft

$h$ = perforation interval length, ft

$H$ = total wellbore measured depth, ft

$k_e$ = formation thermal conductivity, Btu/ hr-ft-˚F

$m$ = parameter defined by Eq. A-30, ˚F/cycle

$N$ = number of flow or shut-in periods, dimensionless

$Q$ = heat flow from or to the wellbore, Btu/ hr

$Q_1$ = heat flow obtained from first shut-in, Btu/ hr

$Q_2$ = heat flow obtained from second shut-in, Btu/ hr

$Q_3$ = heat flow obtained from third shut-in, Btu/ hr

$r_w$ = wellbore radius, ft

$t$ = total time, hr

$t_1$ = first shut-in total time, hr

$t_2$ = second shut-in total time, hr

$t_3$ = third shut-in total time, hr

$T_e$ = formation temperature, ˚F

$T_{ei}$ = initial formation temperature, ˚F

$T_f$ = fluid temperature at wellbore, ˚F

$T_{ws}$ = fluid shut-in temperature, ˚F

$T_s$ = surface temperature, ˚F

$z$ = any vertical well depth, ft

$\alpha$ = heat diffusivity of formation (= $k_e/ c_e \rho_e$), $ft^2/hr$

$\rho_e$ = formation density, $lb_m/ft^3$

## ACKNOWLEDGMENT

The first author (A.Q.A. Al-Saedi) gratefully acknowledges the financial support provided by the Higher Committee for Education Development in Iraq (HCED) in pursuit of his Ph.D. study.

# APPENDIX A

# LINE-SOURCE SOLUTION OF THE TEMPERATURE DIFFUSIVITY EQUATION

Many studies presented the line-source solution for pressure diffusivity equation, such as those given by van Everdingen and Hurst (1949), Mathews et al. (1967), and Dake (1978). The analogy between the pressure and temperature diffusivity equations allowed us to use the same procedure presented by Dake (1978) to solve the temperature diffusivity equation. We can represent the formation-temperature as a function of time and radius in the reservoir by adapting the line-source solution of the temperature-diffusivity equation, following the imposition of initial and boundary conditions given by

1. $T=T_{ei}$ at $t = 0$, for all $r$
2. $T=T_{ei}$ at $r$ = infinity, for all $t$
3. $\lim_{r\to 0} r\frac{\mathrm{d}T}{\mathrm{d}r} = \frac{-Q_r}{2\pi k_e h}$

These conditions led to the final form of the temperature diffusivity equation given by

$$\frac{\partial^2 T}{\partial r^2} + \frac{1}{r}\frac{\partial T}{\partial r} = \frac{c_e \rho_e}{k_e}\frac{\partial T}{\partial t} \tag{A-1}$$

The left-side of Eq. A-1 can be written as

$$\frac{1}{r}\frac{\partial}{\partial r}\left(r\frac{\partial T}{\partial r}\right) = \frac{c_e \rho_e}{k_e}\frac{\partial T}{\partial t} \tag{A-2}$$

where the diffusivity constant is given by $\alpha = k_e/c_e.\rho_e$). By introducing the Boltzmann's transformation with symbol $s$, we can write

$$s = \frac{r^2}{4(\alpha)t} \tag{A-3}$$

Substituting the diffusivity constant into Eq. A-3 will result in

$$s = \frac{c_e \rho_e r^2}{4k_e t} \tag{A-4}$$

Differentiating Eq. A-4 with respect to the radius and time result in the following expressions:

$$\frac{\partial s}{\partial r} = \frac{c_e \rho_e r}{2 k_e t} \tag{A-5}$$

$$\frac{\partial s}{\partial t} = \frac{-c_e \rho_e r^2}{4 k_e t^2} \tag{A-6}$$

Then, by using the chain rule, Eq. A-2 can be rewritten as

$$\frac{1}{r}\frac{\partial}{\partial s}\left( r \frac{\partial T}{\partial s}\frac{\partial s}{\partial r}\right)\frac{\partial s}{\partial r} = \frac{c_e \rho_e}{k_e}\frac{\partial T}{\partial s}\frac{\partial s}{\partial t} \tag{A-7}$$

Substituting Eqs. A-5 and A-6 into Eq. A-7 will result

$$\frac{1}{r}\frac{\partial}{\partial s}\left( r \frac{\partial T}{\partial s}\frac{c_e \rho_e r}{2 k_e t}\right)\frac{c_e \rho_e r}{2 k_e t} = \frac{c_e \rho_e}{k_e}\frac{\partial T}{\partial s}\frac{-c_e \rho_e r^2}{4 k_e t^2} \tag{A-8}$$

or

$$\frac{r}{r}\frac{\partial}{\partial s}\left( \frac{\partial T}{\partial s}\left( \frac{c_e \rho_e r^2}{4 k_e t}\right)\right)\frac{c_e \rho_e}{k_e t} = \frac{-c_e \rho_e}{k_e t}\left( \frac{c_e \rho_e r^2}{4 k_e t}\right)\frac{\partial T}{\partial s} \tag{A-9}$$

By using the Boltzmann's transformation term given by Eq. A-4, we can rewrite Eq. A-9 as

$$\frac{\partial}{\partial s}\left( \frac{\partial T}{\partial s} s\right) = -s\frac{\partial T}{\partial s} \tag{A-10}$$

Eq. A-10 shows that temperature changes only with variable *s*, which is a function of radius and time. Therefore, we can change Eq. A-10 from PDE to ODE in the following manner:

$$\frac{\mathrm{d}}{\mathrm{d}s}\left( \frac{\mathrm{d}T}{\mathrm{d}s} s\right) = -s\frac{\mathrm{d}T}{\mathrm{d}s} \tag{A-11}$$

Eq. A-11 can be simplified as

$$s\frac{\mathrm{d}^2 T}{\mathrm{d}s^2} + \frac{\mathrm{d}T}{\mathrm{d}s} = -s\frac{\mathrm{d}T}{\mathrm{d}s} \tag{A-12}$$

Now, let us consider

$$\frac{\mathrm{d}T}{\mathrm{d}s} = T' \text{ and } \frac{\mathrm{d}^2T}{\mathrm{d}s^2} = \frac{\mathrm{d}T'}{\mathrm{d}s} = T'' \tag{A-13}$$

Then, Eq. A-12 becomes

$$s\frac{\mathrm{d}T'}{\mathrm{d}s} + T'(1+s) = 0 \tag{A-14}$$

By integrating Eq. A-14, we have

$$\ln|T'| = -\ln|s| - s + c_1$$

or

$$\frac{\mathrm{d}T}{\mathrm{d}s} = T' = \frac{e^{-s}.c_2}{s} \tag{A-15}$$

where $C_1$ and $C_2$ are the constants of integration and $C_2$ can be evaluated using the line-source boundary condition. The heat transfer from the formation into the wellbore by conduction in radial coordinates can be written as (Fourier's law):

$$\lim_{r\to 0} r\frac{\mathrm{d}T}{\mathrm{d}r} = \frac{-Q_r}{2\pi k_e h} = r\frac{\mathrm{d}T}{\mathrm{d}s}.\frac{\mathrm{d}s}{\mathrm{d}r} = \frac{4k_e t}{c_e\rho_e r}s\frac{\mathrm{d}T}{\mathrm{d}s}\frac{c_e\rho_e r}{2k_e t} = 2s\frac{\mathrm{d}T}{\mathrm{d}s} \tag{A-16}$$

Therefore,

$$2\left(s.\frac{\mathrm{d}T}{\mathrm{d}s}\right) = \frac{-Q_r}{2\pi h k_e} \tag{A-17}$$

Substituting Eqs. A-15 into Eq. A-17, and considering when *r* goes to zero and *s* equals to zero, we can write

$$C_2 = \frac{-Q_r}{4\pi h k_e} \tag{A-18}$$

Then, Eq. A-15 can be rewritten as

$$T' = \frac{\mathrm{d}T}{\mathrm{d}s} = \frac{-Q_r}{4\pi h k_e} . \frac{e^{-s}}{s} \tag{A-19}$$

or

$$\mathrm{d}T = \frac{-Q_r}{4\pi h k_e} . \frac{e^{-s}}{s} \mathrm{d}s \tag{A-20}$$

Integration of Eq. A-20 with the limit of *s* up to infinity, and the current value of *t*, for which *s* = *x*; the current temperature *T* leads to the following expression:

$$\int_{T_{ei}}^{T} \mathrm{d}T = \frac{-Q_r}{4\pi h k_e} \int_{\infty}^{x} \frac{e^{-s}}{s} \mathrm{d}s \tag{A-21}$$

which yields

$$\left(T - T_{ei}\right) = \frac{Q_r}{4\pi h k_e} \int_{x=\frac{c_e \rho_e r^2}{4 k_e t}}^{\infty} \frac{e^{-s}}{s} \mathrm{d}s \tag{A-22}$$

By introducing the exponential integral, denoted by $E_i(-X)$, which is defined by the following expression:

$$\int_{x}^{\infty} \frac{e^{-s}}{s} \mathrm{d}s = \int_{x=\frac{c_e \rho_e r^2}{4 k_e t}}^{\infty} \frac{e^{-s}}{s} \mathrm{d}s \tag{A-23}$$

we can rewrite Eq. A-22 as follows:

$$T_{(r,t)} = T_{ei} + \frac{Q_r}{4\pi h k_e} E_i \left[ \frac{-c_e \rho_e r^2}{4 k_e t} \right] \tag{A-24}$$

Eq. A-24 represents the line-source solution of the temperature diffusivity equation that expresses temperature as a function of position and time. In field units, Eq. A-24 can be rewritten as

$$T_{(r,t)} = T_{ei} + 0.68\frac{Q_r}{hk_e}E_i\left[\frac{-r^2}{4\alpha t}\right] \tag{A-25}$$

where $\alpha$ represents the formation diffusivity constant and is given as ($k_e/\rho_e c_e$). By considering the log-approximation of the $E_i$ function, Eq. A-25 can be expressed as follows:

$$\begin{aligned} &E_i\left(-x\right) = \ln(1.781x), \qquad x \le 0.01 \\ &\ln(x) = 2.303\log(x) \end{aligned} \tag{A-26}$$

Then, Eq. A-25 becomes

$$T_{ws} = T_{ei} + \left(\frac{1.566Q}{hk_e}\right)\log\left(0.44525\frac{r_w^2}{\alpha t}\right) \tag{A-27}$$

or

$$T_{ws} = T_{ei} + \left(\frac{1.566Q}{hk_e}\right)\left[\log\left(\frac{r_w^2}{\alpha\Delta t}\right) - 0.352\right] \tag{A-28}$$

Eq. A-28 can be simplified as

$$T_{ws} = T_{ei} - \left(\frac{1.566Q}{hk_e}\right)\left[\log\left(\frac{\alpha}{r_w^2}\right) + 0.352\right] - \left(\frac{1.566Q}{hk_e}\right)\log\left(\Delta t\right) \tag{A-29}$$

Thus, we can rewrite Eq. A-29 as follows:

$$T_{ws} = b - m\log\left(\Delta t\right) \tag{A-30}$$

where

$$m = \left(\frac{1.566Q}{hk_e}\right), \qquad b = T_{ei} - m\left[\log\left(\frac{\alpha}{r_w^2}\right) + 0.352\right] \tag{A-31}$$

However, we can apply the same procedure used in pressure-transient test analysis to that in a temperature-transient test. As long as we have a temperature difference, then heat transfer always occurs until the temperature reaches equilibrium, which usually requires an

extended period. Then the superposition of time may apply for a temperature-transient test by using Eq. A-30, and it can be expressed for the second shut-in period as

$$T_{ei} - T_f = -\left(\frac{0.68}{hk_e}\right)\left\{\begin{array}{l}\left[\left(Q_1 - 0\right)E_i\left(\frac{-r_w^2}{4\alpha\left(t_1 - 0\right)}\right)\right] \\ +\left[\left(Q_2 - Q_1\right)E_i\left(\frac{-r_w^2}{4\alpha\left(t_2 - t_1\right)}\right)\right]\end{array}\right\} \tag{A-32}$$

In Eq. A-32, $Q_1$, and $t_1$ represent the heat flow and the total test time, respectively, which were obtained from the first shut-in period, and $Q_2$ and $t_2$ represent the same entities for the second shut-in period, and so on. Therefore, we can rewrite Eq. A-33 for $N$ number of flow and shut-in periods as follows:

$$T_{ei} - T_f = \left(\frac{-0.68}{hk_e}\right)\sum_{j=0}^{N}\left[\left(Q_{j+1} - Q_j\right)E_i\left(\frac{-c_e\rho_e {r_w}^2}{4k_e\left(t_N - t_j\right)}\right)\right] \tag{A-33}$$

# APPENDIX B

# EXAMPLE APPLICATIONS

## B.1. EXAMPLE-1, APPLICATION OF THE SUPERPOSITION PRINCIPLE

The initial formation temperature and the amount of heat flow for each shut-in period were estimated by using the Eq. A-29, as given by Table 1. Wherein, we used the three shut-ins dataset given by Figure 1, and we assumed the other necessary data from the literature such as wellbore radius about 0.329 ft and the 0.043 $ft^2$/hr for formation thermal diffusivity, and the perforation interval about 30 ft. Table B-1 presents the production and shut-in time for each period.

Table B.1 Shut-in and production durations.

| Shut-in period | $t_p$, hr | $t_s$, hr | $t_{total}$, hr |
|---|---|---|---|
| 1 | 0.81 | 0.83 | 1.63 |
| 2 | 5.05 | 9.81 | 14.86 |
| 3 | 92.50 | 98.05 | 190.55 |

Then, for the station located at 3,777 ft, and by using the required data presented in Table 1 and Table B-1, we can apply Eq. A-31 to do superposition between the second and first shut-in periods as follows:

$$T_{ei}-T_r=-\left(\frac{0.68}{30\times 1.303}\right)\left\{\begin{array}{l}\left[\left(78.69-0\right)E_i\left(\frac{-0.392^2}{4\times 0.043\left(1.63-0\right)}\right)\right]\\ +\left[\left(1912.77-78.69\right)E_i\left(\frac{-0.392^2}{4\times 0.043\left(14.86-1.63\right)}\right)\right]\end{array}\right\} \quad \text{(B-1)}$$

$$\begin{aligned}T_{ei}-T_r&=80.18\ ^\circ\text{F}\\ T_r&=171.02-80.18=90.82\ ^\circ\text{F}\end{aligned} \quad \text{(B-2)}$$

The same procedure was applied to all the station's point, and the result presented by Figure 5a. For the same depth point and by using Eq. A-32, we can determine the fluid temperature for the third shut-in period as

$$T_{ei}-T_r=-\left(\frac{0.68}{30\times 1.303}\right)\left\{\begin{array}{l}\left[\left(1912.77-78.69\right)E_i\left(\frac{-0.392^2}{4\times 0.043\left(14.86-1.63\right)}\right)\right]\\ +\left[\left(1324.01-1912.77\right)E_i\left(\frac{-0.392^2}{4\times 0.043\left(190.55-14.86\right)}\right)\right]\end{array}\right\} \tag{B-3}$$

$$\begin{aligned}&T_{ei}-T_r=28.4\ ^\circ\text{F}\\&T_r=171.42-28.4=143.02\ ^\circ\text{F}\end{aligned} \tag{B-4}$$

Figure 5b presents the application of superposition for all depth points of the third shut-in period.

## B.2. EXAMPLE-2, APPLICATION OF KUTASOV AND EPPELBAUM (2018) MODEL

Kutasov and Eppelbaum (2018) presented the line-source solution for the temperature-diffusivity equation based on Carslaw and Jaeger (1959). Their version of the modified-Horner method can be written as

$$T_{s\,(r_w,t_s)}=T_i+B\,X \tag{B-5}$$

where parameter $B$ can be obtained from the slope, and the intercept will give the initial-formation temperature, $T_i$. The parameter $X$ can be written as

$$X=\ln\left(1+\frac{t_c^*}{t_{s(N-1)}^*}\right) \tag{B-6}$$

where

$$t_c=t_{total}\left(1-\frac{z}{H}\right)$$

$$t_c^* = t_c + t_{s1}$$
$$t_{s(N-1)}^* = t_{sN}^* - t_0 \quad \text{(B-7)}$$

Kutasov and Eppelbaum (2018) defined all parameters for their model. For the first shut-in period at 3,777 ft, and total depth of about 16,000 ft, the thermal disturbance period ($t^*_c$) can be estimated by

$$t_c = 1.63\left(1 - \frac{3777}{16000}\right) = 1.247 \text{ hr}$$
$$t_c^* = 1.247 + 0.83 = 2.055 \text{ hr} \quad \text{(B-8)}$$

Table B-2 shows the procedure to find parameter *X*, the slope, and the initial-formation temperature.

Table B.2 Steps involving estimation of $T_{ei}$.

| Iteration | Test time (hr) | $T_s$, ˚F | $t^*_{sN}$ | $1+(t^*_c/t^*_{S(N-1)})$ | $X$ | Slope, ˚F | $T_{ei}$, ˚F |
|---|---|---|---|---|---|---|---|
| 1 | 107.83 | 101.525 | | | | | |
| 2 | 108.00 | 99.613 | 0.167 | 13.323 | 2.589 | | |
| 3 | 108.17 | 97.925 | 0.333 | 7.162 | 1.969 | | |
| 4 | 108.33 | 96.463 | 0.500 | 5.108 | 1.631 | | |
| 5 | 108.50 | 96.856 | 0.667 | 4.081 | 1.406 | 1.755 | 99.32 |

Then, by choosing the iteration number from 4 to 5, the formation temperature obtained by the intercept equals 99.32 ˚F, and the slope that represents the parameter *B* equals 1.755 ˚F. We applied the same procedure for all test data points, and Table 3 presents the result of the first shut-in period in the text.

# REFERENCES


Carslaw, H.S., Jaeger, J.C., 1959. Conduction of Heat in Solids, 2nd ed. Oxford University Press, London.

Dake, L.P., 1978. Fundamentals of Reservoir Engineering. Elsevier Scientific Publishing Company, pp. 149-155, New York.

Dowdle, W., and Cobb, W., 1975. Static formation temperature from well logs - An empirical method. J. Pet. Technol. 27 (11), 1326-1330. https://doi.org/10.2118/5036-pa.

Hasan, A. R. and Kabir, C. S., 1994a. Determination of static reservoir temperature from transient data following mud circulation. SPE Drill. & Compl. 9 (01), 17-24. https://doi.org/10.2118/24085-pa.

Hasan, A.R. and Kabir, C.S., 1994b. Aspects of wellbore heat transfer during two-phase flow (includes associated papers 30226 and 30970). SPE Prod. & Faci. 9 (03), 211-216. https://doi.org/10.2118/22948-pa.

Hasan, A. R. and Kabir, C. S., 2018. Fluid Flow and Heat Transfer in Wellbores, 2nd ed., p. 121, SPE, Richardson, Texas.

Hasan, A. R., Kabir, C. S., and Wang, X., 2009. A robust steady-state model for flowing-fluid temperature in complex wells. SPE Prod. & Oper. 24 (02), 269-276. https://doi.org/10.2118/109765-pa.

Hashmi, G., Kabir, C.S., and Hasan, A.R., 2015. Estimating reliable gas rate with transient-temperature modeling for interpreting early-time cleanup data during transient testing. J. Pet. Sci. & Eng. 133, 285-295. https://doi.org/10.1016/j.petrol.2015.06.001.

Horner, D. R., 1951. Pressure buildup in wells, Proc., Third World Pet. Cong., The Hague Ⅱ, 503.

Izgec, B., Hasan, A. R., Lin, D., and Kabir, C. S., 2010. Flow-rate estimation from wellhead-pressure and -temperature data. SPE Prod. & Oper. 25 (01), 31-39. https://doi.org/10.2118/115790-pa.

Kabir, C. S., Yi, X., Jakymec, M., and Hasan, A. R., 2014. Interpreting distributed-temperature measurements in deepwater gas-well testing: estimation of static and dynamic thermal gradients, and flow rates. SPE Prod. & Oper. 29 (02), 097-104. https://doi.org/10.2118/166333-pa.

Kutasov, I. M. and Eppelbaum, L. V., 2005. Determination of formation temperature from bottom-hole temperature logs—a generalized Horner method. J. Geophys. & Eng. 2 (2), 90-96. https://doi.org/10.1088/1742-2132/2/2/002.

Kutasov, I. M. and Eppelbaum, L. V., 2018. Utilization of the Horner plot for determining the temperature of frozen formations — A novel approach. Geothermics 71, 259-263. https://doi.org/10.1016/j.geothermics.2017.10.005.

Lee, J., Rollins, J. B., Spivey, J. P. 2003. Pressure Transient Testing. SPE, Richardson, Texas.

Matthews, C. S. and Russell, D. G., 1967. Pressure Buildup and Flow Tests in Wells. Monograph Series, SPE of AIME, Dallas, 1, 48.

Roux, B., Sanyal, S. K., and Brown, S. L., 1980. An Improved Approach to Estimating True Reservoir Temperature from Transient Temperature Data. SPE California Regional Meeting. https://doi.org/10.2118/8888-ms.

Schoeppel, R. and Gilarranz, S. 1966. Use of well log temperatures to evaluate regional geothermal gradients. J. Pet. Technol. 18 (06), 667-673. https://doi.org/10.2118/1297-pa.

van Everdingen, A., and Hurst, W., 1949. The application of the Laplace transformation to flow problems in reservoirs. J. Pet. Technol. 1 (12), 305-324. https: //doi.org/10.2118/949305-g.

# SECTION

# 3. CONCLUSIONS AND RECOMMENDATIONS

## 3.1. CONCLUSIONS

In this dissertation, a comprehensive study of wellbore temperature behavior was investigated by including four parts. In first part, and for decades, the traditional heat energy system to represent the thermal behavior at the wellbore was solved by using one type of boundary condition. And for the first time, two new boundary conditions were used to solve the thermal energy system. Those boundary conditions helped to expand the possible range of predicting temperature profile for both forward and reverse circulations.

In the second part, two mathematical models for rotational and frictional kinetic energy were presented. These models yield the same solution if we do not include the energy source, and they can apply equally well for any energy-balance system. The proposed mathematical models provide new insights into different energy terms that can be included to compute the temperature profiles in the drillpipe and annulus.

The third part includes a mathematical model that shows that the heat transfer occurs from the wellbore/formation interface, not from some distance away from the wellbore wherein the initial formation temperature profile remains undisturbed. This new model allows investigation of heat transfer behavior from the formation into the wellbore during drilling or fluid circulation, and from the wellbore into the reservoir in the production mode.

Finally, the analogy between the pressure and temperature diffusivity equations helped many authors to adopt the same final pressure solution form and use it for the wellbore

temperature applications. Wherein, the pressure transient analysis depends on the fluid-flow rate behavior, and the temperature transient analysis depends on the heat-flow rate. However, the major findings of this research are summarized below:

- A new type of boundary condition was used to investigate the wellbore temperature profile for forward and reverse circulations.
- Despite all other studies, using those boundary conditions shows that the maximum temperature happened at the well bottom depth.
- A sensitive application including uncertainty in geothermal gradient and heat-transfer parameters, presence of gas-hydrate interval, presence of a salt-dome interval, and change in geothermal gradient were also investigated.
- For the first time, rotational kinetic energy resulting from the rotating of the drill string in drilling operation was mathematically presented to study its effect on the wellbore temperature profile.
- New mathematical models helped to determine the rate of heat transfer involving the entire wellbore profile during fluid circulation and production.
- Both models showed that the temperature gradient is time-dependent and that the initial-formation temperature does not remaind static neither at the well bottom nor in the entire wellbore profile.
- Application of the line-source solution of the temperature-diffusivity equation allows estimation of the wellbore temperature profiles at total depth, regardless of the direction of heat flow.

- The initial formation temperature at the well bottom and the geothermal gradient depend on time, and second-order polynomial expressions can describe their nonlinearity.
- A complete derivation of the temperature line-source solution from the temperature-diffusivity equation was presented.
- This study presents two new analytical approaches for estimating the fluid temperature in the formation. The first approach helped determine the initial-formation temperature and heat-flow rate for three different shut-in periods of transient temperature data for a day-gas well. And the second one presented helped to investigate the temperature profiles for the multi-rate flow situations by application of the superposition principle.
- The line-source solution derived from the temperature-diffusivity equation led to establishing the radius of the thermal influence.

## 3.2. RECOMMENDATIONS

The main objective of this study is to provide a comprehensive understanding of the using the wellbore temperature behavior to investigate the undisturbed formation temperature and the heat-flow rate. The line-source temperature solution for temperature diffusivity equation helped proposed suitable mathematical models for analyzing the buildup and falloff temperature.

The future academic research potentials are outlined to extend the current research in the following points:

- Explore a deeper understanding of the other mathematical solution methods for temperature diffusivity equation and comparing the results with the existing one.

- Investigate the application of the heat energy system for injection, deep-water wells, directional-drilling applications.
- Apply the peoposed mathematical models in other field applications, such as Stimulation, steam and CO2 injection, and gel treatment.
- Predict the heat flow-rate from the fluid flow rate and study the formation thermal properties in the same way of the pressure-transient analysis.

# BIBLIOGRAPHY


Aadnoy, B. S. and Djurhuus, J. (2008). Theory and Application of a New Generalized Model for Torque and Drag. *IADC/SPE Asia Pacific Drilling Technology Conference and Exhibition*, 25-27 August, Jakarta, Indonesia. http://dx.doi.org/10.2118/114684-MS.

Al Saedi, A., Flori, R.E., and Kabir, C.S. (2018). New analytical solutions of wellbore fluid temperature profiles during drilling, circulating and cementing operations. *J. Pet. Sci. & Eng*. 170 (2018), 206-217. http://dx.doi:10.1016/j.petrol.2018.06.027.

Arnold, F. C. (1990). Temperature variation in a circulating wellbore fluid. *J. Energy Resour*. Technol. 112 (2), 79. http://dx.doi.org/10.1115/1.2905726.

Beirute, R. (1991). A circulating and shut-in well-temperature-profile simulator. *J Pet Technol* 43 (9), 1140-1146. http://dx.doi.org/10.2118/17591-PA.

Carslaw, H.S., Jaeger, J.C., (1959). Conduction of Heat in Solids, 2nd ed. Oxford University Press, London.

Dake, L.P., (1978). Fundamentals of Reservoir Engineering. *Elsevier Scientific Publishing Company*, pp. 149-155, New York.

Davies, S., Gunningham, M., Bittleston, S. (1994). Field studies of circulating temperatures under cementing conditions. *SPE Drill & Compl* 9 (1), 12-16. http://dx.doi.org/10.2118/21973-PA.

Dowdle, W. L., and Cobb, W. M. (1975). Static formation temperature from well logs ─ An empirical method. *J. Petrol. Technol*. 27 (11), 1326-1330. http://dx.doi.org/10.2118/5036-PA.

Edwardson, M., Girner, H., Parkison, H. (1962). Calculation of formation temperature disturbances caused by mud circulation. *J Pet Technol 14* (4), 416-426. http://dx.doi.org/10.2118/124-PA.

Forrest, J., Marcucci, E., and Scott, P. (2007). Geothermal gradients and subsurface temperatures in the Northern Gulf of Mexico. *Trans*. GCAGS.55: 233–248.

Gao, Y., Sun, B., and Xu, B. (2017). A wellbore/formation-coupled heat-transfer model in deepwater drilling and its application in the prediction of hydrate-reservoir dissociation. *SPE J*. 22 (3), 756-766. http://dx.doi.org/10.2118/184398-PA.



Gao, Y., Sun, B., Xu, B. (2017). A wellbore/formation-coupled heat-transfer model in deepwater drilling and its application in the prediction of hydrate-reservoir dissociation. *SPE J*. 22 (3), 756-766. http://dx.doi.org/10.2118/184398-PA.

Guo, B., Li, G., and Shan, L. (2016). Mathematical model provides annular temperature profile for thermal hydraulics in drilling gas hydrates. *IADC/SPE* Asia-Pacific Drill. Technol. Conf. http://dx.doi.org/10.2118/180560-MS.

Hasan, A. R. and Kabir, C. S., (1994a). Determination of static reservoir temperature from transient data following mud circulation. *SPE Drill. & Compl*. 9 (01), 17-24. https://doi.org/10.2118/24085-pa.

Hasan, A. R., Kabir, C. S., and Wang, X., (2009). A robust steady-state model for flowing-fluid temperature in complex wells. *SPE Prod. & Oper*. 24 (02), 269-276. https://doi.org/10.2118/109765-pa.

Hasan, A.R., and Kabir, C.S. (1994). Aspects of wellbore heat transfer during two-phase flow (includes associated papers 30226 and 30970). *SPE Prod. & Facil*. 9 (03), 211-216. http://dx.doi.org/10.2118/22948-PA.

Hasan, A.R., Kabir, C.S., and Ameen, M. (1996). A Fluid Circulating Temperature Model for Workover Operations. *SPE J.* 1 (2): 133-144. http://dx.doi.org/10.2118/27848-PA.

Hashmi, G., Kabir, C.S., and Hasan, A.R., (2015). Estimating reliable gas rate with transient-temperature modeling for interpreting early-time cleanup data during transient testing. *J. Pet. Sci. & Eng*. 133, 285-295. https://doi.org/10.1016/j.petrol.2015.06.001.

Holmes, C. S., & Swift, S. C. (1970). Calculation of circulating mud temperatures. *J Pet Technol* 22 (6), 670-674. http://dx.doi.org/10.2118/2318-PA.

Horner, D. R., (1951). Pressure buildup in wells, Proc., Third World Pet. Cong., The Hague Ⅱ, 503.

Kabir, C.S., Hasan, A.R., and Kouba, G. (1996). Determining Circulating Fluid Temperature in Drilling, Workover, and Well Control Operations. *SPE Drill & Compl* 11 (2): 74-79. http://dx.doi.org/10.2118/24581-PA.

Keller, H., Couch, E., and Berry, P. (1973). Temperature distribution in circulating mud columns. *SPE J*. 13 (1), 23-30. http://dx.doi.org/10.2118/3605-PA.

Kritikos, W.R., and Kutasov, I. M. (1988). Two-point method for determination of undisturbed reservoir temperature. *SPE Form. Eval*. 3 (1), 222-226. http://dx.doi.org/10.2118/15204-PA.

Kumar, A., and Samuel, R. (2012). Analytical Model to Estimate the Downhole Temperatures for Casing while Drilling Operations. *SPE Annual Technical Conference and Exhibition*, 8-10 October, San Antonio, Texas, USA. http://dx.doi.org/10.2118/159278-MS.

Kumar, A., Singh, A. P., and Samuel, R. (2012b). Field Application of an Analytical Model for Estimating the Downhole Temperatures due to Wellbore Friction. Paper SPE-156307-MS presented at the *IADC/SPE Asia Pacific Drilling Technology Conference and Exhibition*, 9-11 July, Tianjin, China. http://dx.doi.org/10.2118/156307-MS.

Kumar, A. and Samuel, R. (2013). Analytical model to predict the effect of pipe friction on downhole fluid temperatures. *SPE Drill & Compl* 28 (3), 270-277. http://dx.doi.org/10.2118/165934-PA.

Kumar, A. and Samuel, R. (2013). Analytical Model to Predict the Effect of Pipe Friction on Downhole Fluid Temperatures. *SPE Drill & Compl* 28 (3): 270-277. http://dx.doi.org/10.2118/165934-PA.

Kumar, A., Singh, A.P., and Samuel, R. (2012a). Analytical Model to Predict the Effect of Pipe Friction on Downhole Temperatures for Extended Reach Drilling (ERD). Paper SPE-151254-MS presented at the *IADC/SPE Drilling Conference and Exhibition*, 6-8 March, San Diego, California, USA. http://dx.doi.org/10.2118/151254-MS.

Kutasov, I. M., and Eppelbaum, L. V. (2005). Determination of formation temperature from bottom-hole temperature logs—a generalized Horner method. *J. Geophys. & Eng*. 2 (2), 90-96. https://doi.org/10.1088/1742-2132/2/2/002.

Kutasov, I. M., and Eppelbaum, L. V. (2018). Utilization of the Horner plot for determining the temperature of frozen formations — A novel approach. *Geothermics* 71, 259-263. https://doi.org/10.1016/j.geothermics.2017.10.005.

Kutasov, I. M. and Eppelbaum, L. V., (2005). Determination of formation temperature from bottom-hole temperature logs—a generalized Horner method. *J. Geophys. & Eng*. 2 (2), 90-96. https://doi.org/10.1088/1742-2132/2/2/002.

Lee, J., Rollins, J. B., Spivey, J. P. (2003). Pressure Transient Testing. *SPE*, Richardson, Texas.

Li, B., Li, H., Guo, B., Cai, X. et al. (2017). A new numerical solution to predict the temperature profile of gas-hydrate-well drilling. *SPE J.* 22 (4), 1201-1212. http://dx.doi.org/10.2118/185177-PA.

Marshall, D. W. and Bentsen, R. G. (1982). A Computer Model to Determine the Temperature Distributions in a Wellbore. *J Can Pet Technol* 21 (1): 63-75. http://dx.doi.org/10.2118/82-01-05.

Matthews, C. S. and Russell, D. G., (1967). Pressure Buildup and Flow Tests in Wells. Monograph Series, *SPE of AIME*, Dallas, 1, 48.

Mirhaj, S. A., Kaarstad, E., and Aadnoy, B. S. (2016). Torque and Drag Modeling; Soft-string versus Stiff-string Models. Paper-178197-MS presented at the *SPE/IADC Middle East Drilling Technology Conference and Exhibition*, 26-28 January, Abu Dhabi, UAE. http://dx.doi.org/10.2118/178197-MS.

Prensky, S., (1992). Temperature Measurements in Boreholes ─ An overview of engineering and scientific applications. Society of *Petrophysicists and Well-Log Analysts*.

Raymond, L. (1969). Temperature distribution in a circulating drilling fluid. *J Pet Technol* 21 (3), 333-341. http://dx.doi.org/10.2118/2320-PA.

Roux, B., Sanyal, S. K., and Brown, S. L., (1980). An Improved Approach to Estimating True Reservoir Temperature from Transient Temperature Data. *SPE California Regional Meeting*. https://doi.org/10.2118/8888-ms.

Sagar, R., Doty, D., & Schmidt, Z., (1991). Predicting temperature profiles in a flowing well. *SPE Prod.* Eng. 6 (04), 441-448. http://dx.doi.org/10.2118/19702-PA.

Samuel, G. R. (2007). Downhole Drilling Tools: Theory and Practice for Engineers and Students. Houston, TX: *Gulf Pub*.

Schoeppel, R., & Gilarranz, S., (1966). Use of well log temperatures to evaluate regional geothermal gradients. *J. Petrol. Technol*. 18 (06), 667-673. http://dx.doi.org/10.2118/1297-PA.

Tragesser, A. F., Crawford, P. B., and Crawford, H. R. (1967). A method for calculating circulating temperatures. *J Pet Technol* 19 (11), 1507-1712. http://dx.doi.org/10.2118/1484-PA.

van Everdingen, A., and Hurst, W., (1949). The application of the Laplace transformation to flow problems in reservoirs. *J. Pet. Technol*. 1 (12), 305-324. https://doi.org/10.2118/949305-g.

Wooley, G. R. (1980). Computing downhole temperatures in circulation, injection, and production wells. *J Pet Technol* 32 (9), 1509-1522. http://dx.doi.org/10.2118/8441-PA.

# VITA

Ahmed Qasim Al Saedi was born in Missan, Iraq. He received BSc and MSc degrees in Petroleum Engineering from University of Baghdad, Baghdad, Iraq in 2005 and 2011, respectively.

Al Saedi worked as a drilling supervisor for Weatherford and then for Baker Hughes in Iraq. He was granted a PhD scholarship by the Higher Committee for Education Development in Iraq. He received a PhD in Petroleum Engineering from Missouri University of Science and Technology, Rolla, MO, in May 2020.

Ahmed Al Saedi was a member of Iraqi Engineers Union and Society of Petroleum Engineering. His research interests included a wellbore temperature modeling and transient well testing. He published four journal papers in these research areas.